Kinetic model for the ammoxidation of ethanol to acetonitrile

Antonio Tripodi[1], Davide Ripamonti[1], Rocco Martinazzo[1], Federico Folco[2], Tommaso Tabanelli[2], Fabrizio Cavani[2], Ilenia Rossetti[1*]

[1] Chemical Plants and Industrial Chemistry Group, Dipartimento di Chimica, Università degli Studi di Milano, INSTM Milano Università-Unit, CNR-ISTM, Via Golgi 19, 20133 Milano (MI) – Italy

[2] Dipartimento di Chimica Industriale "Toso Montanari", Alma Mater Studiorum Università di Bologna, Viale Risorgimento 4, 40136 Bologna - Italy

Abstract

A comprehensive kinetic study, based on V-based catalysts (Vanadium Pyro-Phosphate, VPP, VO_x/TiO_2 and VO_x/ZrO_2), was modelled to retrieve the surface reaction mechanism and kinetic parameters for the ammoxidation of ethanol to acetonitrile. In all the cases, the catalysts showed a moderate to good acetonitrile selectivity, that in turn resulted correlated primarily to the reaction temperature, while the byproducts distribution was more influenced by the thermodynamic stability of the reacting mixture.

A large and comprehensive collection of data on ammoxidation of C2 substrates for acetonitrile production was analysed and 5 groups of experiments on VO_x-based catalysts (operating in the temperature range 250 – 450 °C) were selected. The base reactant was ethanol and ammonia and oxygen were fed in optimal ratios of 1:3-1:4 mol/mol.

A kinetic model was then derived applying the Langmuir-Hinshelwood-Hougen-Watson (LHHW) approach to accepted catalytic oxidation mechanisms: for every catalytic material, eight to ten reactions with rates described by the Arrhenius formula were employed. Fixing the reaction orders

---

[*] Corresponding author: ilenia.rossetti@unimi.it; fax +390250314300.

according to the mechanistic assumption and adjusting only the kinetic and adsorption parameters, the calculated molar fractions of ethanol, ammonia, acetonitrile and ethylene resulted in good agreement with the extensive collection of experimental data available.

Keywords: Acetonitrile; Ethanol; Ammoxidation; Kinetic modeling; Biorefinery.

1. Introduction

The chemical importance of acetonitrile comes from its very particular polarity, affinity with both organic liquids and water and its relatively high boiling point. It is used as a solvent for pharmaceutical industry and laboratory applications (nearly 70%) (Mcconvey et al., 2012), in the extractive separation of butadiene from C4 alkanes (Evans et al., 1991) and in other similar processes (Liao et al., 2001).

Routes to acetonitrile as the main reaction outcome, rather than as an acrylonitrile byproduct (ACS Office of Public Outreach, 1996; Grasselli, 1981), were sought (Evans et al., 1991) and an efficient atom-economy could be achieved using C2 reactants, such as ethanol, ethane and ethylene. All these reactions are characterized by the alkylation of ammonia. In fact, also using ethane, the ethylene molecule is the reactive intermediate, while its further conversion may be not faster than its desorption from the catalyst, due to the competitive occupation of the same active sites by ammonia. Mechanism details, conversion and selectivity vary according to the peculiarities of the catalyst (generally a zeolite or acidic oxide loaded with metals such as Ni, Co, V and others) within the above established context (Ayari et al., 2012; Bondareva et al., 2006; Li and Armor, 1998; Mannei et al., 2017; Mies et al., 2007; Pan et al., 2005; Rhimi et al., 2016; Rojas et al., 2012, 2009).

Ethanol as a reactant, on the other hand, is a promising alternative (Sun and Wang, 2014) being a renewable resource, readily available from well known and operative fermentation processes (Schuster and Chinn, 2013) and usable for this process without particular purification requirements.

In the recent past, we focused on process design from the grass roots for a fully new, integrated process for the ethanol ammoxidation to acetonitrile. After a first investigation on alternative acetonitrile distillation strategies, we have presented an integrated process layout, consisting in a reactor, an ammonia and CO_2 separation section (recovered as $(NH_4)_2CO_3$), HCN elimination as salt and resolution of the water/acetonitrile azeotrope (Tripodi et al., 2017; A. Tripodi et al., 2018; Antonio Tripodi et al., 2018). Then, we have laid down the full plant description as a basis for life cycle assessment (LCA), which demonstrated the lower impact of this alternative route to acetonitrile with respect to the Sohio process to acrylonitrile, of which acetonitrile is the valorized byproduct (Antonio Tripodi et al., 2018).

In this context, the huge missing parameter to optimize and size the process is *reaction kinetics*, needed to design the reactor and to rate its performance during multivariate optimization. The search for kinetic data is limited by the unavailability of consistent datasets collected on purpose. Therefore, in this work, we are filling this gap by building a robust kinetic model to interpret activity data as a basis for process design, based on the most comprehensive dataset we have retrieved for this application. In particular, we considered different catalyst formulations Vanadium Pyro-Phosphate (VPP), VO_x/TiO_2 and VO_x/ZrO_2 in the temperature range from 250 to 450°C.

These catalysts were investigated by Folco et al. (2017), based on the following arguments: (a) catalysts based on Vanadium oxide are well known to be efficient in the gas-phase ammoxidation of activated organic substrates (F.Cavani et al., 1987; P.Cavalli et al., 1987) and in the gas-phase oxidation of alcohols into aldehydes (Malmusi et al., 2019); (b) among mixed oxide catalysts, VPP shows multifunctional properties which are involved in complex transformations involving several in-series steps, as in the case of ethanol ammoxidation to acetonitrile (Ballarini et al., 2006; Chieregato et al., 2015; F. Cavani and Trifirò, 1997); (c) concerning the catalyst made of vanadium oxide supported over titania and zirconia, the amount of active phase was chosen based on the amount needed for the development of the so-called "monolayer" species (N. Ballarini, F. Cavani, A.

Cericola, C. Cortelli, M. Ferrari, F. Trifirò, G. Capannelli, A. Comite, R. Catani, 2004; P.Cavalli, F.Cavani, I.Manenti, 1987).

2. Models and methods

2.1 Investigation on the reaction mechanism

In the case of ethanol ammoxidation the mechanism is different with respect to alkanes and alkenes, because, starting from an already partially oxidized molecule, the alkylating agent is mostly the derived aldehyde rather than the alkene. The alkylation of ammonia with ethanol (whose C-O bond is activated by the initial dehydrogenation or oxidation into acetaldehyde) and the further oxidation of the C-N into the nitrile group, was studied on different catalysts and conditions.

Recently, Folco et al. (Folco, 2013; Folco et al., 2017; Tanganelli, 2011) tested the activity of different vanadium-based catalysts. This large dataset is well suited to the scope of this analysis, because the systematic variation of temperatures and contact times allowed the estimation of both kinetic prefactors and activation energies. Moreover, these data are very interesting for a possible industrial scaling of the process, thanks to the generally low ammonia:ethanol ratio (never higher than 5:1 and usually of 3:1 mol/mol, only), the mild temperature conditions (< 440 °C), the use of non-noble metals, the use of oxygen in mixture with nitrogen (which lets foresee the direct use of air) and the employment of ethanol as C2 substrate. These authors confirmed also the kinetic relevance of the enamine intermediate using it as the starting feed. Simplifications in the catalysts formulation are also relevant in this work with respect to other options (Grasselli, 1999).

Different reports were discarded. Data presented in (Zhang et al., 2011) never accounted for a complete ethanol conversion, which would pose considerable separation issues in a real plant (A. Tripodi et al., 2018; Antonio Tripodi et al., 2018; Tripodi et al., 2017), while the work of Belov et al. (Belov et al., 2016) assumed a co-feed of pure hydrogen. Other experiments (Hamill et al., 2015; Hu

et al., 2012; Zhang et al., 2009) were performed with too high ammonia:ethanol ratios, while the data obtained by Feng et al. (Feng et al., 2011) on a Co doped Ni/alumina were instead characterized by a more balanced feed mixture. In any case, most papers deal with the material-temperature-selectivity scheme (Hu et al., 2012) without the systematic screening of process parameters needed for kinetic modelling.

A more comprehensive series of experiments, ammoxidating a fully oxidized substrate such as acetic acid (Card and Schmitt, 1981; Galanov et al., 2014) or comparing C2/C3 substrates to obtain different nitriles (Bulánek et al., 2002), showed interesting results, but these dataset was here excluded because the pathway through acetamide implies a too different mechanism. The issue of the actual route to the nitrile (acetic acid or enamine-amine) was actually debated and the opposite experimental outcomes (Reddy and Manohar, 1993; S. J. Kulkarni et al., 1994) are likely due to the different metal loading of the supports. The ethanol ammoxidation pathway can be interpreted through the enamine path, which accounts also for propane ammoxidation data (Hinz and Andersson, 1999). On this basis, we discarded all the data regarding C3 and superior substrates and the reaction for CO conversion (Hummel et al., 1993).

The main goal of this analysis, in fact, was not the full and detailed unraveling of the mechanism details, but a rationalization of kinetic data into a chemical and algebraic formulation, as simple and robust as possible, in view of its implementation for reactors design.
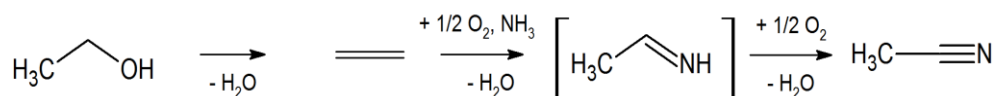
2.2 Reactions network

The overall reaction network is depicted in Figure 1.

The main reaction path for ethanol ammoxidation involves an enamine intermediate:
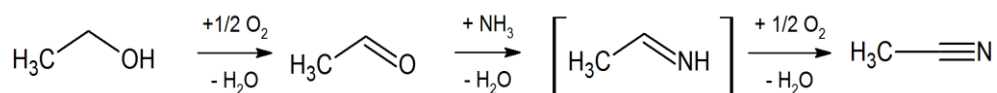
Acidic catalysts can also trigger the dehydration to ethylene, which in turn can contribute to the acetonitrile production:

$$H_3C\text{-}OH \xrightarrow{-H_2O} \text{=} \xrightarrow[\text{-H}_2O]{+1/2\ O_2,\ NH_3} \left[H_3C\text{-}NH \right] \xrightarrow[\text{-H}_2O]{+1/2\ O_2} H_3C\text{-}\equiv N$$

This side route was considered only for the more acidic catalyst of those involved in this work (VPP (Folco, 2013)) because the others (VO_x/TiO_2) showed a much lower ethylene yield. Other authors (Hamill et al., 2015) obtained pretty similar outcomes, using TiO_2.

Other reported side-routes, such as the condensation of ethylene and ethanol into diethyl-ether (Hu et al., 2012) on acidic supports, was not considered as the desorbed products are missing in the reviewed data collection.

The relevant difference between the VPP catalyst and the others, in this regard, may reduce to the ethylene desorption step. Non negligible ethylene yields were reported on other acidic supports (Feng et al., 2011) at any ammonia/ethanol ratio, confirming also that the ammoxidation step is rate-determining for the acetaldehyde conversion but might be kinetically irrelevant towards ethylene. The presence of active metals is likely the more important method to have a low ethylene selectivity, together with relatively low temperatures (Feng et al., 2011; Folco et al., 2017; Hu et al., 2012). It is yet possible that the metal doping enhances the C-C breaking paths, leading to low HCN and ethylene fractions, negligible heavy compounds in the spectra and consistent CO_x production (Rojas et al., 2013). However, as long as the conversion into nitriles of several substrates can take place on zeolites (Bulánek et al., 2002; Huang et al., 2015; Mies et al., 2007; Rhimi et al., 2016), aluminas (Zhang et al., 2011) or other V-containing oxydes (Rojas et al., 2012), the ethanol – ethylene – acetonitrile path ought to be included in any case.

Another issue is represented by the combustion reactions. In principle, the partial pressures of ammonia, ethanol and oxygen employed are within the flammability region at the tested temperatures

(Coronado et al., 2012; Gutiérrez Velásquez et al., 2017; Harris and Macdermott, 1964; Mendiburu et al., 2017), so that a mixed Langmuir-Hinshelwood (LH) and Eley-Rideal (ER) kinetic model ought to be adopted. This figure, however, becomes more complex as the water vapor partial pressure builds up, changing the combustion curves of both fuels. On the other hand, it cannot be excluded that also oxygen participates to any reaction as an adsorbed species (especially on the zirconia support). For these reasons, a simple LH adsorption term was considered a sufficiently good approximation to model oxygen role and the combustion reactions were treated as catalytic ones. Also the suggestions for the possible gas-phase formation of the enamine itself (Oishi et al., 2010) were neglected at this stage of the work.

The condensation reactions leading to high-boiling components were considered having acetaldehyde as main precursor. This (Feng et al., 2011) reflects also two qualitative experimental outcomes: i) heavy molecules appear only on the more acidic catalyst (VPP) when acetaldehyde fractions are zero, and ii) among them, long-chain nitriles were not prevalent. The data indicate that acetonitrile acts as a reactant more towards the production of HCN than towards longer molecules. The choice of having HCN itself as a byproduct of acetonitrile, rather than directly of acetaldehyde or ethylene (Bharadwaj and Schmidt, 1996), comes after the review of many data entries at low contact times, showing an increase of the acid in front of a decrease of the nitrile at negligible aldehyde quantities. Other intermediates can give condensation (Hamill et al., 2015; Zhang et al., 2009), but not in the oxidative conditions considered in this work. The used data, moreover, never account for the presence of acetic acid, which made it possible to neglect the issue of the parallel ethanol full oxidation and the nitrile hydrolysis (Corker et al., 2013).

2.3 Experimental data treatment

The collection of experimental data was already partially published (Folco, 2013; Folco et al., 2017). The whole data-set is reported in the supplementary information, from Table S1 to S5. All the details

on the catalyst preparation and the laboratory reactor set-up can be found in the cited works. The analysis of the products was always performed by gas-chromatography in the gas-phase, after calibration with pure standards.

The molar flow of the reactants at the reaction conditions was extrapolated, for this work, using the ideal gas equation, knowing the original volumetric flow of the mixture. The tests at different contact times were originally performed letting vary the volumetric flowrate while keeping the catalyst load fixed. Anyway, in order to calculate directly reaction rates as a function of the catalyst load, the data were rearranged according to equality (3), which holds for the steady state an ideal reacting mixture passing over a homogenous, isothermal catalytic bed where radial and axial diffusion phenomena are negligible (these conditions are usually achieved in standard laboratory practice once the catalyst and the other packing materials are properly ground (Afandizadeh and Foumeny, 2001; Kagyrmanova et al., 2007)).

The huge body of data was divided into five groups according to the different catalysts employed. Within these groups, each stabilized reaction condition is considered as one relevant data entry, regardless of how many GC spectra were originally taken before observing a steady behavior of the reactor. Each data entry is considered as a database object with four main categories of attributes:

1) general conditions (pressure, inlet molar flow, reaction temperature, flowmeter temperature, reference temperature for the Arrhenius prefactor – see also equation (1), catalytic load);

2) starting chemical conditions (*i.e.* the species molar fraction at the reactor inlet);

3) final chemical conditions (species outlet fractions);

4) statistical weights (used to exclude outliers from the error calculation).

The first two groups of values are sequentially loaded as inputs for the numerical integration of the steady-state continuity equation (in the form of equation (3)), then the results were compared automatically with the group-3 values, and checked against the weight to associate an overall calculation error to each data entry. The calculation output is then a duplicate of each database entry,

with the addition of a fifth group of numbers consisting of the predicted (calculated) final chemical conditions.

3. Results and Discussion

3.1 Data analysis

A family of data based on the same catalytic material shares a common group of associated values that describe quantitatively the reactions network, *i.e.* the kinetic parameters. Selecting four independent variables to represent the reaction conditions (temperature, catalyst load, oxygen and ethanol inlet concentrations), then for each catalysts data entry the dependent variables (the chemicals outlet fractions) are a non-linear function of the inputs, with the kinetic constants as parameters. The goal of the data analysis was at first to trace (or quantify) the correlations between the independent and the dependent variables, and then to evaluate the values of the kinetic parameters that provide the best description and reproduction of this correlation. The following procedure was followed:

a) a set of data with variable catalyst load, *i.e.* different contact time, and the other three variables fixed was selected and used to produce a first guess of the reaction constants. Using the following kinetic formulation (1), and choosing the reference temperature equal to those of the reaction data, the activation energy has no role on this first fit;

$$\ln(k) = \ln(k_0) - \frac{E_a}{R}\left(\frac{1}{T} - \frac{1}{T_0}\right) \tag{1}$$

b) if a similar set of data was available for different reactant concentrations (but at the same temperature), the reaction constants were furtherly adjusted to achieve a better and more comprehensive description of all the points;

c) when a group of data with variable contact time was not available, the kinetic pre-factors were adjusted aiming at a good reproduction of the ethanol decomposition, exploiting the fact that,

using a reference temperature within the range of that data set, the effect of the activation

energy on the reaction rate is reduced (see also equation (1));

d) data sets with different temperatures (but other parameters constants) were picked up to adjust

the activation energies, keeping the kinetic constant pre-factors unchanged;

e) as much data entries as possible were finally considered at the same time, trying to vary the

pre-factors and activation energies in order to achieve the best data interpolation with a unique

ensemble of parameters for each catalyst;

f) for the VPP catalyst only, it was employed an automatic simplex algorithm optimization, as

implemented in the Matlab 2017b release, because in this case there were enough points to

have a meaningful least-squares minimization letting vary as much as 10-15 parameters at a

time – the Objective Function (OF) is described in equation (2):

$$OF = \sum_i \sum_j w_{ij} \left[2 \frac{y_{ij,calc} - y_{ij,exp}}{y_{ij,calc} + y_{ij,exp}} \right]^2 \tag{2}$$

.

for the *j-th* species molar fraction at the reactor outlet in the *i-th* experiment – *w* represents a

weight. The optimisation of the kinetic parameters has been carried out using specific weights

for the different species. For instance, the parameters have been forced to better reproduce the

experimental acetonitrile productivity, while other species (for instance the excess ones) were

assigned lower impact on the optimisation. The weights were also set according to the

reliability of the experiments, according to a preliminary sensitivity analysis. A workaround

prevented the obtainment of negative values of *k* during optimisation (formally allowed by

the simplex method) and we have not optimised at once all the kinetic parameters, to avoid

chemically unreliable solutions.

A summary of the reaction conditions tested for the different catalysts and their general outcome is

reported in Table 1.

The numerical integration of the reactor mass balance was performed according to equation (3):

$$\lambda \frac{\partial n}{\partial w} = \frac{\partial n}{\partial x} = \frac{r}{v} = r \frac{\partial \tau}{\partial x} \implies \Delta n = \int d\tau(r) = \int dw(r')$$

(3)

where n are moles, λ is the linear catalyst density, w the catalyst mass occupying a control volume, v the space velocity in m/s, and r, r' are the reaction rates in mol/s and in mol/kg_{cat} respectively – if the reactions are equimolar or the inert gases molar flow is large with respect to the mole consumption/production, the equation can be expressed in terms of molar fractions rather than of moles. The Runge-Kutta method was implemented in the Ordinary Differential Equation function of the Matworks Matlab r2018® software. The simplex algorithm used for the parameter optimization was similarly run under the 'Function MINimum SEARCH' tool of the same software, which was used also to produce the record of the calculation output. The Matlab version of the simplex algorithm does not handle automatically minimum and maximum bounds for the parameters to be optimized, so the objective function (2) was actually modified in order to introduce an upward bias whenever at least one parameter exceeded its assigned bounds.

The results of data regression are reported in Tables 2-6.

3.2 Models

A complete model should also include an ER mechanism, especially for combustion, but in general for all the oxygen-related steps: this is shown by the fact that the heuristic reactions exponents cannot fully reproduce the reaction rates at different O_2 and ethanol partial pressures and that data groups with different O_2 content cannot be reproduced at the same time with models relying on the same adsorption denominator term. The rigorous expression of the reactions used and the relative rates can be found in the Supplementary Information.

The strongly oxidizing environment causes the combustion of all the chemical species (except water, carbon dioxide and nitrogen), but since the overall carbon balance introduces a bound, at least one carbon-containing species was excluded from the possible fuels to avoid an algebraic redundancy. The choice of the intermediates undergoing combustion to CO_x is simplified by the fact that, starting from C2 rather than longer substrates, there is no need to discriminate by two consecutive C-C cleavages to identify the slowest one (Sanati et al., 1998).

Neglecting possible ER passages also allows to circumvent the problem of discriminating between oxidation alternatives such as (Creaser et al., 1999):

1) $CH_3CH_2OH^* + O_2 + * \rightarrow CH_3CH_2O^* + OH^* + O^*$

2) $CH_3CH_2OH + O^* + * \rightarrow CH_3CHO^* + OH^*$
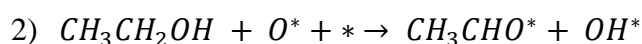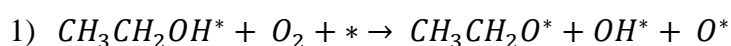
that depend crucially on the catalyst coverage characteristics (* represents a free active site, where X^* represents adsorbed X species).

The heavy compounds generated by acetaldehyde on the VPP included a variety of molecules, then a proper reaction network for their own generation could not be set up: to satisfy the mass balances, it was postulated a brute formula C_4H_7N following the suggestions by Folco et al. (Folco, 2013). This prevented the exact reproduction of the yet limited nitrogen increase, so ammonia combustion reaction could be tuned only in relation to ammonia data.

Most of the data entries, moreover, report a lump quantity for carbon monoxide and dioxide. Due to the fact that each species carries just half of the injected carbon but, with respect to the acetonitrile / HCN couple, the combustion of the monoxide into the dioxide is much faster and the latter can be generated without having the former as precursor, an extra rate determining step (*rds*) leading from CO to CO_2 was not added and every combustion was rather treated as potentially incomplete, yielding one mole of CO and one of CO_2 per two moles of carbon burned. When separated data for CO_2 and CO fractions were available (as for the VO_x/TiO_2 and VO_x/ZrO_2 catalysts (Folco, 2013)), the

stoichiometry of the combustion could be modulated and the transition CO → CO₂ implicitly considered (for simplicity, this is not reported in the passages below).
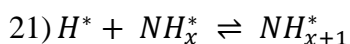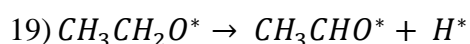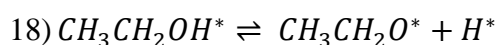
Partial pressures of water were not available, which reduced the experimental points against whom testing the kinetic constants and, moreover, precluded the use of oxygen and hydrogen balances in consistency checks. Carbon and nitrogen balances were themselves biased for every dataset containing an appreciable amount of condensate species (of unknown brute formula).

The derivation of the kinetic model according to a LH framework proceeds as reported below:

1) $CH_3CH_2OH + * \rightleftharpoons CH_3CH_2OH^*$

2) $O_2 + 2* \rightleftharpoons 2O^*$

3) $CH_3CH_2OH^* + O^* \rightleftharpoons CH_3CH_2O^* + OH^*$

4) $CH_3CH_2O^* + OH^* \rightarrow CH_3CHO^* + H_2O^*$

5) $H_2O^* \rightleftharpoons H_2O + *$

6) $NH_3 + * \rightleftharpoons NH_3^*$

7) $CH_3CHO^* + NH_3^* \rightleftharpoons CH_3CHNH^* + H_2O^*$

8) $CH_3CHNH^* + O^* \rightarrow CH_3CN^* + H_2O^*$

9) $NH_3^* + O^* + OH^* \rightarrow N^* + 2H_2O^*$

10) $N_2 + 2* \rightleftharpoons 2N^*$

11) $CH_3CN^* + 2O^* \rightleftharpoons CO^* + HCN^* + H_2O^*$

12) $2HCN^* + 4O^* \rightarrow CO^* + CO_2^* + H_2O^* + 2N^* + *$

13) $CH_3CN + * \rightleftharpoons CH_3CN^*$

14) $CO + * \rightleftharpoons CO^*$

15) $CO_2 + * \rightleftharpoons CO_2^*$

16) $HCN + * \rightleftharpoons HCN^*$

17) $CH_3CHO + * \rightleftharpoons CH_3CHO^*$

The stoichiometry and the kinetic formulation derived to describe the VPP catalyst are reported in the supporting material. The main ethanol-acetaldehyde-enamine-acetonitrile path was treated with two rate-determining steps only, because the enamine was never present in the reaction mixture while acetaldehyde was always detected, because of the pronounced kinetic effects in the strongly oxidizing environment and we considered the final oxidation 8) (rather than the ammonia attack 7) as rate-determining (Corker et al., 2013).

The dehydrogenation steps were not resolved in details, because the absence of hydrogen itself from the products, meaning that the direct path $H_2 + 2 * \rightleftharpoons 2H^*$ is forbidden, makes it impossible to asses the rate-determining step in a chain of the kind: $RH_n^* + O^* \rightleftharpoons RH_{n-1}^* + OH^* \rightleftharpoons RH_{n-2}^* + H_2O^*$, while the presence of both water and oxygen makes it hard to clarify whether the oxidizing agent is the O* or the OH* moiety. In summary, an oxidative dehydrogenation path is active on this point. For example, passages 3) and 4) may as well take place as:

18) $CH_3CH_2OH^* \rightleftharpoons CH_3CH_2O^* + H^*$

19) $CH_3CH_2O^* \rightarrow CH_3CHO^* + H^*$

20) $H^* + OH^* \rightleftharpoons H_2O^*$

21) $H^* + NH_x^* \rightleftharpoons NH_{x+1}^*$

This does not correspond to the strict application of the 'Mars van Krevelen' mechanism (MvK), nevertheless the basic OH* unity can be considered as an effective dehydrating agent when the acid-base properties of a material are as important as its redox ones (Védrine, 2002). Accordingly, also other authors dealing with V-containing oxides proposed for passage 20), relevant to water formation, a passage where hydrogen is not explicitly considered (Chen et al., 1999):

$OH^* + OH^* \rightleftharpoons H_2O + O^* + *$
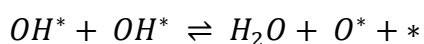
The same authors, however, report a preferential LH mechanism (rather than an ER step) for the H abstraction from the reactants molecules operated by absorbed oxygen, as here postulated, though their analysis is referred to saturated, rather than already partially oxidized substrates.

As a matter of fact, though all the passages relevant to the stoichiometry were considered non-reversible, this issue led to introduce a negative reaction pseudo-order for water in the acetonitrile formation reaction for several catalysts, since the rate-damping effect due to the increase of the Langmuir adsorption term (see also equation 90 in the Supplementary Information) was not sufficient to achieve a good data interpolation. This means a reaction order for water that derives from experimental data and not from the microkinetic steps. Notice that also the ammonia decomposition may take place only via O* or OH* mediated steps (*i.e.* as a combustion), then its conversion into acetonitrile had to be simply based on the NH_3* species. A -OH displacement from catalytic sites, moreover, is probably involved in the very adsorption step of ammonia (Bredow et al., 2004). The same reasoning holds for ethylene ammoxidation. Passage 11) likely follows the route:

22) $CH_3CN^* + OH^* \rightleftharpoons CH_2CN^* + H_2O^*$

23) $CH_2CN^* + OH^* \rightleftharpoons CHCN^* + H_2O^*$

24) $CHCN^* + OH^* + O^* \rightarrow CO^* + CN^* + H_2O^*$

25) $CN^* + OH^* \rightleftharpoons HCN^* + O^*$
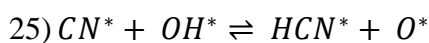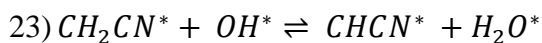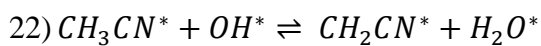
The above passages leading to HCN, though affected by the same uncertainty, are anyway based on the C-C break as rate-determining step. Step 12), moreover, shows the superposition of the combustion of a carbon-containing species and of ammonia and can be taken as a model for the other combustions: though their details are not resolved, we point out that the catalyst coverage with any carbon- or nitrogen- intermediate is likely to be much less important than its coverage by O*, OH* and NH* species, which in turn are in equilibrium with oxygen, water and ammonia. Then an adsorption term accounting for these latter three species gives a coherent figure of the process.

All these considerations should also be applied to the CO_2 production, coming from CO oxidation via an irreversible step (if the Bouduard reaction is neglected), but this issue could not be considered due to the fact that CO and CO_2 are not resolved in most of the reviewed data.

For the ethylene-acetonitrile route, the first rate-determining step is ethanol dehydration. In this case the oxidizing species could also be the ethoxide or ethanol itself (Alexopoulos et al., 2016; Fang et al., 2015; Kim et al., 2015), but the interpolated pseudo-order for the reaction is unitary due to the exclusion of water from the rate expression and possibly from the exclusion of ethylene end the other intermediates from the denominator. Or, more simply, as if the actually relevant step is either 28) or 29) below, that are kinetically equivalent except for a different dependence on the surface concentration of free sites:

26) $CH_3CH_2OH^* + O^* \rightleftharpoons CH_3CH_2O^* + OH^*$

27) $CH_3CH_2O^* + CH_3CH_2O^* + 2* \rightarrow 2\,CH_2CH_2{}^* + H_2O^* + O^*$

28) $CH_3CH_2OH^* + OH^* + * \rightarrow CH_2CH_2{}^* + H_2O^* + OH^*$

29) $CH_3CH_2OH^* + * \rightarrow CH_2CH_2{}^* + H_2O^*$

30) $CH_2CH_2{}^* + NH_3^* + O^* \rightleftharpoons CH_3CHNH^* + H_2O^* + *$

31) $CH_2CH_2 + * \rightleftharpoons CH_2CH_2{}^*$
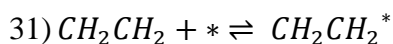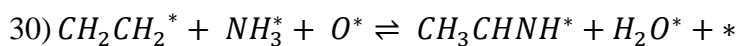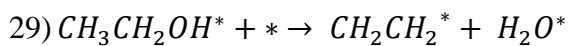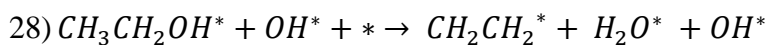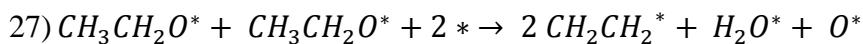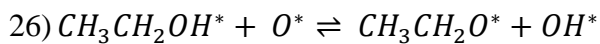
The ethylene combustion had to be made dependent, from a kinetic point of view, from ethanol concentration because of two reasons: i) the ethylene fraction actually stabilizes at high catalyst loads, while the CO_x concentration rises linearly as ethanol completes its decrease and ii) considering the overall carbon balance, this reaction is equivalent to the direct ethanol combustion.

Actually, the steady increase of carbon monoxide and dioxide (with respect to both temperature and catalyst load) makes it necessary the addition of multiple combustion passages.

The kinetic models derived from the above described passages are reported, for each catalyst, through equations 5-n. During the analysis, it was found that different reaction orders and, in some cases, also

the modification of the combustion stoichiometries could help to interpolate better some data subsets belonging to the same catalyst: anyway, we preferred to achieve a unified kinetic description for each of them (though mechanism shifts are still possible, on the same material, at different temperatures and sites covering), even if it meant a slightly greater cumulative error, to reach a compromise between the good reproduction of the experimental outcomes and the general validity of the model.

None of the rate-determining steps was considered as reversible, meaning that no reaction belonging to the stoichiometric balance was limited by the thermodynamic conditions. This approach was chosen on the basis of the experimental data themselves, characterized by an oxidative environment and by a constantly decreasing trend for ammonia at any catalyst load and temperature. Nevertheless, a thermodynamic analysis for the possible reaction mixture composition was performed calculating the gas-phase fugacities via the Redlich-Kwong-Soave Equation of State, and then minimizing the total Gibbs energy as a function of the molar concentrations for every compound appearing in the datasets plus acetic acid. The fugacity calculation and the energy minimization were both performed resorting to the AVP32 Databank and the 'Gibbs Reactor' tool included in the Aspen Plus® v. 9.0 software by Aspen Technology Inc.™.

3.3. Data interpolation

The screening of the thermodynamic conditions for the reaction products is reported synthetically from Figure 2: Theoretical reactions advancement as relative mole increment for a mixture composed originally of (mol/mol): ethanol (0.045), water (0.05), ammonia (0.13), oxygen (0.13), nitrogen (0.69).for a couple of representative tests. The stability of CO_2 and H_2O drives the mixture towards an overall increase of the total moles, but the relatively high fraction and stability of nitrogen damp this effect, reducing the effect of pressure. Moreover, the consumption of oxygen and ammonia via the combustions accounted for a global positive effect of the pressure towards the ethanol conversion, so that the global mole increment depends crucially on the temperature and loosely on the pressure.

This mixed behavior is recognizable in the trends exhibited by NH_3, N_2 and ethylene: in principle at least this latter ought to be treated with a reversible reaction for the VPP catalyst, but the addition of its combustion and ammoxidation in the reactions network, together with the inclusion of water in the denominators, act likely in the same sense. The acetonitrile fraction in the products seems to benefit from higher pressures, nevertheless it has to be pointed out that its reaction pathway is made up of equimolar passages and, moreover, all the catalysts show yields exceedingly larger than what would be expected on a thermodynamic ground. This is another confirmation that the enamine conversion is effectively pushed forward by oxygen, while scarcely hindered by water (the negative reaction term adopted for water in several rate equations – see supporting material – is likely the representation of an 'extra adsorption effect') and of the little importance of gas-phase combustions as well.

Also the equilibrium: $CH_3CN + 2H_2O \rightleftarrows CH_3COOH + NH_3$, otherwise considered an effective route to acetonitrile on acidic catalysts (Tollefson et al., 1970), is actually suppressed in the reaction conditions studied.

The overall performance of the VPP catalyst is synthetically visualized in Figure 6 and the outcome of the quantitative analysis performed on the data, *i.e.* the kinetic pre-factors and activation energies, are reported in Table 2. The sensitivity of the sum of square residues (SSR) respect to the kinetic pre-factors k_0 was calculated altering in turn each constant of $\pm5\%$ of its base value while the others were kept fixed.

When the automatic optimization was performed, several data entries received a null weight according to the following criteria:

   a) the first, manual adjustment of the parameters gave an unacceptable error on the ethanol final fraction (this quantity has also the meaning of a carbon balance – these points are marked in red in the reported figures);

b) for ten data points, the extrapolation of the total molar flow was arbitrary, since the volumetric reactants flowrate could not be retrieved;

c) a single group of reaction tests with enhanced oxygen content was not satisfactorily described by the surmised reaction orders: this may imply a limit of the model, but also a possible shift in the reaction mechanism or the development of different rate-determining steps.

The adsorption term was kept as simple as possible, assuming that the reaction products desorb rapidly except water and the enamine intermediate is in negligible quantity. Oxygen was kept outside the Langmuir term, in this analysis, because it likely reacts also via the ER mechanism. It has to be pointed out that small changes in the adsorption exponents and constants had little influence on the model behavior, while large changes had actually the effect of a rescaling factor. The assigned values are then somehow arbitrary, nevertheless the following heuristic observation could be made (at least for the TiO_2 and ZrO_2-supported catalysts):

- the adsorption constants helped to achieve a better fit of the data taken at different concentration of reactants;

- the higher-importance term is the one depending on ethanol, either because its conversion actually takes place on the catalyst surface, or because ammonia and oxygen are always fed in excess;

- for the $VO_x(2\%)/TiO_2$ catalyst, the adopted oxygen adsorption constant was relatively high, probably because this material is more sensitive to effects of competitive adsorption between the reactants.

This aspect of the model is the one that deserves more development in future works (Sanati et al., 1998).

The overall dependence of the acetonitrile selectivity on the ethanol inlet fraction, on the catalyst load and reaction temperature was also evaluated via a correlation analysis for the VPP dataset, the richest

one. In this case, the data were first normalized and then two linear correlations were tried as reported in the following equations:

$$\begin{cases} \theta = \dfrac{T}{440\ ^{\circ}C} - 1 \\ \sigma = \dfrac{S}{50\ \%} - 1 \end{cases} \quad \begin{cases} \upsilon = \dfrac{y_{etoh,in}}{0.045\ mol/mol} - 1 \\ \gamma = \dfrac{g}{1333\ mg} - 1 \end{cases} \quad \begin{cases} \sigma = a_1 + b_1 \upsilon \\ \sigma = a_2 + b_2 \theta + c_2 \gamma \end{cases} \quad (4)$$

where s stands for the percent acetonitrile selectivity and g for the catalyst load.

The general Design of Experiments (DOE) (Oehlert, 2003) approach was followed. The regression coefficients t-tests are reported in Table 7, together with the F-tests on the fraction of the total error accounted by the model. Though the data were quite dispersed, the statistical analysis indicates a good degree of dependence between the parameters, especially for the second correlation. Figure 77 helps to appreciate that the resolution of the temperature and catalyst contributions can actually account too a good qualitative level for the variation of the acetonitrile selectivity. The test statistic values are in line with those obtained via a conceptually similar analysis for oxidative reactions on Vanadium oxides (Fattahi et al., 2014).

It is worth noticing that the higher selectivity of this catalyst towards ethylene (Figure 8 and 9) could be apparent, because it was due to the faster combustion of acetonitrile into HCN (Figure) with respect to the slower ammoxidation of ethylene itself. Also the fact that the yields of acetonitrile, HCN and ethylene are positively correlated stems from the fact that almost all the available data refers to a condition of incomplete ethanol conversion, and then the parallel production of these products dominates the reactions network, before the species can convert into each other once ethanol is completely consumed.

Figure 10 shows clearly that, at the same temperature (440 °C), the molar fractions, as a function of the reaction coordinate, are satisfactorily interpolated until ethanol was still present, while the model

is actually "delayed" in reproducing conditions of fast and complete ethanol conversion. Nevertheless, since this latter situation involves only a small subgroup of available data, the model was necessarily trained to fit better data of the former kind. Moreover, the data group showing $\chi=100\%$ contains several outliers (*e.g.* the ethylene and HCN fractions at the second catalyst load value and, likely, the acetonitrile value at the fourth x coordinate) and is characterized by a lower ethanol inlet fraction. This could be due to the fact that, in some cases, the ethanol adsorption on the catalyst can have a slowing effect due to sites occupation, as important as the accelerating role due to the increased reactant availability. More likely, an apparent reaction order lower than one (which implies a faster development of the reaction kinetic also as the precursor is consumed) hints to the early onset of all the combustions, possibly via mixed EL and LH paths, as also hinted by the final decrease of the HCN itself. This last point seems also partially confirmed by other analysis carried out within the already cited workgroup (Tanganelli, 2011), showing an appreciably enhanced CO_x productivity associated to low ethanol inlet fractions.

With these limitations, the overall model performance (summarized with the parity plots in Figure 11 - Figure 12 - Figure 13) can still be considered sufficient for general purposes such as the prediction of the products fractions at the reactor outlet (the highest error on acetonitrile is at low fractions, *i.e.* at the kinetic onset), the calculation of the overall heat balance and a reasonable quantification of the byproducts.

The VPP catalyst itself, with respect to the others, showed a high selectivity to ethylene, a too high activity towards undesired poly-condensations and the opening of acetonitrile consumption paths in the same conditions that enhanced its productivity. The apparently "ceiled" acetonitrile selectivity for this material, accompanied by increased ethylene yields, may also be explained in terms of the tendency of the alkene to be lost into byproducts (*i.e.* CO_x) when its partial pressure is not high enough to increase the importance of its own parallel ammoxidation (Costine and Hodnett, 2005), though the

analysis of these authors comes from a reaction environment where the aldehyde intermediate is not present and can be here used just for a qualitative review of the VPP data.

Of the other catalysts, only the VO_x/ZrO_2 ensemble is large enough to be treated with a correlation analysis as the one discussed above:

$$\begin{cases} \theta = \dfrac{T}{440\ °C} - 1 \\ \sigma' = \dfrac{s}{100\ \%} - 1 \\ c = \dfrac{y_{CO}}{0.0406} - 1 \end{cases} \begin{cases} \sigma' = a_1 + b_1\theta \\ \quad \theta < 400\ °C \\ \sigma' = a_2 + b_2 c \\ \quad \theta \geq 400\ °C \end{cases} \tag{5}$$

(where *s* stands for the percent acetonitrile selectivity).

In this case, the direct correlation between the normalized temperature and the acetonitrile selectivity is good up to an effective temperature (Figure **77** 7 and Table 8**:** Statistical description of the acetonitrile selectivity as a function of normalized temperature (up to 400 °C) or correlated to CO yield (for higher temperatures) on the VO_x/ZrO_2 catalyst.), after which the selectivity does not worsen, but becomes loosely dependent on the controlled reaction conditions. An inverse correlation is shown, at high temperatures, between the acetonitrile selectivity and the CO yield. Bearing in mind that these data are all characterized by null oxygen outlets, it can be surmised that the acetonitrile yield, in these conditions, fluctuates according to the higher or lower importance gained by the parasitic and uncontrolled combustions.

The high conversions and the lower ethylene selectivity obtained with the less-acidic TiO_2 supports are qualitatively in line with the results of other oxidative-dehydrogenation reactions for C3 substrates on similar V-based materials (Khodakov et al., 1999). Also the Zirconia-based catalyst behaves generally like the 'titania dataset'. The quantitative description given for these materials is generally as good as that of the acid catalyst, though their working temperature range is roughly 80 °C down-shifted (Figure S14 to Figure S29).

The three calculation outliers for the HCN on the $VO_x(7\%)/TiO_2$(Folco, 2013) catalyst are for relatively high temperatures (two of them) or oxygen quantities. It cannot be excluded that,

calculating HCN as an acetonitrile byproduct and focusing on the correct interpolation of this latter, the resulting algebraic link cannot yield the same precision on both the observed quantities: at milder temperatures the absolute error is reduced either by the lower reaction rate, or by the more robust statistic available. Other three outliers are observed for the acetonitrile production on the $VO_x(2\%)/TiO_2$ at high temperature, because in this case the parameters were optimized focusing on the low-temperature runs, that show the higher acetonitrile selectivity.

The mismatch in the combustion products (CO and CO_2) observed (Figure S29, Supplementary Information) as a kind of "horizontally shifted clouds" depends probably on the higher importance given to the correct reproduction of ethanol conversion, anyway the results here presented are not qualitatively worse than similar predictions for Oxidative DeHydrogenation (ODH) reactions on VO_x/TiO_2 (Grabowski, 2004). Since the error is greater for the data entries at high oxygen concentration, it is also possible that these conditions enhance the ethanol combustion beyond the adopted reaction order, or that a single adsorption term cannot represent all the parallel reaction paths, as would be the case if different kind of active sites were involved.

Anyway, the good results achieved for the TiO_2-based materials, whose datasets comprise reactions at many different temperatures but less variable contact times, confirms the general reliability of the model, since in this case the optimization had to be shifted towards the activation energies. The least accurate values of the parameters are those for the Cs-doped catalyst (Folco, 2013), because the experiments on this material are relative to a single contact time and just one combination of reagents fractions: this made it difficult to adjust the Ahrrenius pre-factors and the adsorption term and to check the reaction orders. At this regard, we point out that the followed calculation procedure, which stated to start any new interpolation from the same first-guess values, fixing the activation energies at a chosen reference temperature, helped much in keeping the parameters values in line with each other and give a coherent figure of the overall experimental work of Folco et al. (Folco, 2013). In practical terms, it is expected that catalysts of similar densities, loaded in beds of equal lengths and

exposed to the same volumetric flows are described by general kinetic parameters whose difference reflects the different selectivity. Different results may be expected if the reaction rates were normalized to the active surfaces, or derived by the micro-kinetic reaction steps treated via the Eyring model.

4. Conclusions

A first statistical screening of the reaction mixtures at the reactor outlet helped to identify the reaction temperature as the leading parameter determining acetonitrile selectivity for a given contact time. The ethanol partial pressure plays an appreciable role, which is, nonetheless, less easily quantified due to the mixed effect of the parasite reactions and active sites occupation phenomena.

A thermodynamic analysis helped to appreciate the capability of the catalysts under study to promote the acetonitrile production with respect to the ammonia combustion and to identify ethylene as the quantitatively more important byproduct. The non-negligible ethylene production on the VPP catalyst is due essentially to its acidity, this material needs also reaction temperatures higher than those of all the others. All catalysts yielded HCN as a minor byproduct, yet in quantities larger than its equilibrium ones, which let surmise its dependence on acetonitrile productivity itself and on the reaction temperatures adopted. The best catalytic formulation seems to be the V/ZrO_2, that grants full conversion and the least byproducts yield.

Basing on known oxidative mechanisms, a simplified series of steps was traced and used to derive one LH kinetic model for each catalyst. While some variation of the reaction orders was allowed, each data group (containing no less than 100 usable experimental molar fractions) were interpolated with a maximum of 20 adjustable parameter. Most of these values were tuned on the basis of our knowledge of the chemical behavior of the system and on the experimental conditions under which

the data were measured, whereas with a dataset of more than 300 experimental points we used a non-linear optimization for a maximum of 10 parameters at a time.

The numerical model describes with good accuracy the ethanol-ammonia-acetonitrile path, while the less precise results on the byproducts, on the acetaldehyde intermediate and on the oxygen reaction order reflect the complex nature of all the possible parasite reactions. Robust estimations are given for the conversion of ethanol and ammonia, together with the yields of acetonitrile and ethylene. Also the temperature effect in shifting the product distribution was correctly accounted, though at the cost of some interdependency between the activation energies and the kinetic pre-factors values. Qualitatively, the adoption of a LHHW model (instead of a mixed LHHW plus ER one) did not result in a limitation.

In summary, we achieved a comprehensive rationalization and a sound numerical description of ethanol ammoxidation with a moderate number of adjustable parameters, which are suitable to be used in further modeling, reactor design and scale-up studies.

Bibliography

ACS Office of Public Outreach, 1996. Sohio Acrylonitrile Process [WWW Document]. Am. Chem. Soc.

Afandizadeh, S., Foumeny, E.A., 2001. Design of packed bed reactors: Guides to catalyst shape, size, and loading selection. Appl. Therm. Eng. 21, 669–682. doi:10.1016/S1359-4311(00)00072-7

Alexopoulos, K., John, M., Borght, K. Van Der, Galvita, V., Reyniers, M., Marin, G.B., 2016. DFT-based microkinetic modeling of ethanol dehydration in H-ZSM-5. J. Catal. 339, 173–185. doi:10.1016/j.jcat.2016.04.020

Ayari, F., Mhamdi, M., Álvarez-Rodríguez, J., Guerrero Ruiz, A.R., Delahay, G., Ghorbel, A., 2012.

Ammoxidation of ethylene over low and over-exchanged Cr-ZSM-5 catalysts. Appl. Catal. A Gen. 415–416, 132–140. doi:10.1016/j.apcata.2011.12.021

Ballarini, N., Cavani, F., Cortelli, C., Ligi, S., Pierelli, F., Trifirò, F., Fumagalli, C., Mazzoni, G., Monti, T., 2006. VPO catalyst for n-butane oxidation to maleic anhydride: A goal achieved, or a still open challenge ? Top. Catal. 38, 147–156.

Belov, V. V., Markov, V.I., Sova, S.B., Golosman, E.Z., Nechugovskii, A.I., 2016. New composite catalysts for the synthesis of acetonitrile from ethanol and ammonia, prepared using calcium aluminates (Talyum). Russ. J. Appl. Chem. 89, 414–420. doi:10.1134/S1070427216030113

Bharadwaj, S.S., Schmidt, L.D., 1996. HCN Synthesis by Ammoxidation of Methane and Ethane on Platinum Monoliths. Ind. Eng. Chem. 35, 1524–1533. doi:10.1021/ie950520g

Bondareva, V.M., Andrushkevich, T. V, Aleshina, G.I., Plyasova, L.M., Dovlitova, L.S., Lapina, O.B., Khabibulin, D.F., Vlasov, A.A., 2006. Ammoxidation of Ethane on V-Mo-Nb Oxide Catalysts 87, 377–386.

Bredow, T., Homann, T., Jug, K., 2004. Adsorption of NO, NH3 and H2O on V2O5/TiO2 catalysts. Res. Chem. Intermed. 30, 65–73. doi:10.1163/156856704322798052

Bulánek, R., Novoveská, K., Wichterlová, B., 2002. Oxidative dehydrogenation and ammoxidation of ethane and propane over pentasil ring Co-zeolites. Appl. Catal. A Gen. 235, 181–191.

Card, R.J., Schmitt, J.L., 1981. Gas-phase synthesis of nitriles. J. Org. Chem. 46, 754–757. doi:10.1021/jo00317a020

Chen, K., Khodakov, A., Yang, J., Bell, A., Iglesia, E., 1999. Isotopic tracer and kinetic studies of oxidative dehydrogenation pathways on vanadium oxide catalysts. J. Catal. 333, 325–333.

Chieregato, A., Nieto, J.M.L., Cavani, F., 2015. Mixed-oxide catalysts with vanadium as the key element for gas-phase reactions. Coord. Chem. Rev. 301, 3–23.

Corker, E.C., Mentzel, U. V., Mielby, J., Riisager, A., Fehrmann, R., 2013. An alternative pathway for production of acetonitrile: ruthenium catalysed aerobic dehydrogenation of ethylamine. Green Chem. 15, 928–933. doi:10.1039/c3gc36513a

Coronado, C.J.R., Carvalho, J.A., Andrade, J.C., Cortez, E. V., Carvalho, F.S., Santos, J.C., Mendiburu, A.Z., 2012. Flammability limits: A review with emphasis on ethanol for aeronautical applications and description of the experimental procedure. J. Hazard. Mater. 241–242, 32–54. doi:10.1016/j.jhazmat.2012.09.035

Costine, A., Hodnett, B.K., 2005. Factors limiting selectivity in C3 and C4 amm(oxidation) reactions. Appl. Catal. A Gen. 290, 9–16. doi:10.1016/j.apcata.2005.05.032

Creaser, D., Andersson, B., Hudgins, R.R., Silveston, P.L., 1999. Transient Kinetic Analysis of the Oxidative Dehydrogenation of Propane. J. Catal. 182, 264–269. doi:10.1006

Evans, B., Hawkins, S., Schulz ed., G., 1991. Ullmann's Encyclopedia of Industrial Chemistry. VCH, Weinheim.

F. Cavani, Trifirò, F., 1997. The characterization of the surface properties of V-P-O-based catalysts by probe molecules. Appl. Catal. A Gen. 157, 195–221.

F.Cavani, E.Foresti, F.Trifirò, G.Busca, 1987. Nature of Active Species in the Ammoxidation of Toluene over V2O5/TiO2 Catalysts Prepared by Flash-Drying. J. Catal. 106.

Fang, Z., Wang, Y., Dixon, D.A., 2015. Computational Study of Ethanol Conversion on Al_8O_{12} as a Model for γ-Al_2O_3. J. Phys. Chem. C 119, 23413–23421. doi:10.1021/acs.jpcc.5b05887

Fattahi, M., Kazemeini, M., Khorasheh, F., Rashidi, A., 2014. Kinetic modeling of oxidative dehydrogenation of propane (ODHP) over a vanadium-graphene catalyst: Application of the DOE and ANN methodologies. J. Ind. Eng. Chem. 20, 2236–2247. doi:10.1016/j.jiec.2013.09.056

Feng, C., Zhang, Yuecheng, Zhang, Yining, Wen, Y., Zhao, J., 2011. Study on alumina-supported cobalt-nickel oxide catalyst for synthesis of acetonitrile from ethanol. Catal. Letters 141, 168–177. doi:10.1007/s10562-010-0468-z

Folco, F., 2013. Catalytic processes for the transformation of ethanol into acetonitrile [Dissertation Thesis]. Alma Mater Studiorum Università di Bologna.

Folco, F., Ochoa, J.V., Cavani, F., Ott, L., Janssen, M., 2017. Ethanol gas-phase ammoxidation to acetonitrile. Catal. Sci. Technol. 7, 200–212. doi:10.1039/C6CY01275B

Galanov, S.I., Sidorova, O.I., Gavrilenko, M.A., 2014. The Process of Acetonitrile Synthesis over γ-Al2O3 Promoted by Phosphoric Acid Catalysts. Procedia Chem. 10, 108–113. doi:10.1016/j.proche.2014.10.020

Grabowski, R., 2004. Kinetics of the oxidative dehydrogenation of propane on vanadia/titania catalysts, pure and doped with rubidium. Appl. Catal. A Gen. 270, 37–47. doi:10.1016/j.apcata.2004.04.021

Grasselli, R., 1981. Selective oxidation and ammoxidation of olefins by heterogeneous catalysis. J. Chem. Educ. 216–221. doi:10.1021/ed063p216

Grasselli, R.K., 1999. Advances and future trends in selective oxidation and ammoxidation catalysis. Catal. Today 49, 141–153. doi:10.1016/S0920-5861(98)00418-0

Gutiérrez Velásquez, E.I., Coronado, C.J.R., Quintero Cartagena, J.C., Carvalho, J.A., Mendiburu, A.Z., Andrade, J.C., Cortez, E. V., Santos, J.C., 2017. Prediction of flammability limits for ethanol-air blends by the Kriging regression model and response surfaces. Fuel 210, 410–424. doi:10.1016/j.fuel.2017.08.089

Hamill, C., Driss, H., Goguet, A., Burch, R., Petrov, L., Daous, M., Rooney, D., 2015. Mild temperature palladium-catalyzed ammoxidation of ethanol to acetonitrile. Appl. Catal. A Gen. 506, 261–267. doi:10.1016/j.apcata.2015.09.030

Harris, G.F.P., Macdermott, P.E., 1964. Flammability and explosibility of ammonia. Inst. Chem. Eng. Symp. Ser. No 49 29–37.

Hinz, A., Andersson, A., 1999. Propane ammoxidation on an Al-Sb-V-W-oxide catalyst. A mechanistic study using the TAP-2 reactor system. Chem. Eng. Sci. 54, 4407–4421. doi:10.1016/S0009-2509(99)00138-4

Hu, Y., Cao, J., Deng, J., Cui, B., Tan, M., Li, J., Zhang, H., 2012. Synthesis of acetonitrile from ethanol via reductive amination over Cu/γ-Al2O3. React. Kinet. Mech. Catal. 106, 127–139. doi:10.1007/s11144-011-0415-z

Huang, Y., Dong, X., Li, M., Yu, Y., Gao, J., Zheng, Y., Fitzgerald, G.B., de Joannis, J., Tang, Y., Wachs, I.E., Podkolzin, S.G., Huang, Y., Dong, X., Li, M., Zhang, M., Yu, Y., 2015. A density functional theory study on ethylene formation and conversion over P modified ZSM-5. Catal. Sci. Technol. 5, 1093–1105. doi:10.1039/C4CY01205D

Hummel, A.A., Badani, M.V., Hummel, K.E., Delgass, W.N., 1993. Acetonitrile synthesis from CO, H2 and NH3 over Iron catalyst. J. Catal. 139, 392–405.

Kagyrmanova, A.P., Zolotarskii, I.A., Smirnov, E.I., Vernikovskaya, N. V., 2007. Optimum dimensions of shaped steam reforming catalysts. Chem. Eng. J. 134, 228–234. doi:10.1016/j.cej.2007.03.035

Khodakov, A., Olthof, B., Bell, a T., Iglesia, E., 1999. Structure and catalytic properties of supported vanadium oxides: Support effects on oxidative dehydrogenation reactions. J. Catal. 181, 205–216. doi:10.1006/jcat.1998.2295

Kim, S., Robichaud, D.J., Beckham, G.T., Paton, R.S., Nimlos, M.R., 2015. Ethanol dehydration in HZSM-5 studied by density functional theory: Evidence for a concerted process. J. Phys. Chem. A 119, 3604–3614. doi:10.1021/jp513024z

Li, Y., Armor, J.N., 1998. A Reaction Pathway for the Ammoxidation of Ethane and Ethylene over

Co-ZSM-5 Catalyst. J. Catal. 176, 495–502.

Liao, B., Lei, Z., Xu, Z., Zhou, R., Duan, Z., 2001. New process for separating propylene and propane by extractive distillation with aqueous acetonitrile. Chem. Eng. J. 84, 581–586.

Malmusi, A., Ochoa, J.V., Tabanelli, T., Basile, F., Lucarelli, C., Agnoli, S., Francesco Carraro, G.G., Cavani, F., 2019. Ethanol aerobic and anaerobic oxidation with FeVO4 and V2O5 catalysts. Appl. Catal. A Gen. 570, 139–147.

Mannei, E., Ayari, F., Petitto, C., Asedegbega-Nieto, E., Guerrero-Ruiz, A.R., Delahay, G., Mhamdi, M., Ghorbel, A., 2017. Light hydrocarbons ammoxidation into acetonitrile over MoeZSM-5 catalysts: Effect of molybdenum precursor. Microporous Mesoporous Mater. 241, 246–257. doi:10.1016/j.micromeso.2016.12.021

Mcconvey, I.F., Woods, D., Lewis, M., Gan, Q., Nancarrow, P., 2012. The Importance of Acetonitrile in the Pharmaceutical Industry and Opportunities for its Recovery from Waste. Org. Process Res. Dev 16, 612–624.

Mendiburu, A.Z., de Carvalho, J.A., Coronado, C.R., Roberts, J.J., 2017. Flammability limits temperature dependence of pure compounds in air at atmospheric pressure. Energy 118, 414–424. doi:10.1016/j.energy.2016.12.036

Mies, M.J.M., Rebrov, E. V, Schiepers, C.J.B.U., Croon, M.H.J.M. De, Schouten, J.C., 2007. High-throughput screening of Co-BEA and Co-ZSM-5 coatings in the ammoxidation of ethylene to acetonitrile in a microstructured reactor. Chem. Eng. Sci. 62, 5097–5101. doi:10.1016/j.ces.2006.12.018

N. Ballarini, F. Cavani, A. Cericola, C. Cortelli, M. Ferrari, F. Trifirò, G. Capannelli, A. Comite, R. Catani, U.C., 2004. Supported vanadium oxide-based catalysts for the oxidehydrogenation of propane under cyclic conditions. Catal. Today 91, 99–104.

Oehlert, G.W., 2003. A First Course in Design and Analysis of Experiments. Am. Stat. 57, 66–67.

doi:10.1198/tas.2003.s210

Oishi, T., Yamaguchi, K., Mizuno, N., 2010. An efficient one-pot synthesis of nitriles from alcohols or aldehydes with NH3 catalyzed by a supported ruthenium hydroxide. Top. Catal. 53, 479–486. doi:10.1007/s11244-010-9475-y

P.Cavalli, F.Cavani, I.Manenti, F.T., 1987. Ammoxidation of Toluene to Benzonitrile on Vanadium-Titanium Oxides Catalysts Prepared by Precipitation. The Role of Catalyst Composition. Ind. Eng. Chemiistry Res. 26, 639–647.

P.Cavalli, F.Cavani, I.Manenti, M.El-Sawi, F.Trifirò, 1987. Kinetic and Mechanistic Analysis of Toluene Ammoxidation to Benzonitrile on Vanadium-Titanium Oxides. Ind. Eng. Chemiistry Res. 26, 804–810.

Pan, W., Jia, M., Lian, H., Shang, Y., Wu, T., Zhang, W., 2005. Selective Oxidation and Aammoxidation of Ethane Over Ion-Exchanged Co-MCM-49 Zeolites. React. Kinet. Catal. Lett. 86, 67–73.

Reddy, B.M., Manohar, B., 1993. One step synthesis of acetonitrile from ethanol via ammoxidation over Sb–V–P–O/Al 2 O 3 catalyst. J. Chem. Soc. Chem. Commun.

Rhimi, B., Mhamdi, M., Ghorbel, A., Kalevaru, V.N., Martin, A., Perez-cadenas, M., Guerrero-ruiz, A., 2016. Ammoxidation of ethylene to acetonitrile over vanadium and molybdenum supported zeolite catalysts prepared by solid-state ion exchange. "Journal Mol. Catal. A, Chem. 416, 127–139. doi:10.1016/j.molcata.2016.02.028

Rojas, E., Calatayud, M., Banares, M., Guerrero-Perez, O., 2012. Theoretical and Experimental Study of Light Hydrocarbon Ammoxidation and Oxidative Dehydrogenation on (110)-VSbO 4 Surfaces. J. Phys. Chem. C 116, 9132–9141. doi:10.1021/jp3017437

Rojas, E., Delgado, J.J., Guerrero-pérez, M.O., Banares, M., 2013. Performance of NiO and Ni–Nb–O active phases during the ethane ammoxidation into acetonitrile. Catal. Sci. Technol. 3173–

3182. doi:10.1039/c3cy00415e

Rojas, E., Guerrero-pérez, M.O., Bañares, M.A., 2009. Direct ammoxidation of ethane : An approach to tackle the worldwide shortage of acetonitrile. Catal. Commun. 10, 1555–1557. doi:10.1016/j.catcom.2009.04.016

S. J. Kulkarni, Rao, R.R., Subrahmanyam, M., Rao, A.V.R., 1994. Ammoxidation of ethanol to acetonitrile over molecular sieves. J. Chem. Soc. Chem. Commun. 3.

Sanati, M., Akbari, R., Masetti, S., Trifirò, F., 1998. Kinetic study on propane ammoxidation to acrylonitrile over V-Sb-O/TiO2(B). Catal. Today 42, 325–332. doi:10.1016/S0920-5861(98)00109-6

Schuster, B.G., Chinn, M.S., 2013. Consolidated Bioprocessing of Lignocellulosic Feedstocks for Ethanol Fuel Production. Bioenergy Resour. 416–435. doi:10.1007/s12155-012-9278-z

Sun, J., Wang, Y., 2014. Recent Advances in Catalytic Conversion of Ethanol to Chemicals. ACS Catal. 4, 1078–1090. doi:10.1080/01614940.2013.816610

Tanganelli, F., 2011. Studio dell'ammonossidazione in fase gas di etanolo ad acetonitrile [Degree Thesis]. Alma Mater Studiorum Università di Bologna.

Tollefson, E.L., Decker, R, M., Johnson, C.B., 1970. Development of a Process for Production of Acetonitrile from Acetic Acid and Ammonia. Can. J. Chem. Eng. 48, 219–223.

Tripodi, Antonio, Bahadori, E., Cespi, D., Passarini, F., Cavani, F., Tabanelli, T., Rossetti, I., 2018. Acetonitrile from Bioethanol Ammoxidation: Process Design from the Grass-Roots and Life Cycle Analysis. ACS Sustain. Chem. Eng. 6, 5441–5451. doi:10.1021/acssuschemeng.8b00215

Tripodi, A., Compagnoni, M., Ramis, G., Rossetti, I., 2017. Pressure-swing or extraction-distillation for the recovery of pure acetonitrile from ethanol ammoxidation process: A comparison of efficiency and cost. Chem. Eng. Res. Des. 127C, 92–102. doi:10.1016/j.cherd.2017.09.018

Tripodi, A., Manzini, D., Compagnoni, M., Ramis, G., Rossetti, I., 2018. Alternative integrated distillation strategies for the purification of acetonitrile from ethanol ammoxidation. J. Ind. Eng. Chem. 59, 35–49. doi:10.1016/j.jiec.2017.10.003

Védrine, J.C., 2002. The Role of Redox, Acid-Base and Collective Properties and of Crystalline State of Heterogeneous Catalysts in the Selective Oxidation of Hydrocarbons. Top. Catal. 21, 97–106. doi:10.1023/A:1020560200125

Zhang, D., Zhang, Y., Wen, Y., Hou, K., Zhao, J., 2011. Intrinsic kinetics for the synthesis of acetonitrile from ethanol and ammonia over Co-Ni/γ-Al2O3 catalyst. Chem. Eng. Res. Des. 89, 2147–2152. doi:10.1016/j.cherd.2011.01.029

Zhang, Yining, Zhang, Yuecheng, Feng, C., Qiu, C., Wen, Y., Zhao, J., 2009. Amination of ethanol to acetonitrile over Ni-doped Co/Al2O3 catalyst. Catal. Commun. 10, 1454–1458. doi:10.1016/j.catcom.2009.03.019

Tables and Figures

ID	catalyst	Ethanol conversion (%)	Selectivity to acetonitrile (%)	Selectivity to main byproduct (%)	Temperature range (°C)
1	Vanadium Pyro-Phosphate (VPP)	6 – 100	10 – 50	8 – 40	350 – 440
2	VO_x (2% wt) / TiO_2	10 – 100	5 – 58	5 – 48	250 – 440
3	VO_x (7% wt) / TiO_2	8 – 100	5 – 54	12 – 51	250 – 440
4	Cs-VO_x (7% wt) / TiO_2	6 – 100	19 – 48	8 – 40	250 – 440
5	VO_x / ZrO_2	2 – 100	0 – 75	7 – 27	250 – 440

Table 1: Overall reaction conditions and outcomes for the experimental data reviewed (Folco, 2013).

Reactions	1	2	3	4	5	6	7	8	9	10
$\ln k_0 \left[\frac{mol/s}{mg_{cat}} / \frac{1\,mol/s}{1\,mg}\right]$	-13.6	-7.82	-13.0	-4.61	-4.96	-10.0	-13.8	-10.4	-6.50	-10.4
$-E_a/R\ \left[\frac{1}{K}\right]$	-8910	-2010	-24700	-17400	-12000	-10200	-21400	-27100	-20100	-20100
$\frac{\Delta SSR}{\Delta k_0}$	14.4	2.94	29.9	0.0286	0.643	2.43	10.6	7.62	8.58	0.717

Denominator	Term 1	Term 2	Term 3	Term 4
$\ln K_{ads}$	2	3	3	-

Table 2: Kinetic constants for the proposed reaction network (equations detailed in the Supporting Information) on the VPP catalyst. The variations ΔSSR and Δk are expressed as relative values.

Reactions	1	2	3	4	5	6	7	8
$\ln k_0 \left[\frac{mol/s}{mg_{cat}} / \frac{1\,mol/s}{1\,mg}\right]$	-13.1	-9.32	-19.6	-10.8	-1.15	-8.52	-9.21	-15.4
$-E_a/R\ \left[\frac{1}{K}\right]$	-15600	-17400	-18000	-16800	-14400	-14400	-16800	-14400
$\frac{\Delta SSR}{\Delta k_0}$	15.5	0.814	0.577	2.36	0.00236	3.15	0.282	0.146

Denominator	Term 1	Term 2	Term 3	Term 4
$\ln K_{ads}$	2.5	-2	2	3.5

Table 3: Kinetic constants for reaction network (equations) on the $VO_x(2\%)/TiO_2$ catalyst.

Reactions	1	2	3	4	5	6	7	8
$\ln k_0 \left[\frac{mol/s}{mg_{cat}} / \frac{1\,mol/s}{1\,mg}\right]$	-11.5	-9.43	-16.6	-10.1	-6.91	-8.52	-8.52	-15.4
$-E_a/R \left[\frac{1}{K}\right]$	-14400	-17400	-18000	-16800	-9620	-14400	-16800	-14400
$\frac{\Delta SSR}{\Delta k_0}$	10.2	2.61	2.15	2.69	0.996	3.15	1.16	0.0932

Denominator	Term 1	Term 2	Term 3	Term 4
$\ln K_{ads}$	3	-2	3	-

Table 4: Kinetic constants for reaction network (equations) on the $VO_x(7\%)/TiO_2$ catalyst.

Reactions	1	2	3	4	5	6	7	8
$\ln k_0 \left[\frac{mol/s}{mg_{cat}} / \frac{1\,mol/s}{1\,mg}\right]$	-14.7	-12.1	-20.0	-14.2	-11.6	-13.8	-13.4	-1.88
$-E_a/R \left[\frac{1}{K}\right]$	-9620	-15000	-13200	-16800	-12000	-12000	-16800	-14400
$\frac{\Delta SSR}{\Delta k_0}$	9.21	1.86	0.170	1.40	1.01	2.89	0.306	0.00496

Denominator	Term 1	Term 2	Term 3	Term 4
$\ln K_{ads}$	-2	-2	-2	-

Table 5: Kinetic constants for reaction network (equations) on the $Cs-VO_x(7\%)/TiO_2$ catalyst.

Reactions	1	2	3	4	5	6	7	8
$\ln k_0 \left[\frac{mol/s}{mg_{cat}} / \frac{1\,mol/s}{1\,mg}\right]$	-10.8	-9.32	-16.5	-10.8	-7.13	-13.8	-7.82	-13.1
$-E_a/R \left[\frac{1}{K}\right]$	-18000	-12400	-21700	-12600	-12000	-15000	-18600	-14400
$\frac{\Delta SSR}{\Delta k_0}$	59.2	18.6	12.9	18.1	8.02	0.014	1.53	2.06

Denominator	Term 1	Term 2	Term 3	Term 4
$\ln K_{ads}$	3	-2	2	-2

Table 6: Kinetic constants for reaction network (equations) on the VO_x/ZrO_2 catalyst.

Parameter	Role	Value	Error	t-rejection	F-value
b_1	Ethanol effect	-0.156	0.0533	< 1 %	8.60
b_2	Temperature	-1.29	0.396	< 1 %	9.49
c_2	Catalyst load	0.155	0.0815	6.5 %	

Table 7: Statistical description of the acetonitrile selectivity as a function of ethanol partial pressure alone, or contact time and reaction temperature for the VPP reactions. The error is given as $\sigma/\sqrt{n}$ where σ is the standard deviation. The t-rejection value is the probability of rejecting a true null hypothesis (uncorrelation).

Parameter	Role	Value	Error	t-rejection	F-value
b_1	Temperature	2.64	0.22	< 1 %	144
b_2	CO fraction	-0.254	0.0513	< 1 %	24

Table 8: Statistical description of the acetonitrile selectivity as a function of normalized temperature (up to 400 °C) or correlated to CO yield (for higher temperatures) on the VO_x/ZrO_2 catalyst.
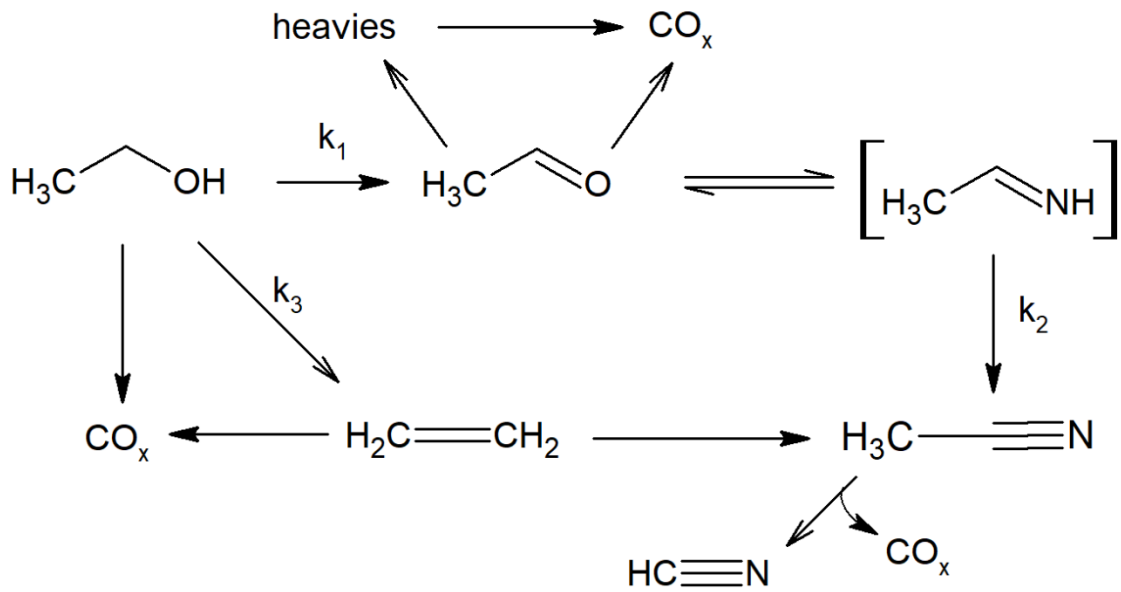
Figure 1: Main reactions for ethanol ammoxidation on acidic catalysts. See (Hamill et al., 2015) for a different account of the parasite condensation reactions.
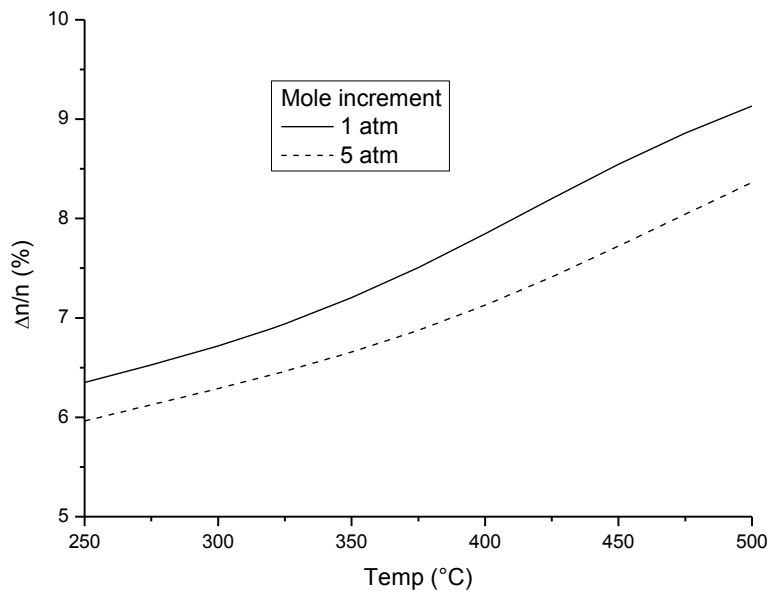
Figure 2: Theoretical reactions advancement as relative mole increment for a mixture composed originally of (mol/mol): ethanol (0.045), water (0.05), ammonia (0.13), oxygen (0.13), nitrogen (0.69).
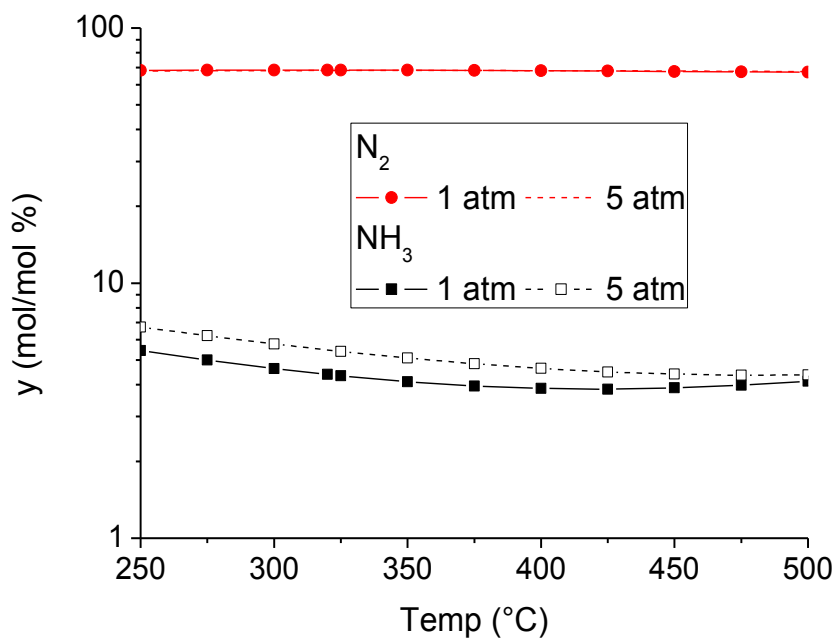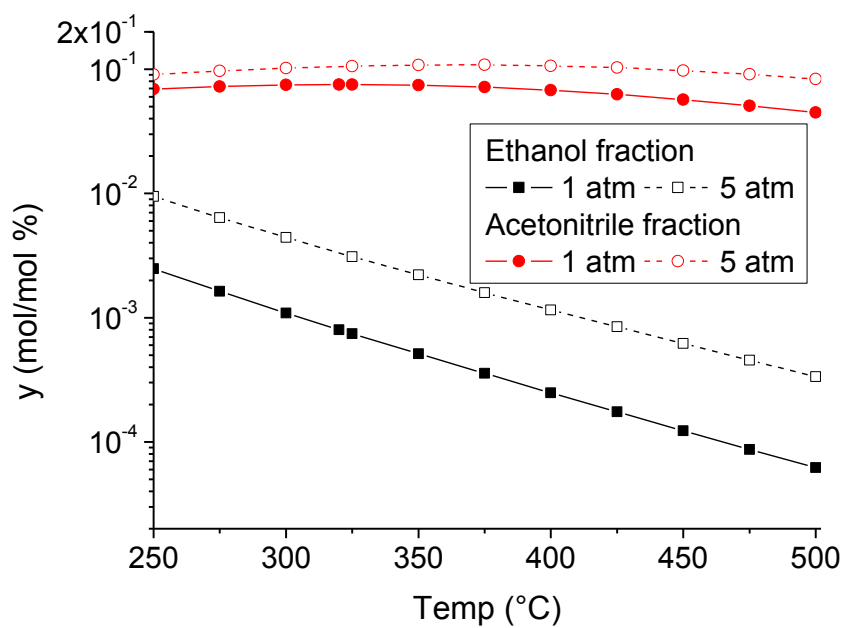
Figure 3: Theoretical fractions for ethanol, acetonitrile (top) and ammonia, nitrogen (bottom).
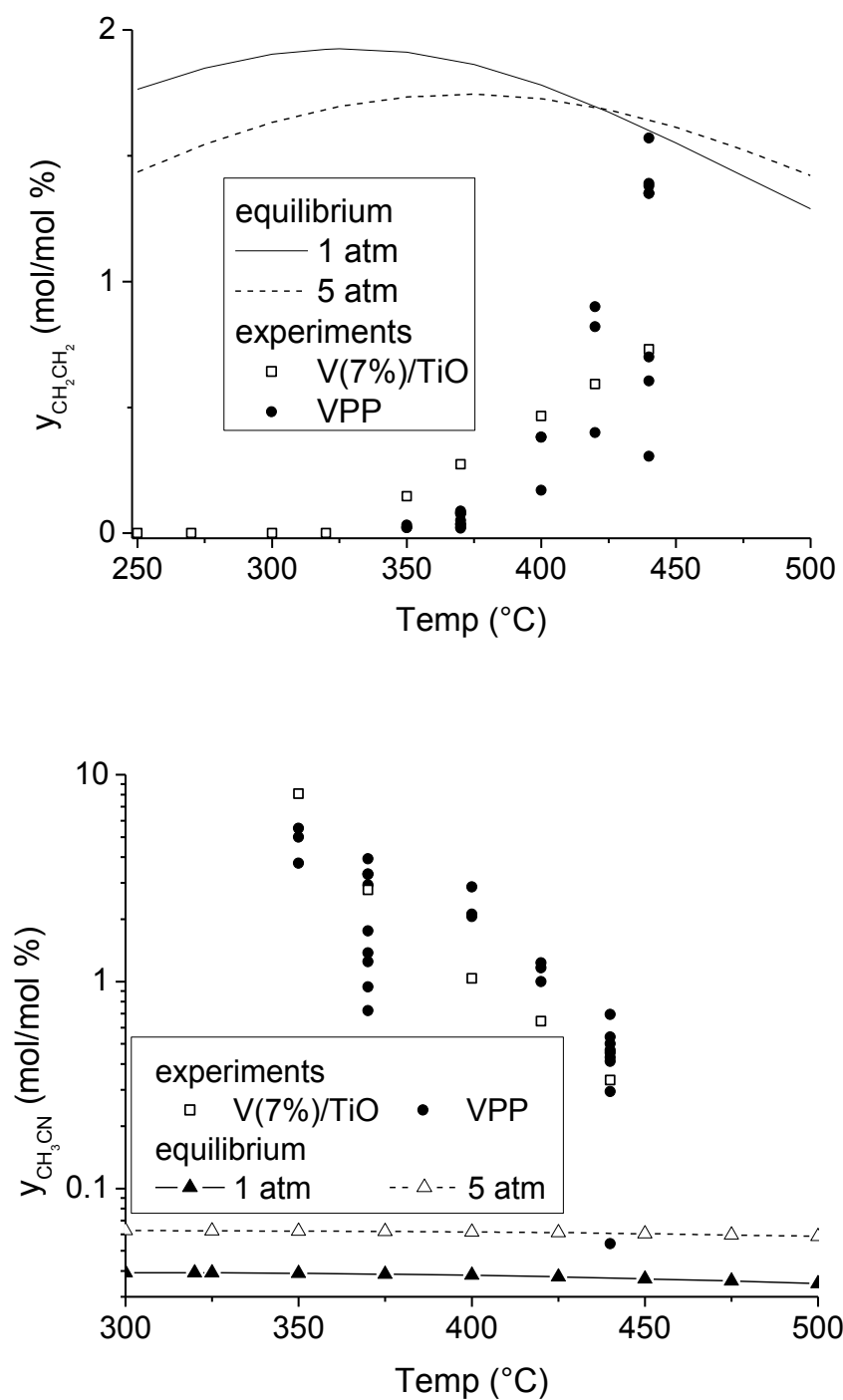
Figure 4: Comparison between the equilibrium fractions and the experimental outcomes for ethylene (top) and the acetonitrile/ethylene ratio (bottom) at different catalyst loads. While only the less acidic catalysts inhibit ethylene formation, the selectivity to acetonitrile is order of magnitudes larger than what expected on the thermodynamic ground.
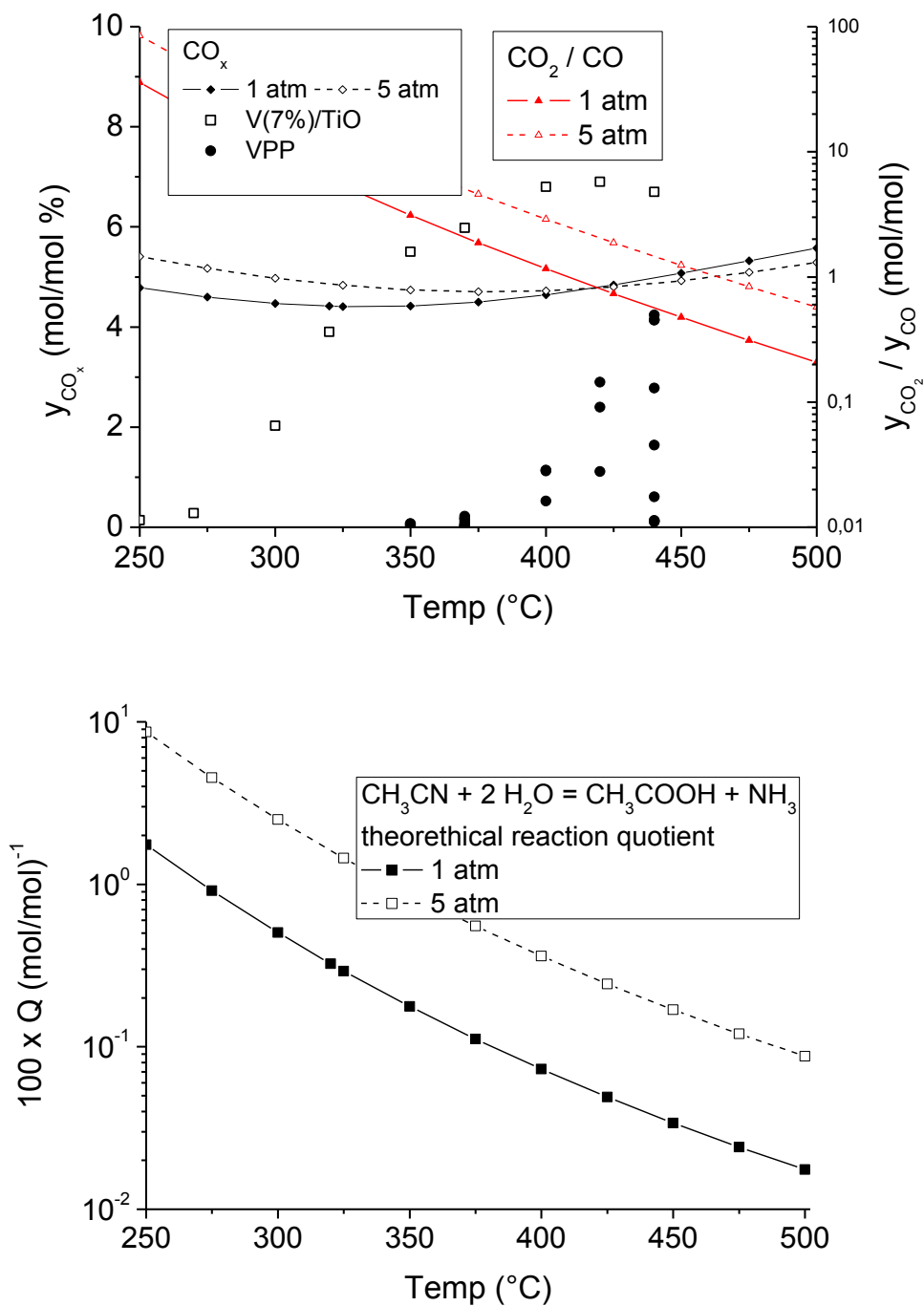
Figure 5: (Top) theoretical *vs* experimental CO_x fraction and CO_2/CO distribution: as the former increases at higher temperatures, so does the CO stability, then the catalysts which yield more carbon oxides (*i.e.* the Titania-based ones) are also modeled with an additional rate-determining step for CO conversion – the high values are likely due to an inhibition of ammonia combustion as an oxygen-consuming path; (Bottom) equilibrium reaction quotient for the acetonitrile hydrolysis.
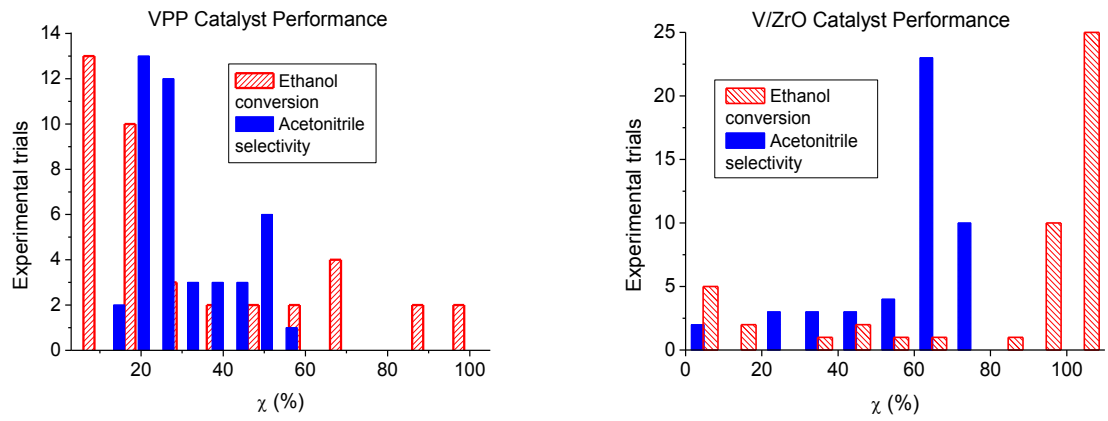
Figure 6: Performance of the VPP (left) and VO_x/ZrO_2 (Folco, 2013) (right) catalysts at a glance (χ is the percent ethanol molar conversion – acetonitrile selectivity is on the same scale).
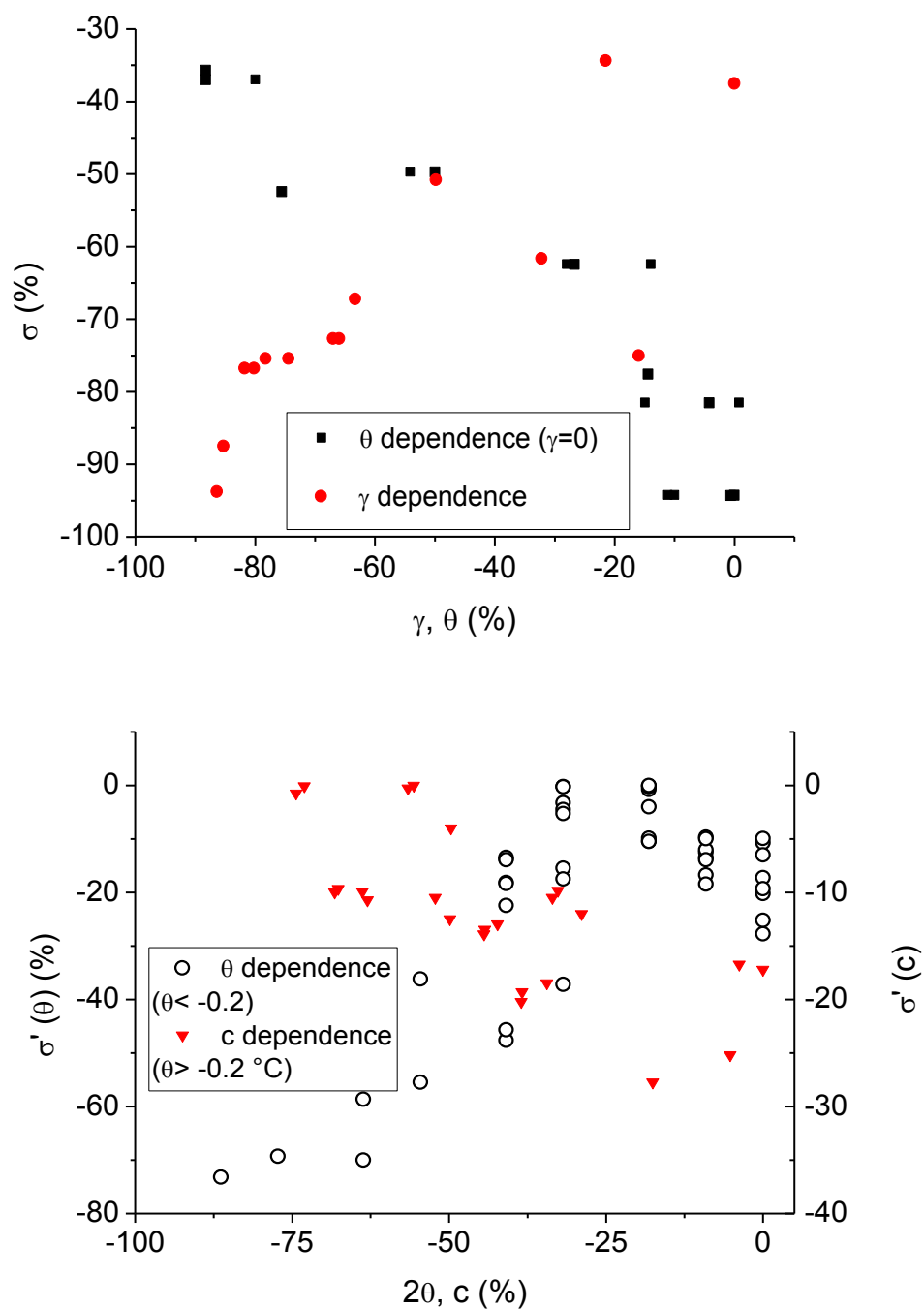
Figure 77: (Top) Normalized acetonitrile selectivity as a function of the reduced temperature and catalyst load for the VPP data: while the contact time has a dominating role (circles, for $\gamma < 0$ only), lower temperatures prevents acetonitrile parasite combustion where the other conditions are fixed; (Bottom) normalized selectivity for the VO_x/ZrO_2 ensemble: the increasing trend with temperature ceases around 400 °C, after which an inverse correlation with CO production can be traced.
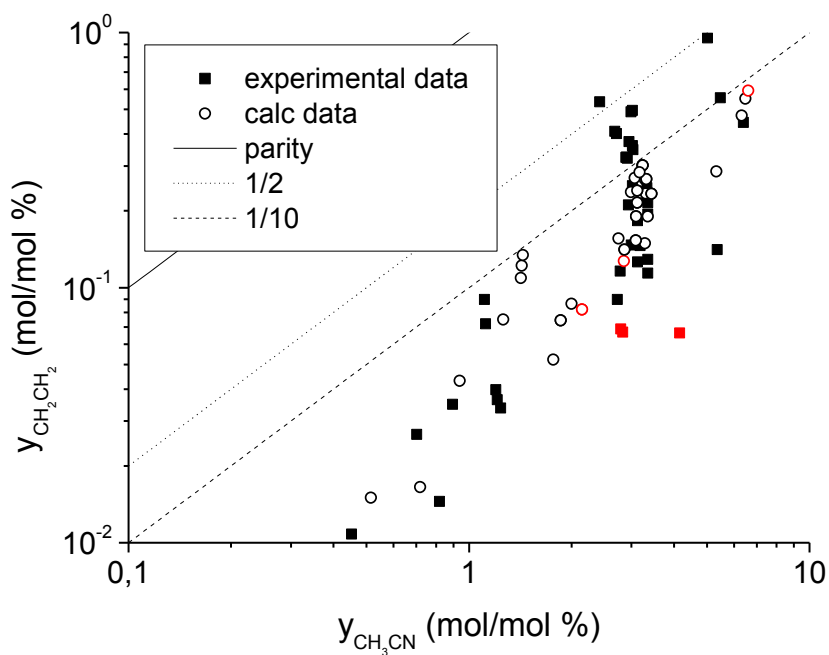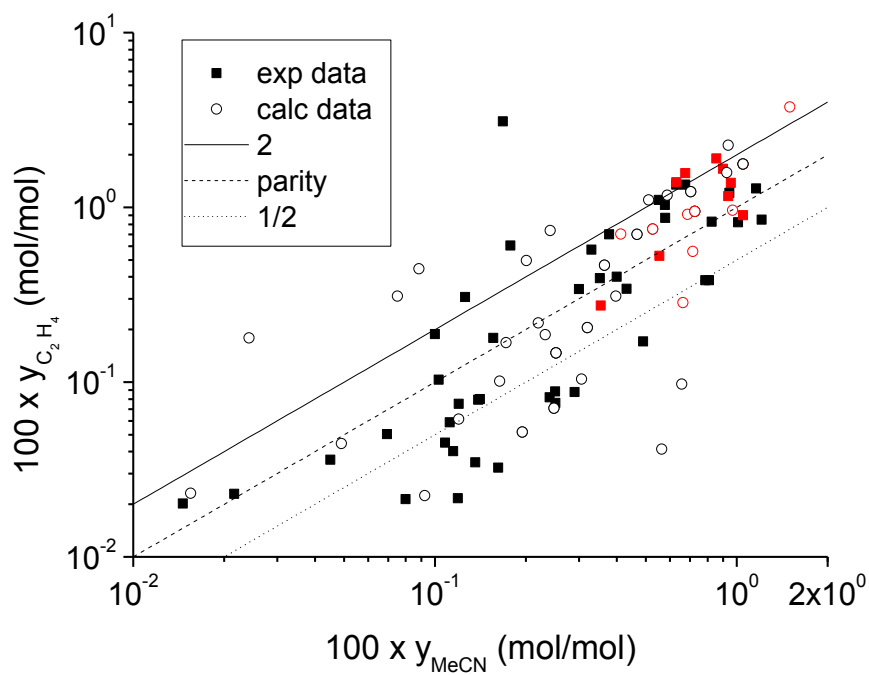
Figure 8: Ethylene *vs* acetonitrile yield for the VPP catalyst (Top) and for the VO_x/ZrO_2 (Folco, 2013) (Bottom). Red points represents data series most difficult to fit.
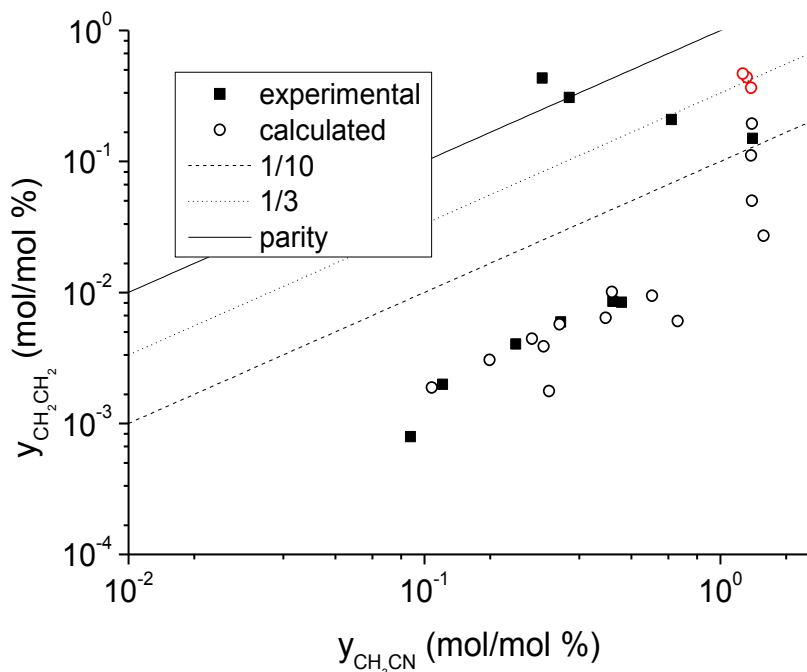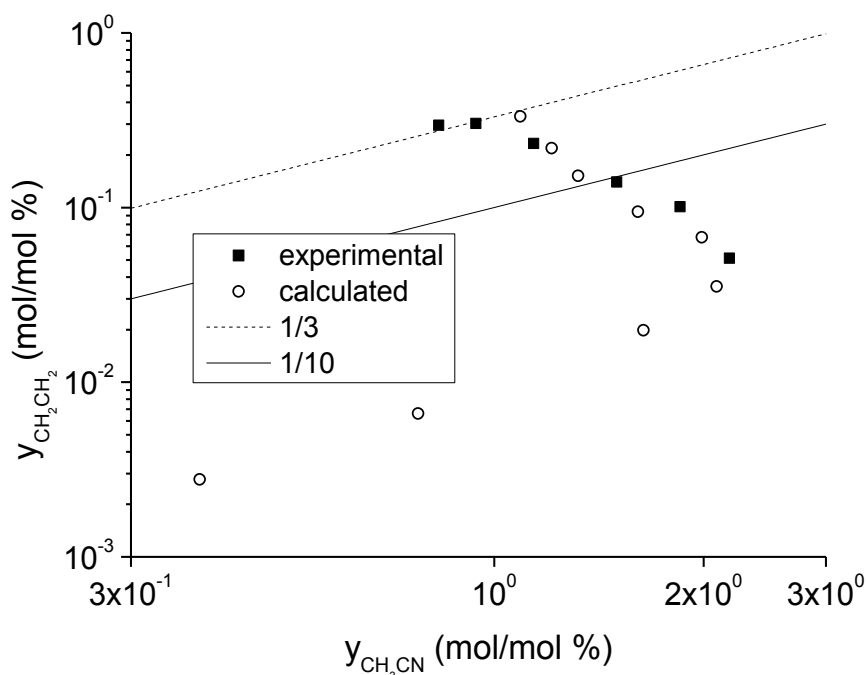
Figure 9: Ethylene *vs* acetonitrile yield for the Cs-VO$_x$/TiO$_2$ catalyst (top) and for the VO$_x$(2%)/TiO$_2$ (Folco, 2013) (bottom). Red points represents data most difficult to fit.
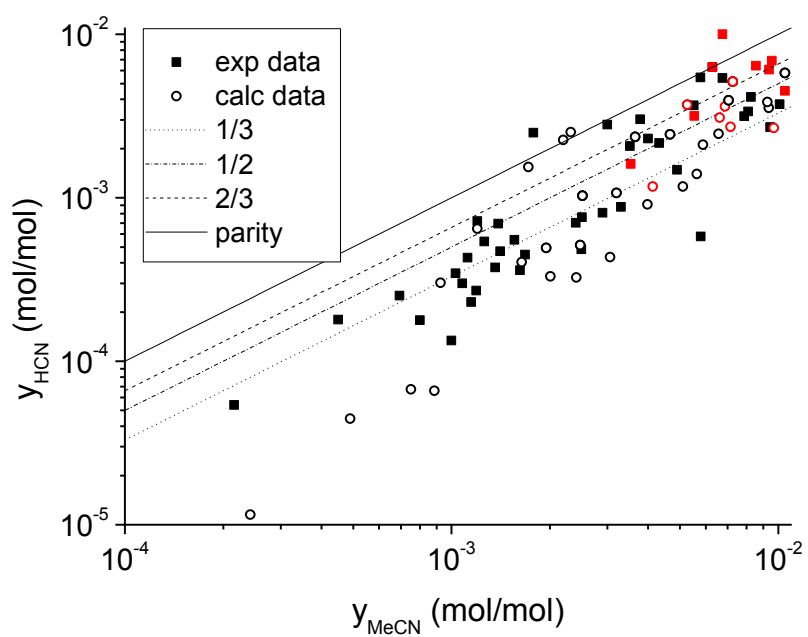
Figure 10: HCN *vs* CH₃CN (MeCN) yield for the VPP catalyst. Red points represents data series most difficult to fit.
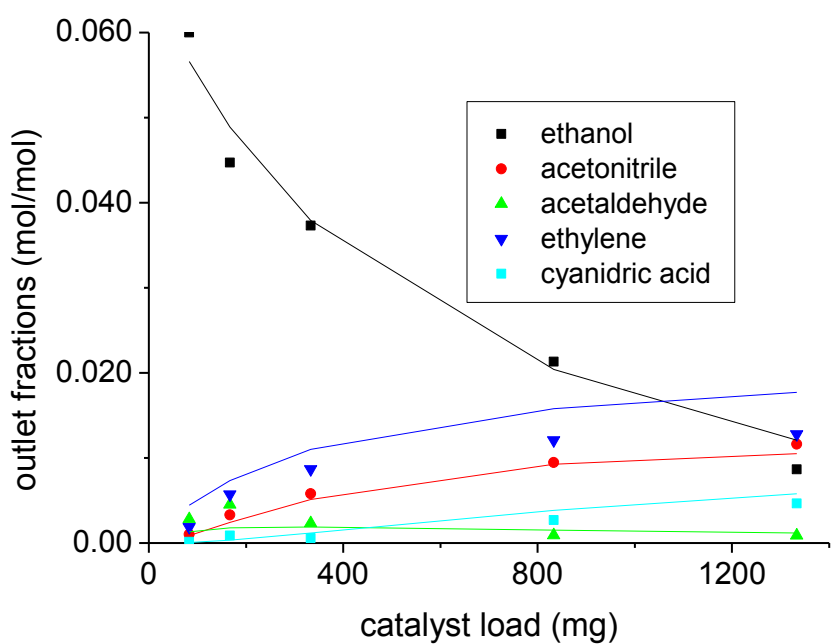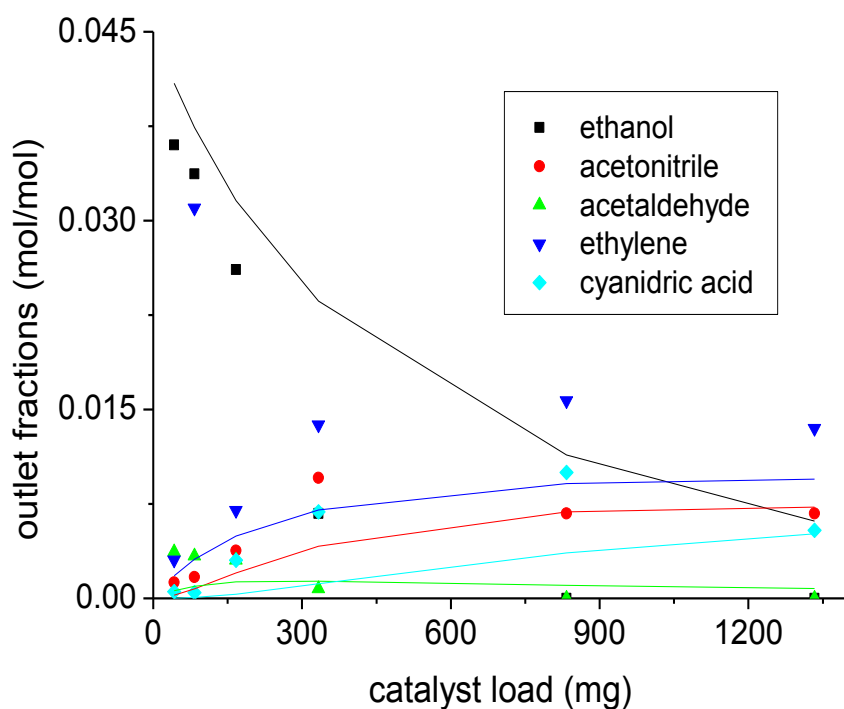
Figure 10: Experimental (points) and calculated (lines) data at 440 °C, for ethanol inlet fractions of 0.045 (top) and 0.067 (bottom), over the largest range of contact times (reworked as different catalyst loads at fixed molar flow) on the VPP catalyst. A faster kinetic associated with lower ethanol inlets may imply a shift in the mechanism, or adsorption phenomena more complex than those considered.
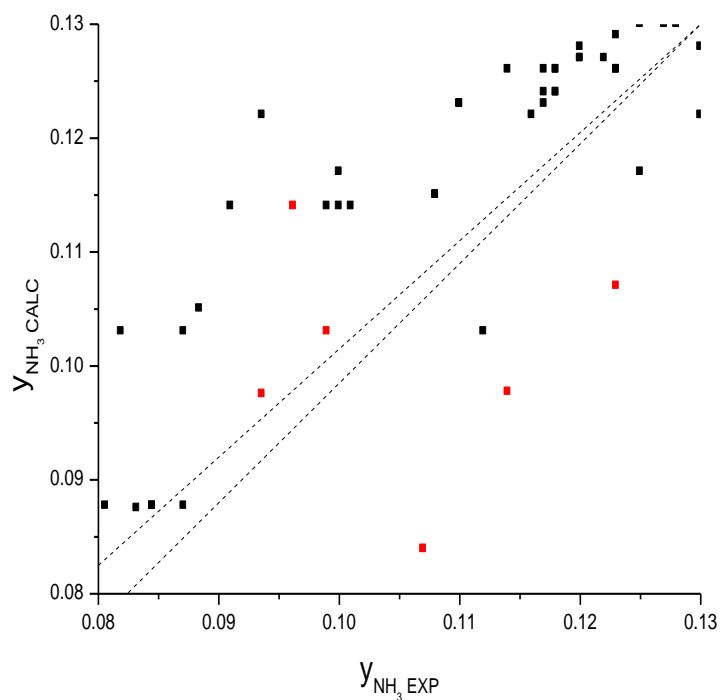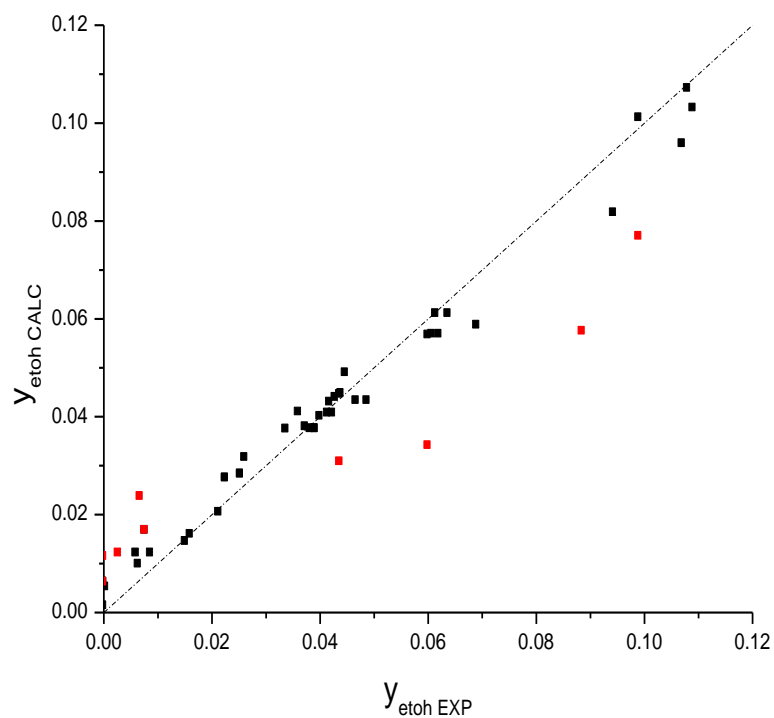
Figure 11: Parity plots of calculated *vs* experimental mole fractions of ethanol (top) and ammonia (bottom) on the VPP catalyst. The dispersion of ammonia data reflects the uncertainty in the nitrogen balance due to the unspecified heavy compounds formulas. Red points mark the outlets with a too high error (outliers). Double dashed lines mark ±10% deviation.
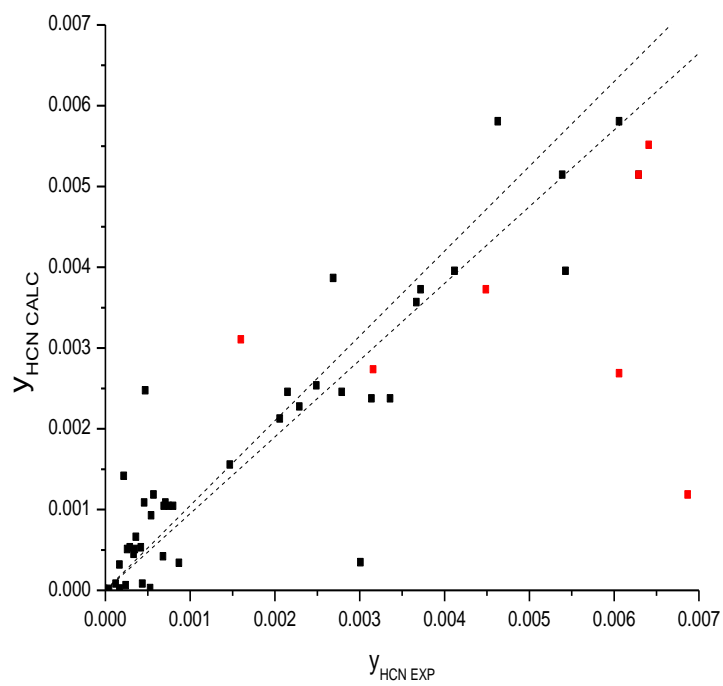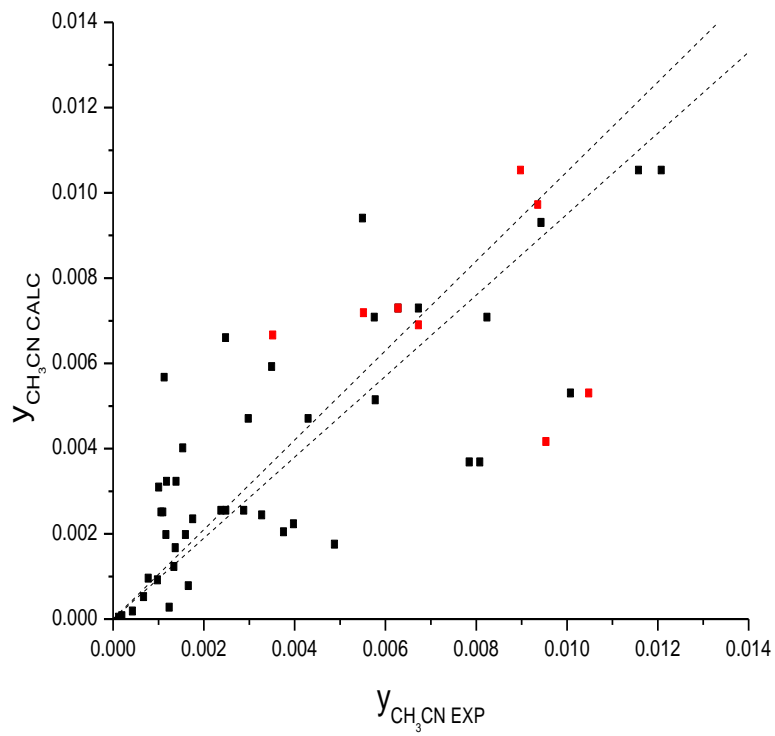
Figure 12: Parity plots of calculated *vs* experimental mole fractions of acetonitrile (top) and HCN (bottom) on VPP. Red points mark the outlets with a too high error (outliers). Double dashed lines marks the ±10% deviation.
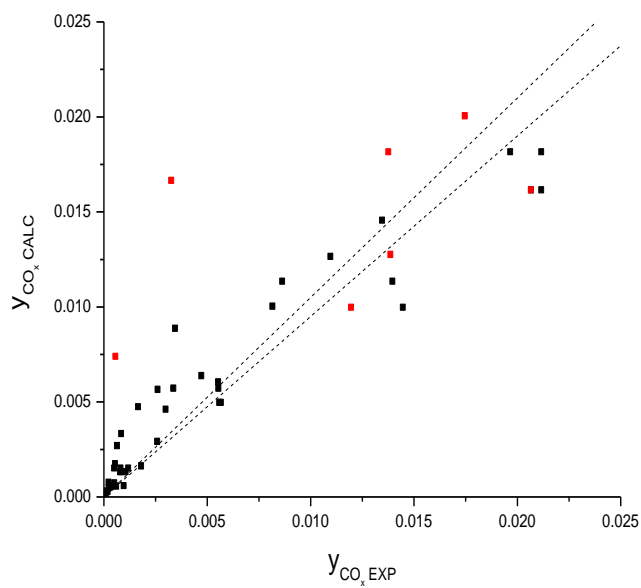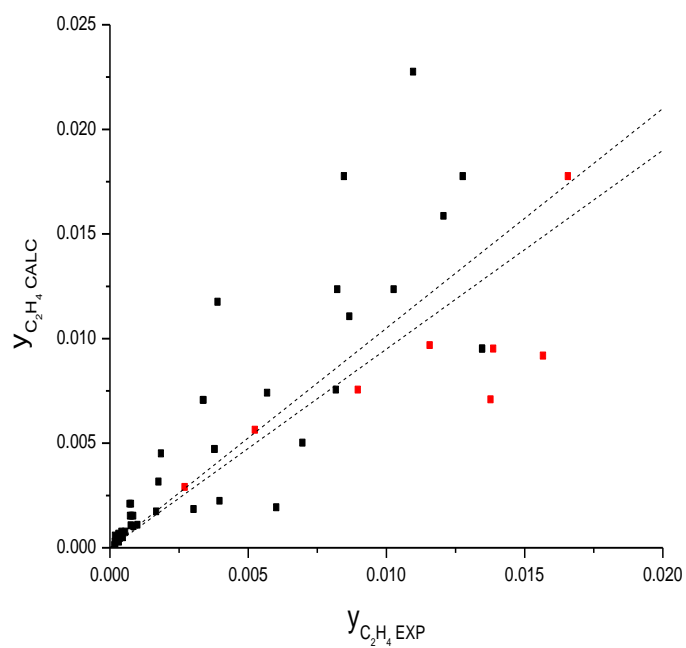
Figure 13: Parity plots of calculated *vs* experimental mole fractions of ethylene (top) and CO/CO$_2$ (bottom) on VPP. Red points mark the outlets with a too high error (outliers). Double dashed lines marks the ±10% deviation.

Supporting Information – full kinetic formulation and graphs

$$CH_3CH_2OH + \frac{1}{2}O_2 \xrightarrow{k1} CH_3CHO + H_2O \qquad (6)$$

$$r_1 = k_1 \frac{y_{EtOH}\, y_{O_2}^{0.5}}{D^2} \qquad (7)$$

$$CH_3CHO + \frac{1}{2}O_2 + NH_3 \xrightarrow{k2} CH_3CN + 2H_2O \qquad (8)$$

$$r_2 = k_2 \frac{y_{AcH}\, y_{NH_3} y_{O_2}^{0.5}}{D^3} \qquad (9)$$

$$CH_3CH_2OH \xrightarrow{k3} C_2H_4 + H_2O \qquad (10)$$

$$r_3 = k_3 \frac{y_{EtOH}}{D^2} \qquad (11)$$

$$C_4H_7N + \frac{19}{4}O_2 \xrightarrow{k4} 2CO_2 + 2CO + \frac{1}{2}N_2 + \frac{7}{2}H_2O \qquad (12)$$

$$r_4 = k_4 \frac{y_{AcH}^2\, y_{O_2}^2}{D^3} \qquad (13)$$

$$2CH_3CHO + NH_3 \xrightarrow{k5} C_4H_7N + 2H_2O \qquad (14)$$

$$r_5 = k_5 \frac{y_{AcH}^2}{D^3} \qquad (15)$$

$$CH_3CN + \frac{5}{4}O_2 \xrightarrow{k6} HCN + \frac{1}{2}CO + \frac{1}{2}CO_2 + H_2O \qquad (16)$$

$$r_6 = k_6 \frac{y_{MeCN} y_{O_2}^{0.5}}{D^3} \qquad (17)$$

$$NH_3 + \frac{3}{4}O_2 \xrightarrow{k7} \frac{1}{2}N_2 + \frac{3}{2}H_2O \qquad (18)$$

$$r_7 = k_7 \frac{y_{NH_3} y_{O_2}^{0.5}}{D^2} \qquad (19)$$

$$C_2H_4 + \frac{5}{2}O_2 \xrightarrow{k8} CO + CO_2 + 2H_2O \qquad (20)$$

$$r_8 = k_8 \frac{y_{EtOH} y_{O_2}}{D^3} \qquad (21)$$

$$C_2H_4 + O_2 + NH_3 \xrightarrow{k9} CH_3CN + 2H_2O \qquad (22)$$

$$r_9 = k_9 \frac{y_{C_2H_4} y_{NH_3} y_{O_2}}{D^3} \qquad (23)$$

$$HCN + O_2 \xrightarrow{k10} \frac{1}{2}CO + \frac{1}{2}CO_2 + \frac{1}{2}H_2O + \frac{1}{2}N_2 \qquad (24)$$

$$r_{10} = k_{10} \frac{y_{HCN} y_{O_2}}{D^2} \qquad (25)$$

Stoichiometry and rates expression for the reactions on the VPP catalyst.

$$CH_3CH_2OH + \frac{1}{2}O_2 \xrightarrow{k1} CH_3CHO + H_2O \qquad (26) \qquad r_1 = k_1 \frac{y_{EtOH}\, y_{O_2}^{0.5}}{D^2} \qquad (27)$$

$$CH_3CHO + \frac{1}{2}O_2 + NH_3 \xrightarrow{k2} CH_3CN + 2H_2O \qquad (28) \qquad r_2 = k_2 \frac{y_{AcH} y_{NH_3}\, y_{O_2}^{0.5} y_{H_2O}^{-1}}{D^2} \qquad (29)$$

$$CH_3CH_2OH \xrightarrow{k3} C_2H_4 + H_2O \qquad (30) \qquad r_3 = k_3 \frac{y_{EtOH}}{D^1} \qquad (31)$$

$$CH_3CN + \frac{5}{4}O_2 \xrightarrow{k4} HCN + \frac{1}{2}CO + \frac{1}{2}CO_2 + H_2O \qquad (32) \qquad r_4 = k_4 \frac{y_{MeCN}\, y_{O_2}^{1}}{D^3} \qquad (33)$$

$$CH_3CHO + 2O_2 \xrightarrow{k5} CO + CO_2 + 2H_2O \qquad (34) \qquad r_5 = k_5 \frac{y_{AcH}\, y_{O_2}^{2}}{D^5} \qquad (35)$$

$$2NH_3 + \frac{3}{2}O_2 \xrightarrow{k6} N_2 + 3H_2O \qquad (36) \qquad r_6 = k_6 \frac{y_{NH_3}^{2}\, y_{O_2}^{1.5}}{D^5} \qquad (37)$$

$$HCN + O_2 \xrightarrow{k7} \frac{1}{2}CO + \frac{1}{2}CO_2 + \frac{1}{2}H_2O + \frac{1}{2}N_2 \qquad (38) \qquad r_7 = k_7 \frac{y_{HCN}\, y_{O_2}}{D^3} \qquad (39)$$

$$CH_3CH_2OH + \frac{5}{2}O_2 \xrightarrow{k8} CO + CO_2 + 3H_2O \qquad (40) \qquad r_8 = k_8 \frac{y_{EtOH}\, y_{O_2}^{2}}{D^2} \qquad (41)$$
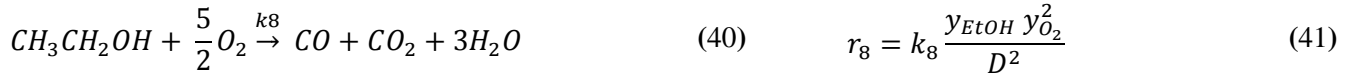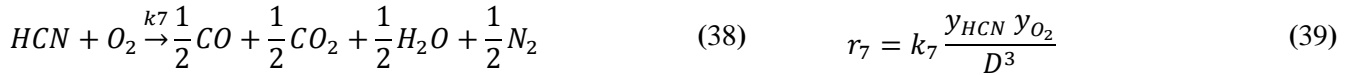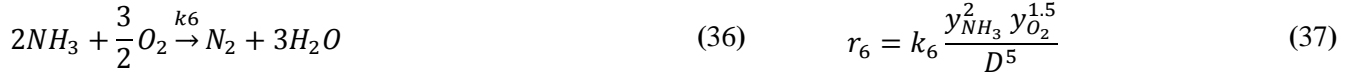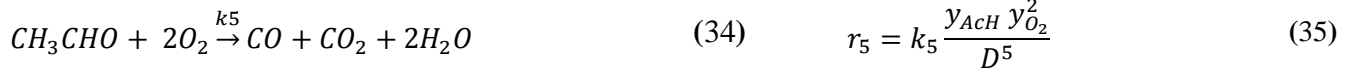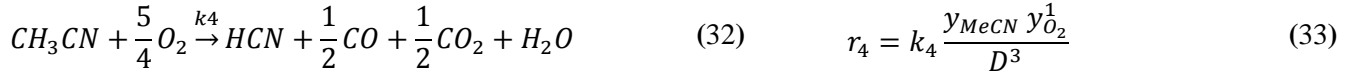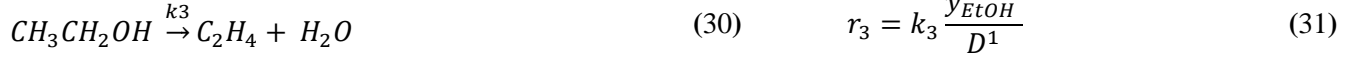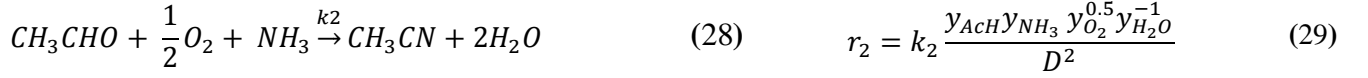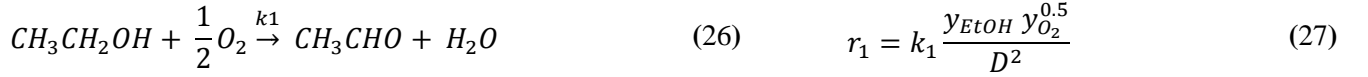
Stoichiometry and rates expression for the reactions on the Vanadium(2%)-Titania catalyst.

$$CH_3CH_2OH + \frac{1}{2}O_2 \xrightarrow{k1} CH_3CHO + H_2O \qquad (42)$$

$$r_1 = k_1 \frac{y_{EtOH}\, y_{O_2}^{0.5}}{D^2} \qquad (43)$$

$$CH_3CHO + \frac{1}{2}O_2 + NH_3 \xrightarrow{k2} CH_3CN + 2H_2O \qquad (44)$$

$$r_2 = k_2 \frac{y_{AcH}\, y_{NH_3}\, y_{O_2}^{0.5}\, y_{H_2O}^{-1}}{D^2} \qquad (45)$$

$$CH_3CH_2OH \xrightarrow{k3} C_2H_4 + H_2O \qquad (46)$$

$$r_3 = k_3 \frac{y_{EtOH}}{D^1} \qquad (47)$$

$$CH_3CN + \frac{5}{4}O_2 \xrightarrow{k4} HCN + \frac{1}{2}CO + \frac{1}{2}CO_2 + H_2O \qquad (48)$$

$$r_4 = k_4 \frac{y_{MeCN}\, y_{O_2}^{1}}{D^3} \qquad (49)$$

$$CH_3CHO + 2O_2 \xrightarrow{k5} CO + CO_2 + 2H_2O \qquad (50)$$

$$r_5 = k_5 \frac{y_{AcH}\, y_{O_2}^{1}}{D^5} \qquad (51)$$

$$2NH_3 + \frac{3}{2}O_2 \xrightarrow{k6} N_2 + 3H_2O \qquad (52)$$

$$r_6 = k_6 \frac{y_{NH_3}^{2}\, y_{O_2}^{1.5}}{D^5} \qquad (53)$$

$$HCN + O_2 \xrightarrow{k7} \frac{1}{2}CO + \frac{1}{2}CO_2 + \frac{1}{2}H_2O + \frac{1}{2}N_2 \qquad (54)$$

$$r_7 = k_7 \frac{y_{HCN}\, y_{O_2}}{D^3} \qquad (55)$$

$$CH_3CH_2OH + \frac{5}{2}O_2 \xrightarrow{k8} CO + CO_2 + 3H_2O \qquad (56)$$

$$r_8 = k_8 \frac{y_{EtOH}\, y_{O_2}}{D^2} \qquad (57)$$
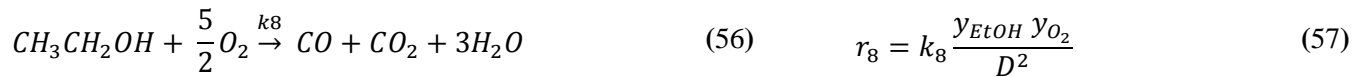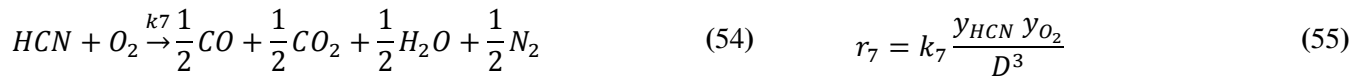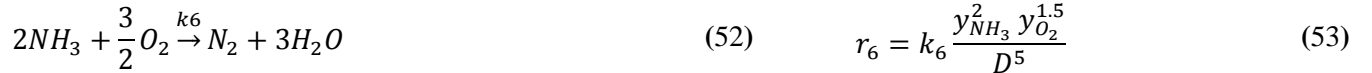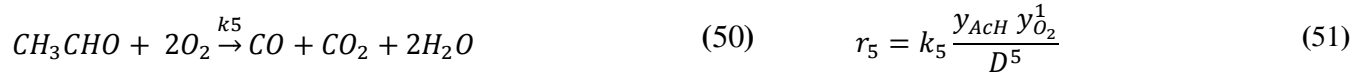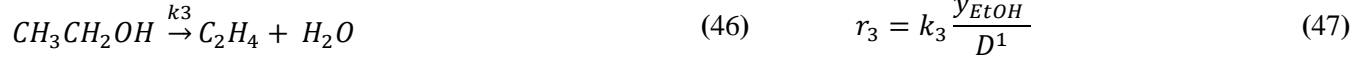
Stoichiometry and rates expression for the reactions on the Vanadium(7%)-Titania catalyst.

$$CH_3CH_2OH + \frac{1}{2}O_2 \xrightarrow{k1} CH_3CHO + H_2O \qquad (58)$$

$$r_1 = k_1 \frac{y_{EtOH}\, y_{O_2}^{0.5}}{D^2} \qquad (59)$$

$$CH_3CHO + \frac{1}{2}O_2 + NH_3 \xrightarrow{k2} CH_3CN + 2H_2O \qquad (60)$$

$$r_2 = k_2 \frac{y_{AcH}y_{NH_3}\, y_{O_2}^{0.5} y_{H_2O}^{-1}}{D^2} \qquad (61)$$

$$CH_3CH_2OH \xrightarrow{k3} C_2H_4 + H_2O \qquad (62)$$

$$r_3 = k_3 \frac{y_{EtOH}}{D^1} \qquad (63)$$

$$CH_3CN + \frac{5}{4}O_2 \xrightarrow{k4} HCN + \frac{1}{2}CO + \frac{1}{2}CO_2 + H_2O \qquad (64)$$

$$r_4 = k_4 \frac{y_{MeCN}\, y_{O_2}^{1}}{D^3} \qquad (65)$$

$$CH_3CHO + 2O_2 \xrightarrow{k5} CO + CO_2 + 2H_2O \qquad (66)$$

$$r_5 = k_5 \frac{y_{AcH}\, y_{O_2}^{1.5}}{D^5} \qquad (67)$$

$$2NH_3 + \frac{3}{2}O_2 \xrightarrow{k6} N_2 + 3H_2O \qquad (68)$$

$$r_6 = k_6 \frac{y_{NH_3}^{1.5}\, y_{O_2}}{D^5} \qquad (69)$$

$$HCN + O_2 \xrightarrow{k7} \frac{1}{2}CO + \frac{1}{2}CO_2 + \frac{1}{2}H_2O + \frac{1}{2}N_2 \qquad (70)$$

$$r_7 = k_7 \frac{y_{HCN}\, y_{O_2}}{D^3} \qquad (71)$$

$$CH_3CH_2OH + \frac{5}{2}O_2 \xrightarrow{k8} CO + CO_2 + 3H_2O \qquad (72)$$

$$r_8 = k_8 \frac{y_{EtOH}\, y_{O_2}^{2}}{D^2} \qquad (73)$$

Stoichiometry and rates expression for the reactions on the Cs-Vanadium-Titania catalyst.

$$CH_3CH_2OH + \frac{1}{2}O_2 \xrightarrow{k1} CH_3CHO + H_2O \qquad (74)$$

$$r_1 = k_1 \frac{y_{EtOH}\, y_{O_2}^{0.5}}{D^2} \qquad (75)$$

$$CH_3CHO + \frac{1}{2}O_2 + NH_3 \xrightarrow{k2} CH_3CN + 2H_2O \qquad (76)$$

$$r_2 = k_2 \frac{y_{AcH}\, y_{NH_3}\, y_{O_2}^{0.5}\, y_{H_2O}^{-1}}{D^2} \qquad (77)$$

$$CH_3CH_2OH \xrightarrow{k3} C_2H_4 + H_2O \qquad (78)$$

$$r_3 = k_3 \frac{y_{EtOH}}{D^1} \qquad (79)$$

$$CH_3CN + \frac{5}{4}O_2 \xrightarrow{k4} HCN + \frac{1}{2}CO + \frac{1}{2}CO_2 + H_2O \qquad (80)$$

$$r_4 = k_4 \frac{y_{MeCN}\, y_{O_2}^{1}}{D^3} \qquad (81)$$

$$CH_3CHO + 2O_2 \xrightarrow{k5} CO + CO_2 + 2H_2O \qquad (82)$$

$$r_5 = k_5 \frac{y_{AcH}\, y_{O_2}^{1.5}}{D^5} \qquad (83)$$

$$2NH_3 + \frac{3}{2}O_2 \xrightarrow{k6} N_2 + 3H_2O \qquad (84)$$

$$r_6 = k_6 \frac{y_{NH_3}^2\, y_{O_2}^{1.5}}{D^5} \qquad (85)$$

$$HCN + O_2 \xrightarrow{k7} \frac{1}{2}CO + \frac{1}{2}CO_2 + \frac{1}{2}H_2O + \frac{1}{2}N_2 \qquad (86)$$

$$r_7 = k_7 \frac{y_{HCN}\, y_{O_2}}{D^3} \qquad (87)$$

$$CH_3CH_2OH + \frac{5}{2}O_2 \xrightarrow{k8} CO + CO_2 + 3H_2O \qquad (88)$$

$$r_8 = k_8 \frac{y_{EtOH}\, y_{O_2}}{D^2} \qquad (89)$$

Stoichiometry and rates expression for the reactions on the Cs-Vanadium-Titania catalyst.

Where the denominator adsorption term is in the form:

$$D = 1 + K_{ads,1}y_{EtOH} + K_{ads,2}y_{H_2O} + K_{ads,3}y_{NH_3} + K_{ads,4}y_{O_2} \qquad (90)$$
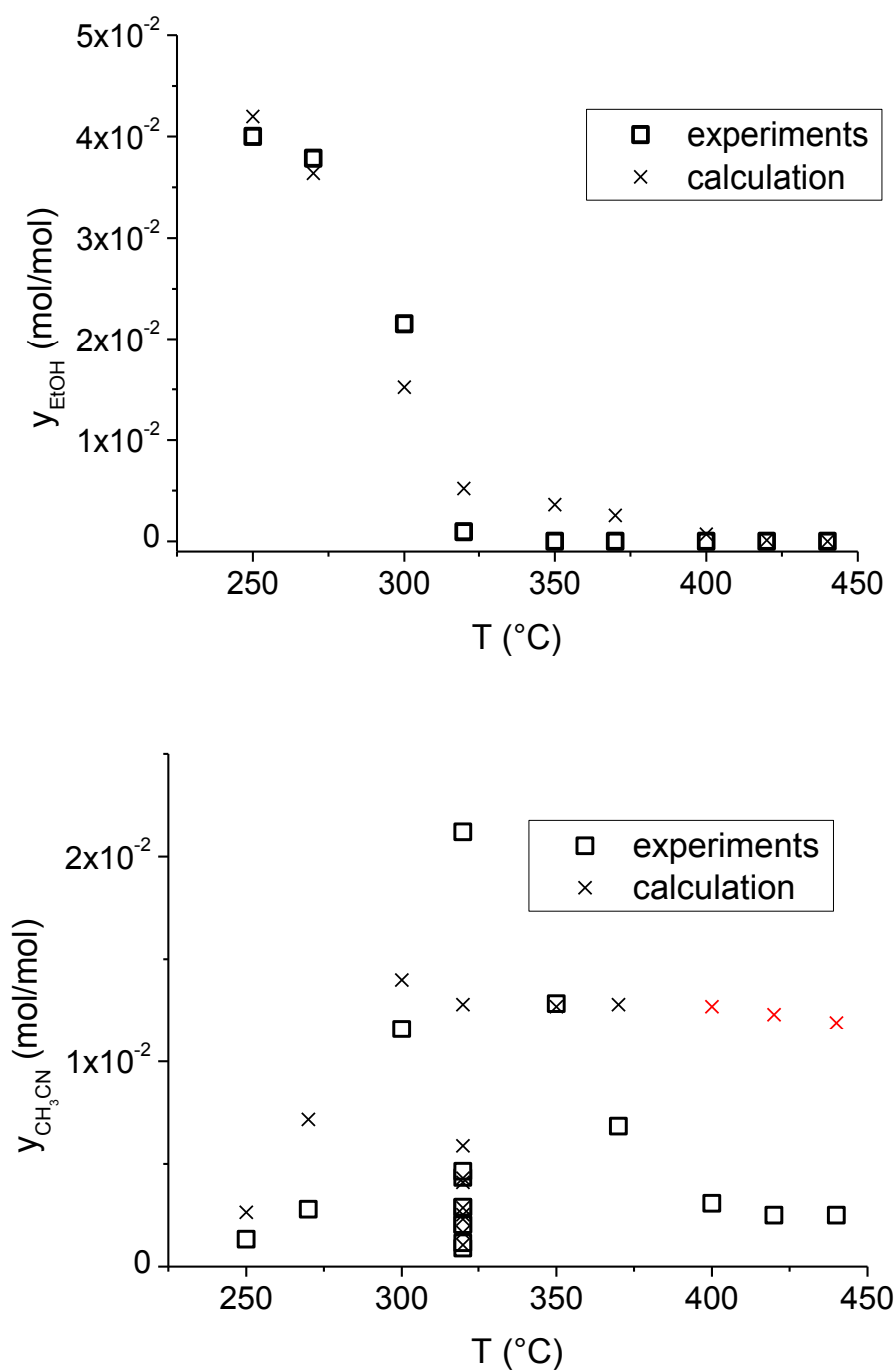
Figure S14: Ethanol (top) and acetonitrile (bottom) molar fractions as a function of reaction temperature for the $VO_x(2\%)/TiO_2$ catalyst (Folco, 2013).
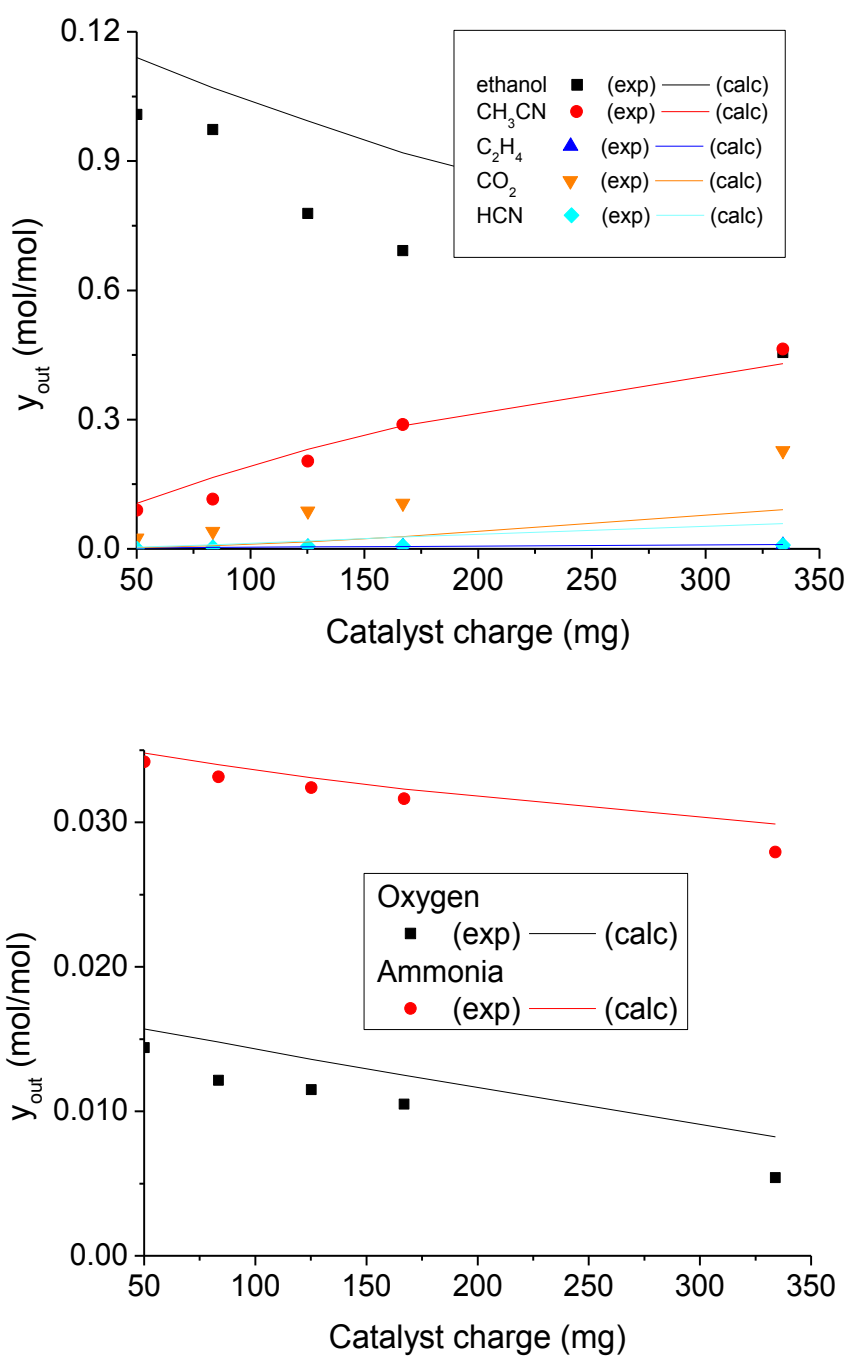
Figure S15: Experimental (points) and calculated (lines) data at 320 °C, for an ethanol inlet fraction of 0.013 over the largest range of contact times (reworked as different catalyst loads at fixed molar flow) on the $VO_x(2\%)/TiO_2$ catalyst (Folco, 2013). Notice that correcting the error on the ethanol and CO_2 balance, acting on the combustion reactions, the resulting oxygen would not allow to predict correctly the acetonitrile formation.
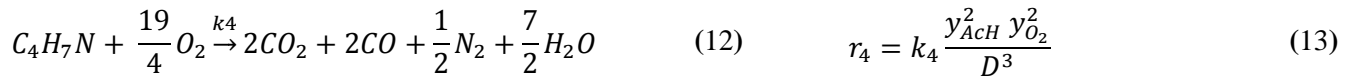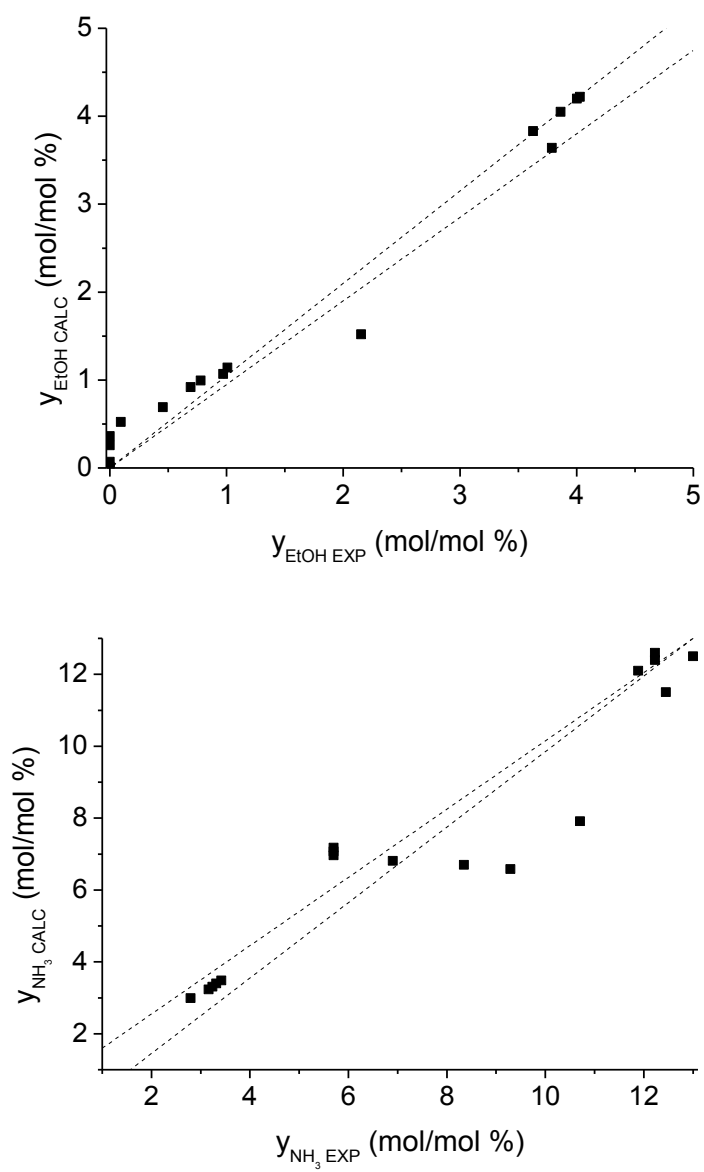
Figure S16: Parity plots of calculated *vs* experimental mole fractions of ethanol (top) and ammonia (bottom) for the $VO_x(2\%)/TiO_2$ catalyst.
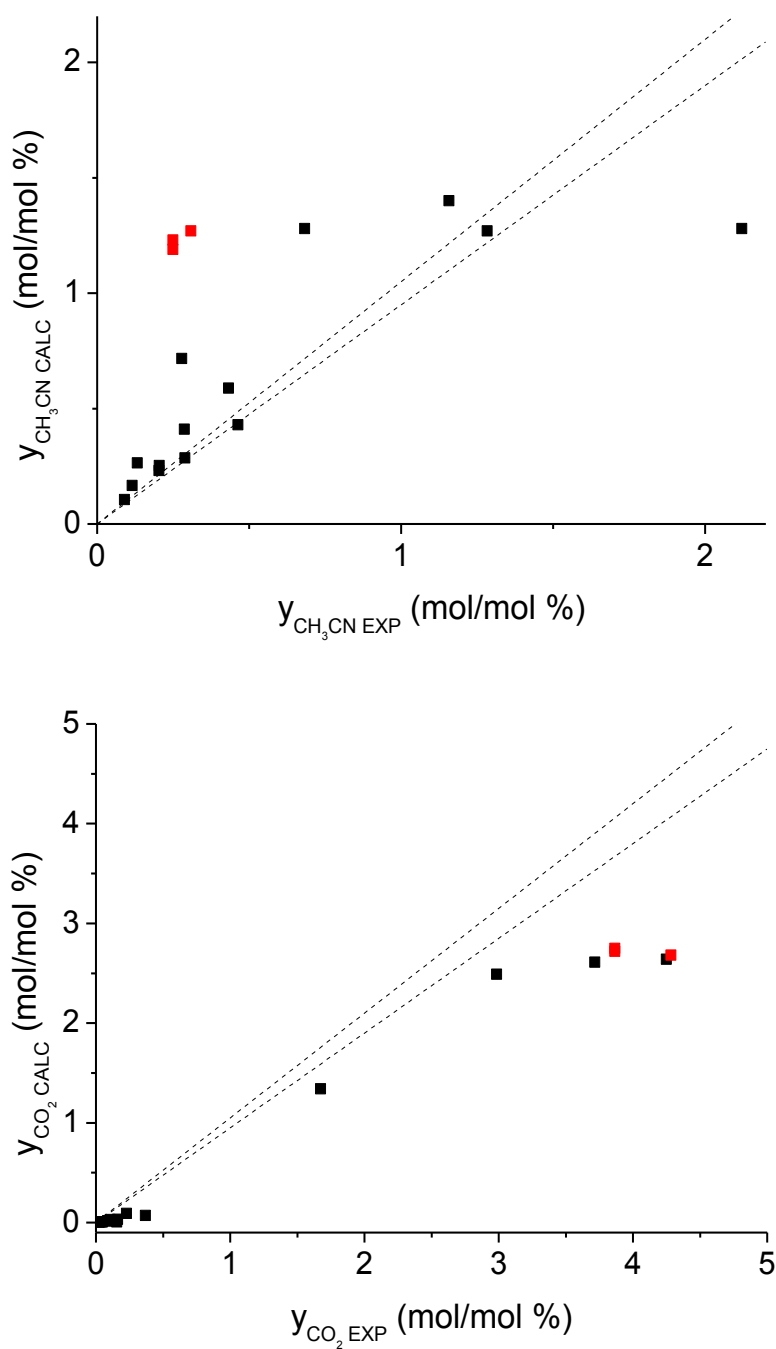
Figure S17: Parity plots of calculated *vs* experimental mole fractions of acetonitrile (top) and CO_2 (bottom) on the $VO_x(2\%)/TiO_2$ catalyst.
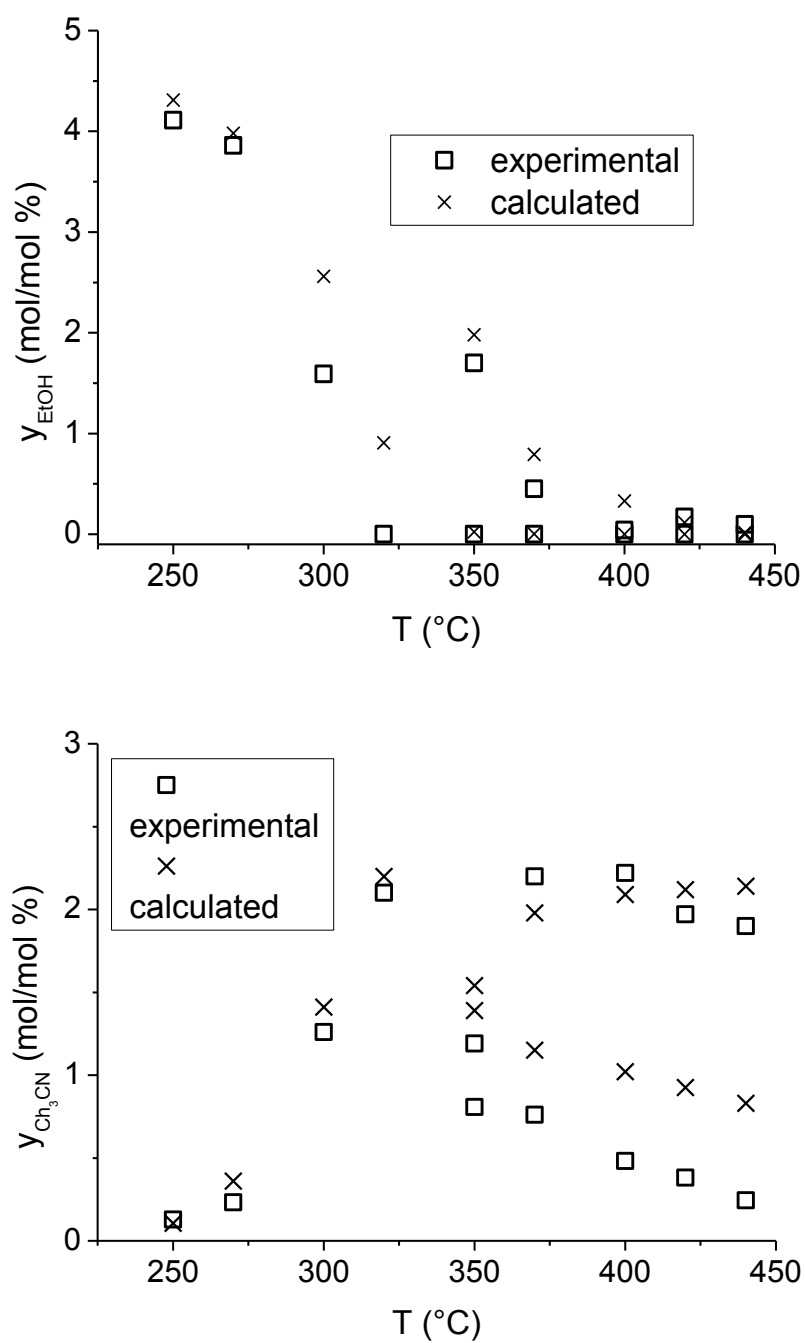
Figure S18: Ethanol (top) and acetonitrile (bottom) molar fractions as a function of reaction temperature for the $VO_x(7\%)/TiO_2$ catalyst (Folco, 2013).
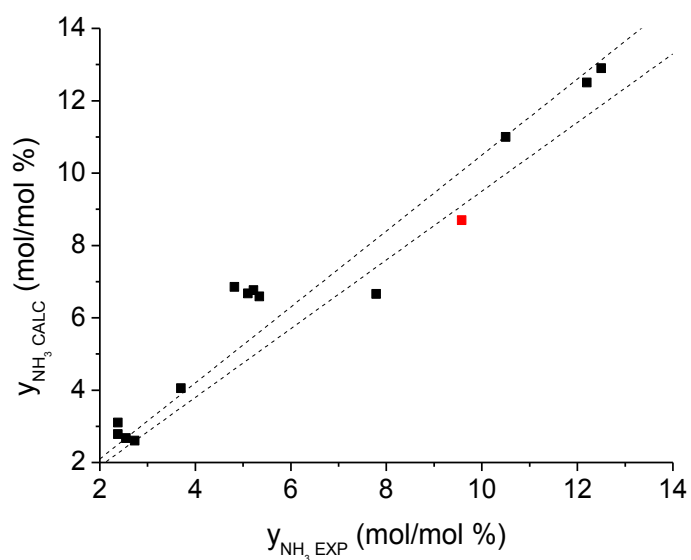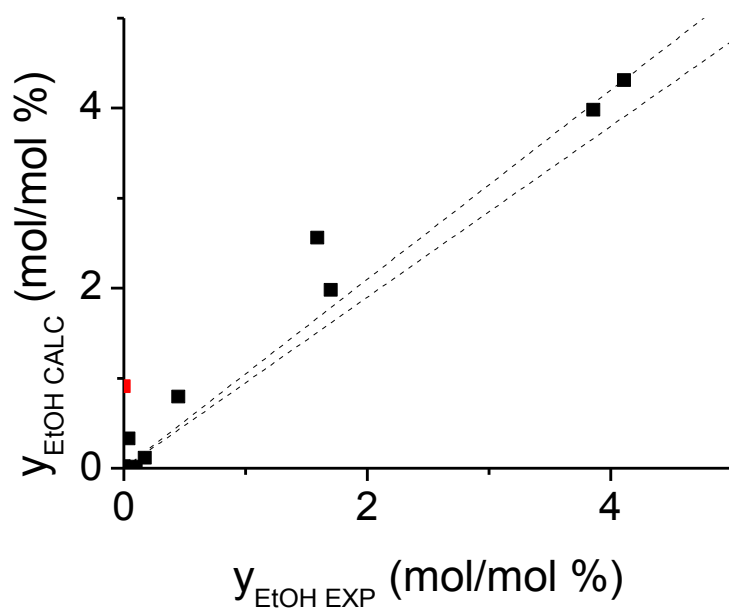
Figure S19: Parity plots of calculated *vs* experimental mole fractions of ethanol (top) and ammonia (bottom) for the $VO_x(7\%)/TiO_2$ catalyst (Folco, 2013).
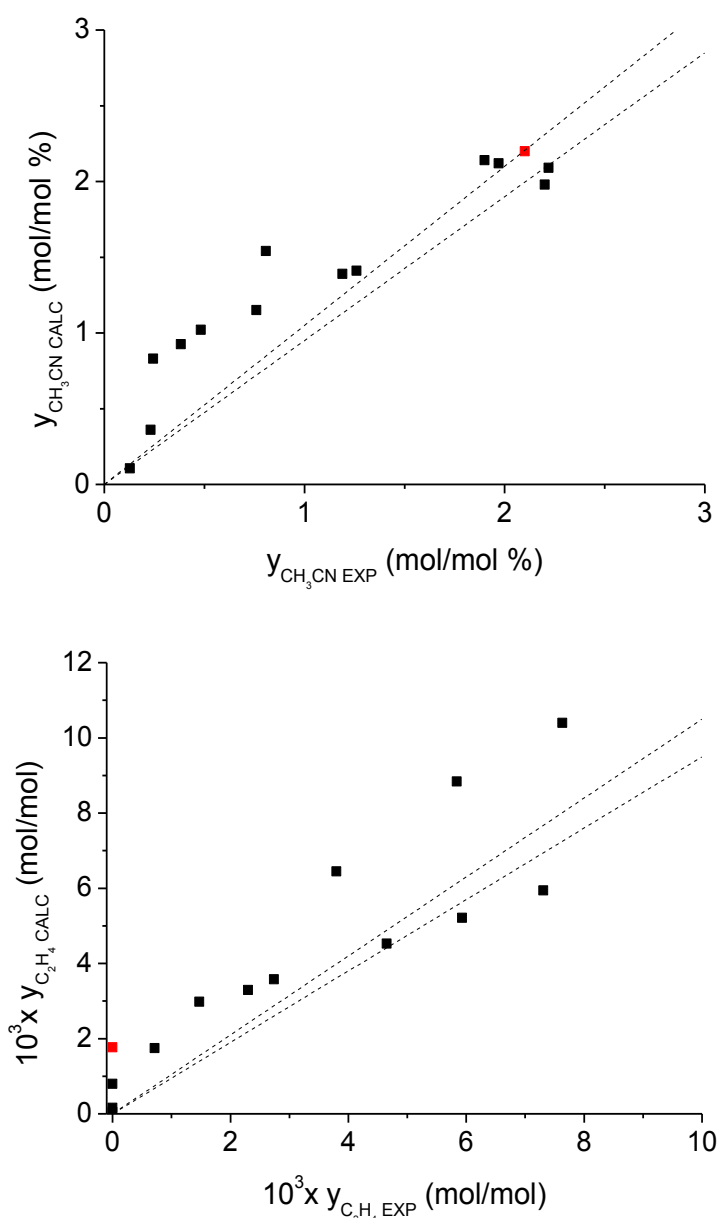
Figure S20: Parity plots of calculated *vs* experimental mole fractions of acetonitrile (top) and ethylene (bottom) for the $VO_x(7\%)/TiO_2$ catalyst (Folco, 2013).
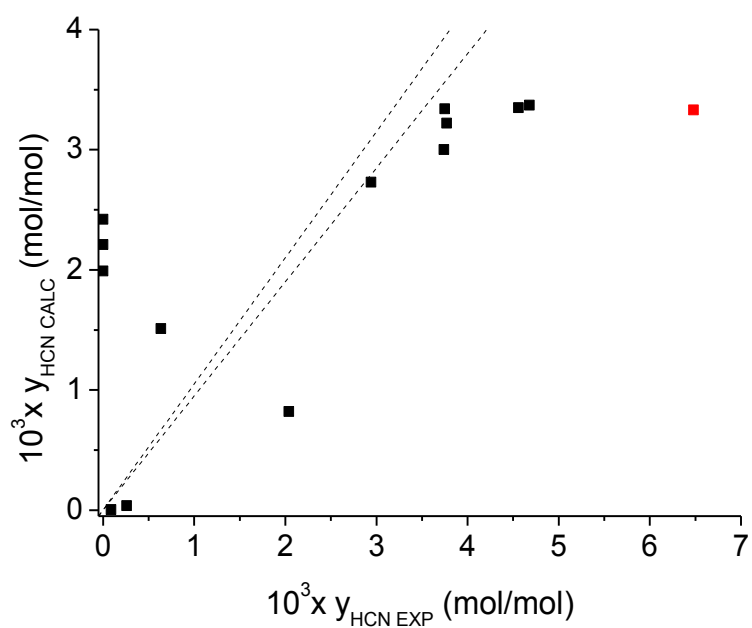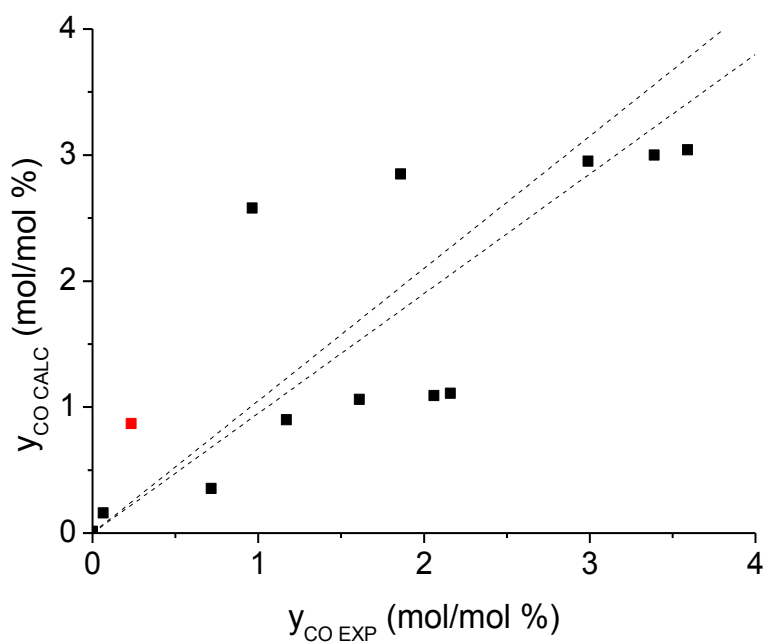
Figure S21: Parity plots of calculated *vs* experimental mole fractions of CO (top) and HCN (bottom) for the $VO_x(7\%)/TiO_2$ catalyst (Folco, 2013).
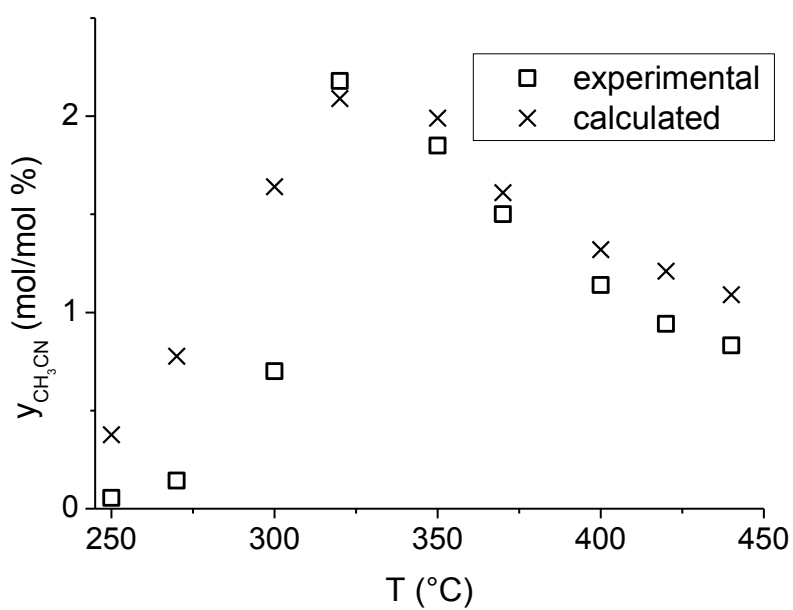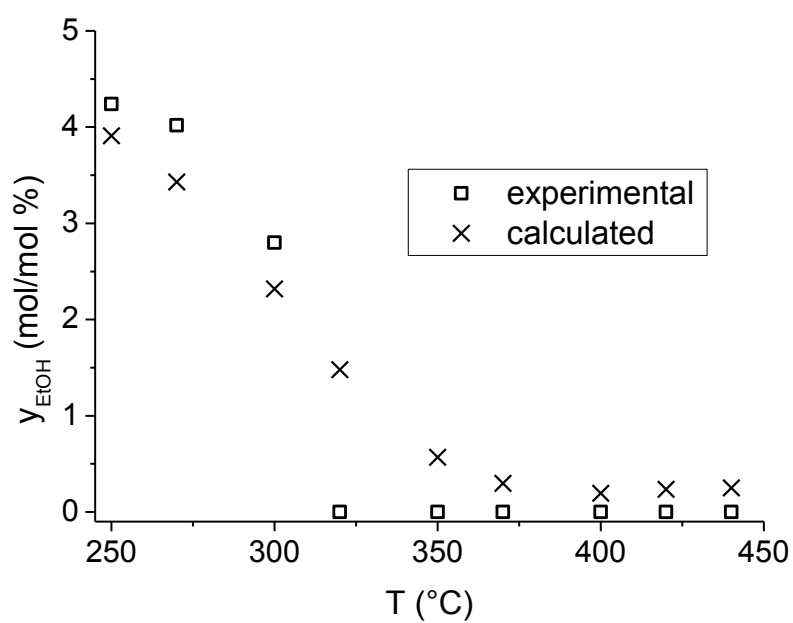
Figure S22: Ethanol (top) and acetonitrile (bottom) molar fractions as a function of reaction temperature for the Cs- $VO_x(7\%)/TiO_2$ catalyst (Folco, 2013).
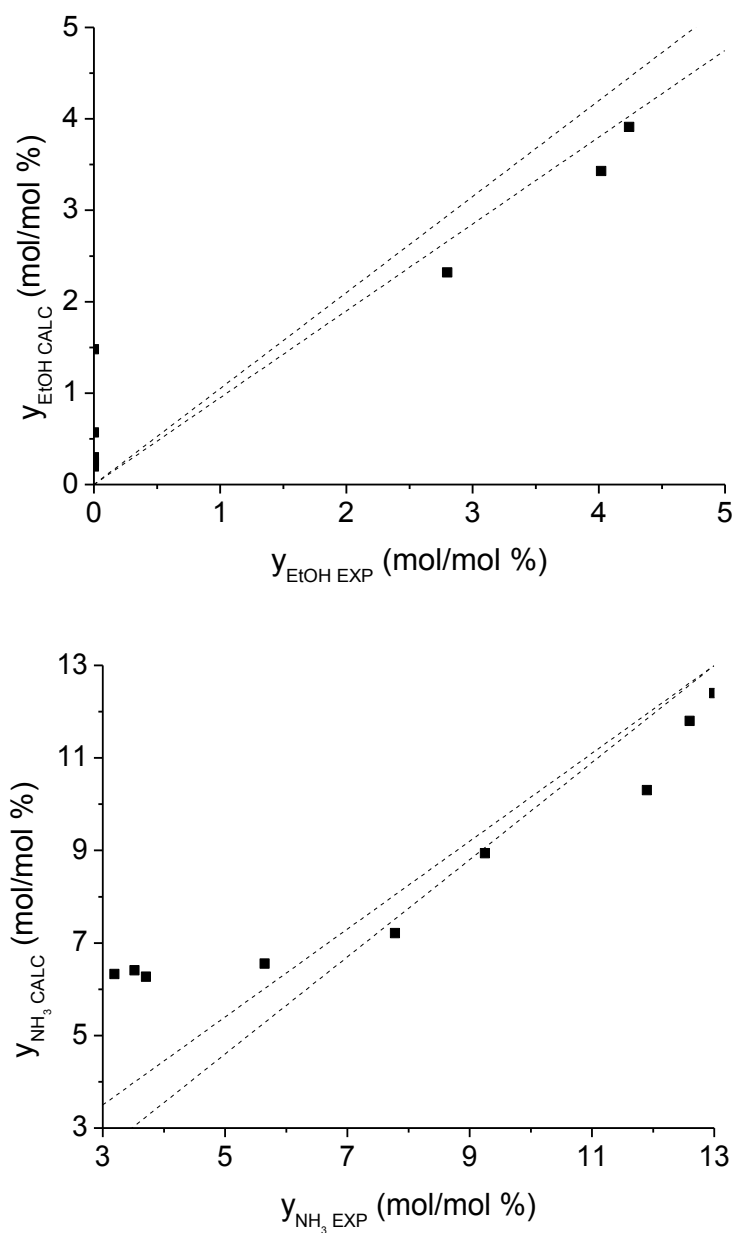
Figure S23: Parity plots of calculated *vs* experimental mole fractions of ethanol (top) and ammonia (bottom) for the $Cs\text{-}VO_x(7\%)/TiO_2$ catalyst (Folco, 2013).
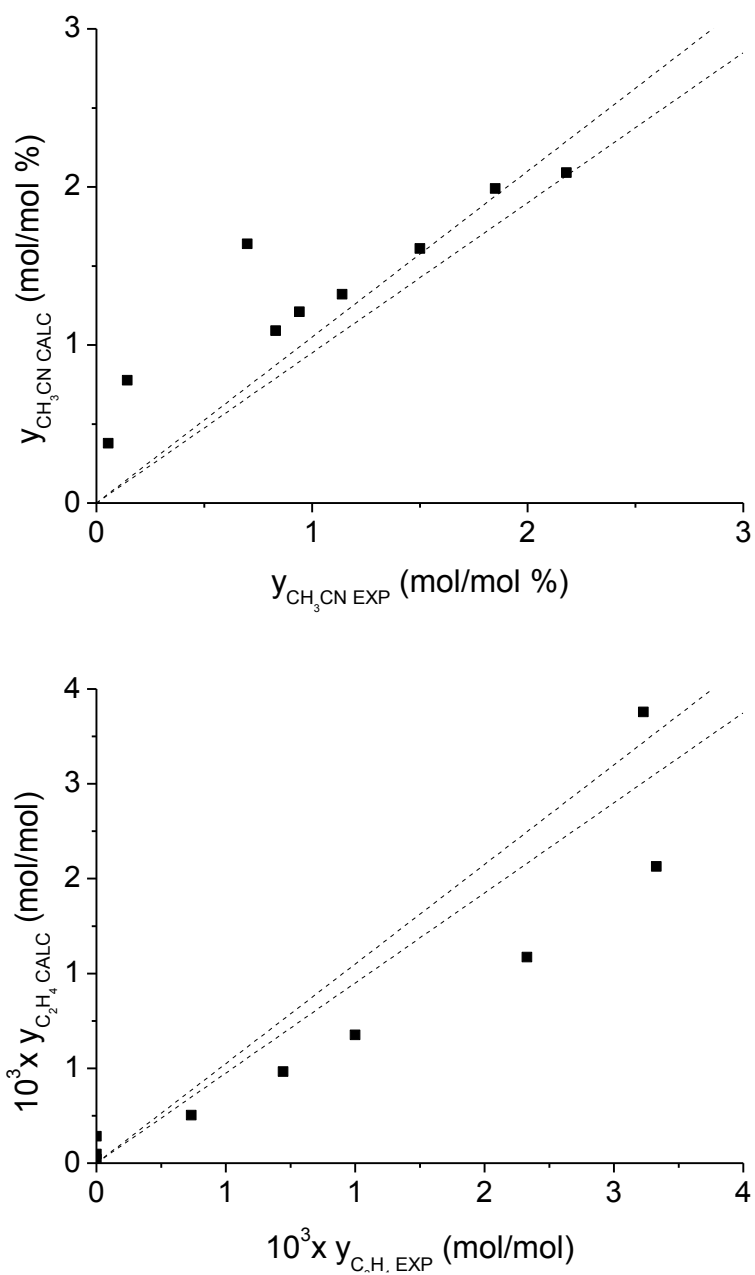
Figure S24: Parity plots of calculated *vs* experimental mole fractions of acetonitrile (top) and ethylene (bottom) for the Cs-VO$_x$(7%)/TiO$_2$ catalyst (Folco, 2013).
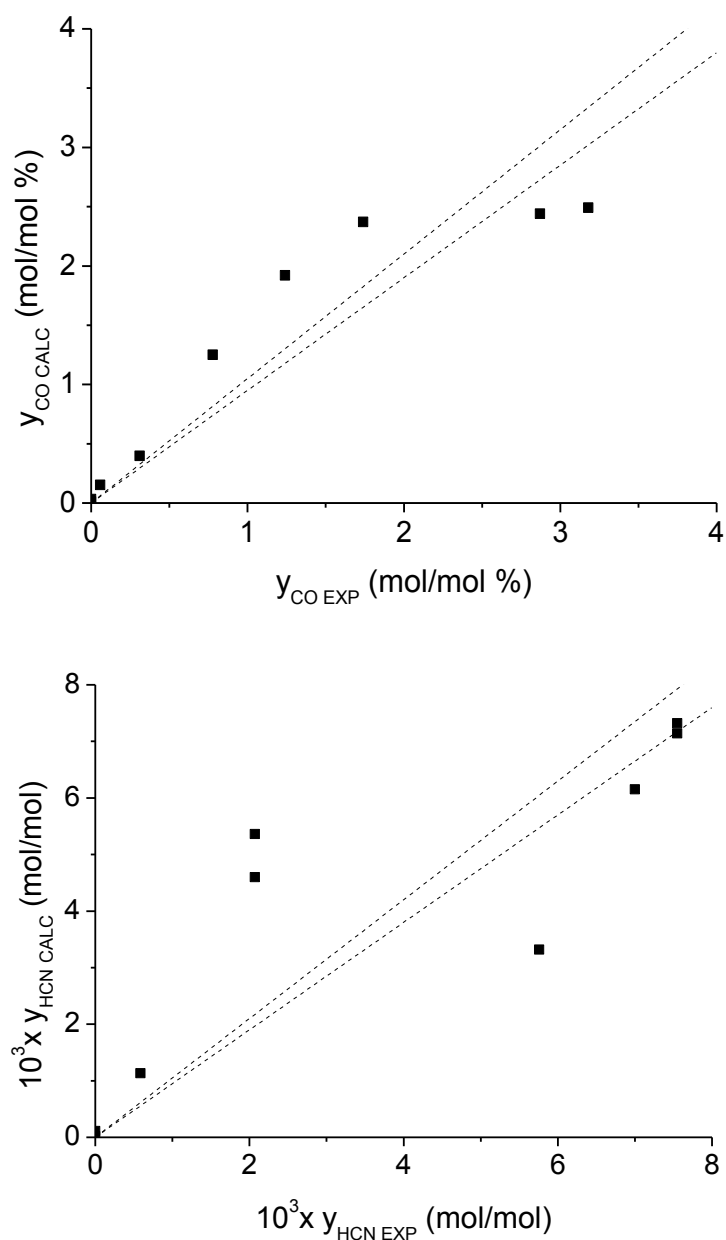
Figure S25: Parity plots of calculated *vs* experimental mole fractions of CO (top) and HCN (bottom) for the Cs-VO$_x$(7%)/TiO$_2$ catalyst (Folco, 2013).
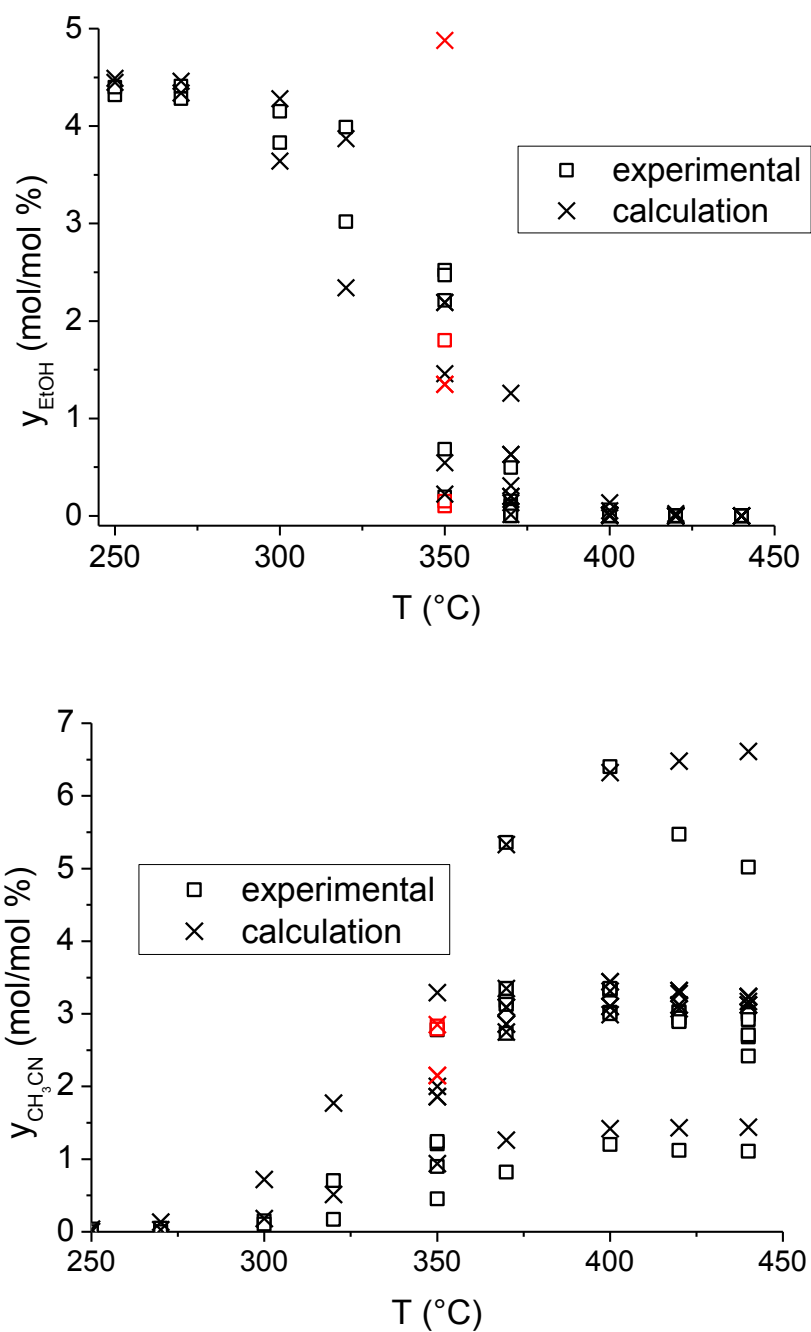
Figure S26: Ethanol (top) and acetonitrile (bottom) molar fractions as a function of reaction temperature for the VO_x/ZrO_2 catalyst (Folco, 2013).
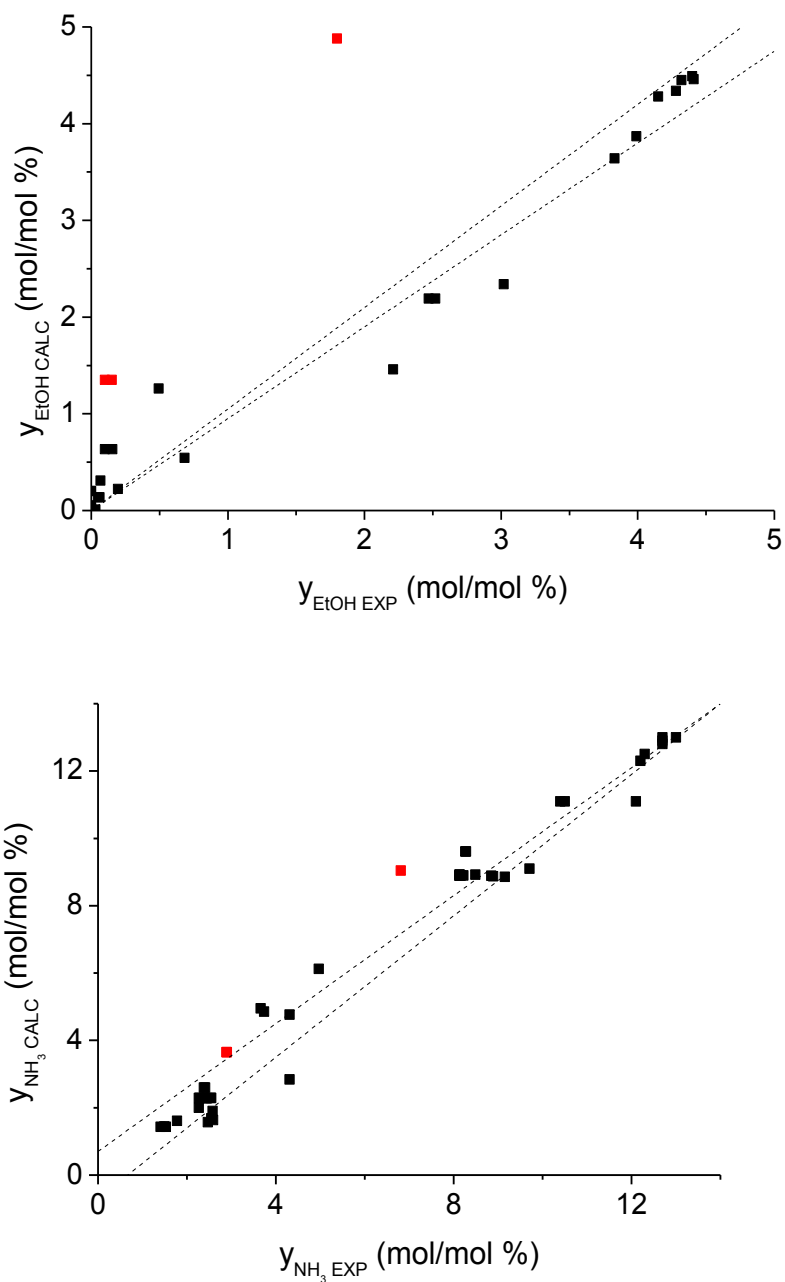
Figure S27: Parity plots of calculated *vs* experimental mole fractions of ethanol (top) and ammonia (bottom) for the VO_x/ZrO_2 catalyst.
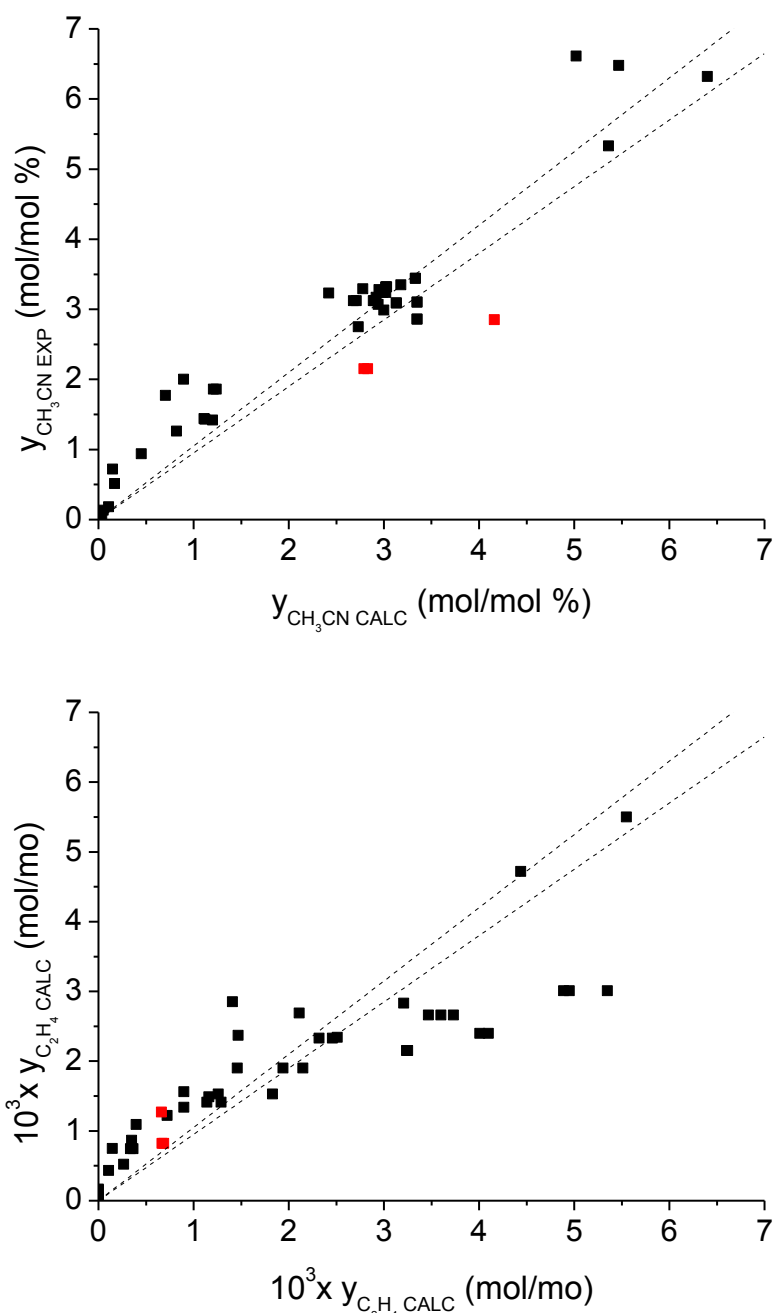
Figure S28: Parity plots of calculated *vs* experimental mole fractions of acetonitrile (top) and ethylene (bottom) for the VO_x/ZrO_2 catalyst.
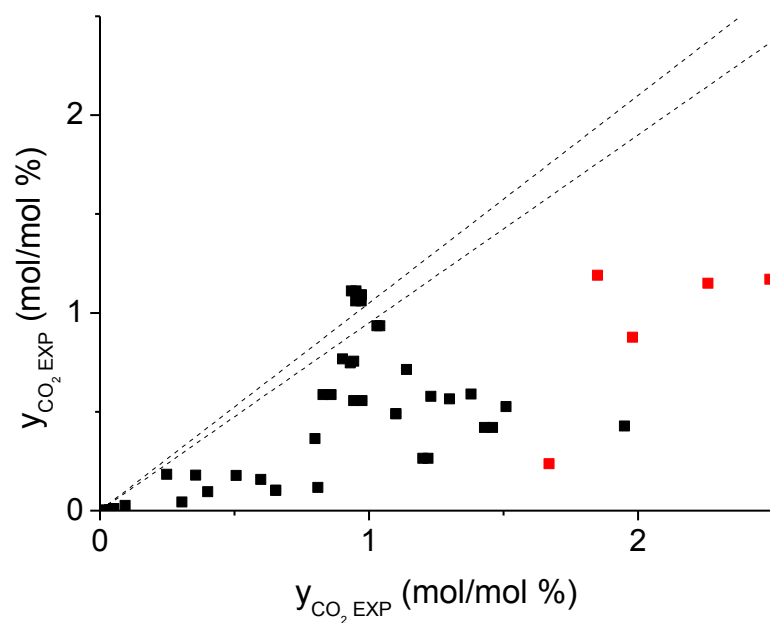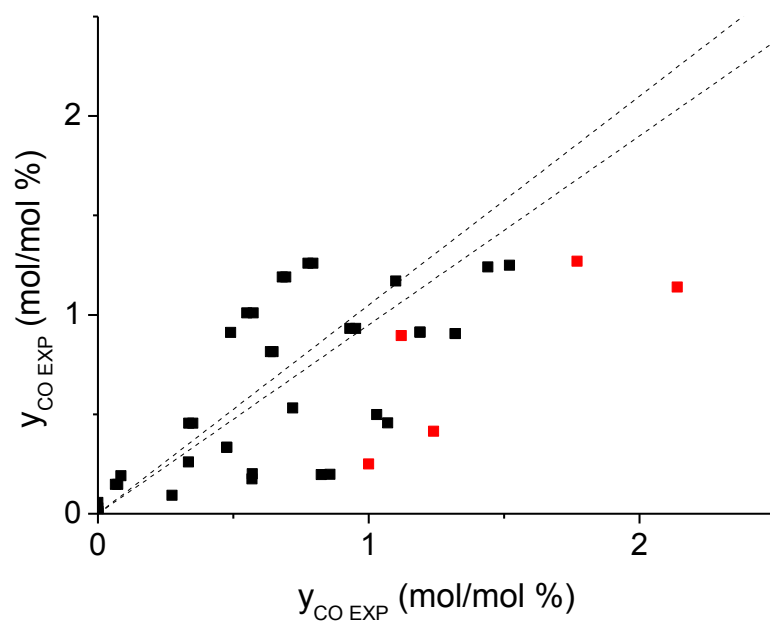
Figure S29: Parity plots of calculated *vs* experimental mole fractions of CO (top) and CO_2 (bottom) for the VO_x/ZrO_2 catalyst. Red marks individuate the trials with the highest ethanol:ammonia:oxygen ratio.

The original data (from Folco et al., Catalysis Science and Technology, 2017 and Università di Bologna, PHD Dissertation Thesis, 2013) as volumetric flowrate, total catalyst load and contact time were converted into molar flowrate and partial catalyst loads assuming ideal-gas behavior and constant catalyst density.

id	T	T0	Flow		Load	inlet fractions					outlet fractions									
#	(°C)	(°C)	(stdml/min)	(10^{-5} mol/s)	(mg)	(mol/mol)					(mol/mol)									
						EtOH	H_2O	NH_3	O_2	N_2	EtOH	NH_3	O_2	MeCN	AcH	C_2H_4	CO	CO_2	HCN	N_2
1	350	440	99.93	6.81	1333	0.045	0.005	0.13	0.13	0.69	0.0423	0.122	0.122	0.00119	0.000675	0.000216	0.00027	0.00027	0.00027	0.69
2	370	440	99.93	6.81	1333	0.045	0.005	0.13	0.13	0.69	0.0382	0.117	0.117	0.0029	0.00108	0.000877	0.0011	0.0011	0.00081	0.69
3	400	440	99.93	6.81	1333	0.045	0.005	0.13	0.13	0.69	0.0225	0.108	0.108	0.00787	0.001125	0.00382	0.0057	0.0057	0.00315	0.6905
4	420	440	99.93	6.81	1333	0.045	0.005	0.13	0.13	0.69	0.00765	0.112	0.0897	0.0101	0	0.00821	0.0145	0.0145	0.00373	0.692
5	440	440	99.93	6.81	1333	0.045	0.005	0.13	0.13	0.69	0	0.0845	0.0806	0.0063	0	0.0135	0.0212	0.0212	0.0063	0.699
6	370	440	99.93	6.81	42	0.045	0.005	0.13	0.13	0.69	0.0439	0.128	0.128	0.000146	0.0009	0.000202	0	0	0	0.69
7	370	440	99.93	6.81	83	0.045	0.005	0.13	0.13	0.69	0.04365	0.127	0.127	0.000216	0.000783	0.000229	$<10^{-4}$	$<10^{-4}$	0.000054	0.69
8	370	440	99.93	6.81	167	0.045	0.005	0.13	0.13	0.69	0.04275	0.125	0.123	0.00045	0.000945	0.00036	0.000135	0.000135	0.00018	0.69
9	370	440	99.93	6.81	333	0.045	0.005	0.13	0.13	0.69	0.0418	0.123	0.121	0.000693	0.00116	0.000504	0.00022	0.00022	0.000252	0.69
10	370	440	99.93	6.81	833	0.045	0.005	0.13	0.13	0.69	0.04	0.12	0.119	0.00139	0.00119	0.000792	0.000544	0.000544	0.000693	0.69
11	370	440	99.93	6.81	1333	0.045	0.005	0.13	0.13	0.69	0.0391	0.118	0.118	0.0024	0.001	0.000819	0.000877	0.000877	0.000702	0.69
12	440	440	99.93	6.81	42	0.045	0.005	0.13	0.13	0.69	0.036	0.13	0.13	0.00126	0.00369	0.00306	0.00054	0.00054	0.00054	0.69
13*	440	440	99.93	6.81	83	0.045	0.005	0.13	0.13	0.69	0.0337	0.123	0.125	0.00168	0.00336	0.031	0.000672	0.000672	0.000448	0.69
14	440	440	99.93	6.81	167	0.045	0.005	0.13	0.13	0.69	0.0261	0.116	0.118	0.00378	0.00302	0.007	0.00302	0.00302	0.00302	0.69
15	440	440	99.93	6.81	333	0.045	0.005	0.13	0.13	0.69	0.00675	0.0962	0.101	0.00956	0.000765	0.0138	0.000601	0.000601	0.00688	0.69
16	440	440	99.93	6.81	833	0.045	0.005	0.13	0.13	0.69	0	0.0936	0.091	0.00675	0	0.0157	0.0139	0.0139	0.01	0.69
17	440	440	99.93	6.81	1333	0.045	0.005	0.13	0.13	0.69	0	0.0871	0.0819	0.00675	0	0.0135	0.0207	0.0207	0.0054	0.69
18*	350	440	99.93	6.81	1333	0.0178	0.0022	0.13	0.13	0.72	0.016	0.12	0.121	0.0008	0.00032	0.000214	0.000125	0.000125	0.000178	0.72
19*	370	440	99.93	6.81	1333	0.0178	0.0022	0.13	0.13	0.72	0.0151	0.118	0.12	0.00136	0.000374	0.000347	0.000267	0.000267	0.000374	0.72
20*	400	440	99.93	6.81	1333	0.0178	0.0022	0.13	0.13	0.72	0.00641	0.1	0.0975	0.0049	0.000342	0.00171	0.00262	0.00262	0.00148	0.72

21*	420	440	99.93	6.81	1333	0.0178	0.0022	0.13	0.13	0.72	0.000356	0.0884	0.0832	0.004	0.00009	0.004	0.00557	0.00557	0.0023	0.727
22*	440	440	99.93	6.81	1333	0.0178	0.0022	0.13	0.13	0.72	0	0.0832	0.0793	0.00178	0	0.00605	0.00819	0.00819	0.0025	0.745
23*	350	440	99.93	6.81	1333	0.045	0.005	0.13	0.13	0.69	0.0414	0.12	0.121	0.00162	0.0009	0.000324	0.00036	0.00036	0.00036	0.69
24*	370	440	99.93	6.81	1333	0.045	0.005	0.13	0.13	0.69	0.0391	0.118	0.12	0.00251	0.000936	0.00076	0.000819	0.000819	0.00076	0.69
25*	400	440	99.93	6.81	1333	0.045	0.005	0.13	0.13	0.69	0.0225	0.108	0.108	0.0081	0.0009	0.00382	0.00562	0.00562	0.003375	0.691
26*	420	440	99.93	6.81	1333	0.045	0.005	0.13	0.13	0.69	0.00765	0.099	0.0858	0.0105	0.000375	0.009	0.012	0.012	0.0045	0.693
27*	440	440	99.93	6.81	1333	0.045	0.005	0.13	0.13	0.69	0	0.078	0.0767	0.0063	0	0.0139	0.0207	0.0207	0.0063	0.7
28	350	440	99.93	6.81	1333	0.0667	0.0083	0.13	0.13	0.66	0.0614	0.117	0.12	0.00112	0.00117	0.000587	0.00064	0.00064	0.00043	0.665
29	370	440	99.93	6.81	1333	0.0667	0.0083	0.13	0.13	0.66	0.0607	0.117	0.12	0.0012	0.00114	0.00075	0.00084	0.00084	0.00072	0.665
30	400	440	99.93	6.81	1333	0.0667	0.0083	0.13	0.13	0.66	0.0467	0.099	0.0975	0.003	0.0028	0.0034	0.0034	0.0034	0.0028	0.666
31	420	440	99.93	6.81	1333	0.0667	0.0083	0.13	0.13	0.66	0.0253	0.0819	0.0663	0.00578	0.00248	0.0103	0.00867	0.00867	0.00544	0.666
32	440	440	99.93	6.81	1333	0.0667	0.0083	0.13	0.13	0.66	0.0027	0.0598	0.0338	0.009	0.00128	0.0166	0.0138	0.0138	0.09	0.669
33	350	440	99.93	6.81	1333	0.115	0.015	0.13	0.13	0.61	0.108	0.114	0.12	0.00103	0.00248	0.00103	0.001	0.001	0.000345	0.61
34	370	440	99.93	6.81	1333	0.115	0.015	0.13	0.13	0.61	0.099	0.11	0.118	0.00156	0.00216	0.00179	0.00184	0.00184	0.000552	0.61
35	400	440	99.93	6.81	1333	0.115	0.015	0.13	0.13	0.61	0.0943	0.1	0.0962	0.00352	0.00186	0.00393	0.00476	0.00476	0.00207	0.61
36	420	440	99.93	6.81	1333	0.115	0.015	0.13	0.13	0.61	0.069	0.0725	0.0533	0.00552	0.00138	0.011	0.011	0.011	0.00368	0.612
37	440	440	99.93	6.81	1333	0.115	0.015	0.13	0.13	0.61	0.0437	0.0503	0.0169	0.00856	0.00143	0.019	0.0175	0.0175	0.00642	0.613
38	440	440	99.93	6.81	83	0.0667	0.0083	0.13	0.13	0.66	0.06	0.123	0.121	0.001	0.0028	0.00188	0	0.00088	0.000134	0.665
39	440	440	99.93	6.81	167	0.0667	0.0083	0.13	0.13	0.66	0.0447	0.0936	0.107	0.0033	0.00451	0.00572	0.00176	0.00264	0.00088	0.665
40	440	440	99.93	6.81	333	0.0667	0.0083	0.13	0.13	0.66	0.0373	0.091	0.091	0.0058	0.00232	0.0087	0.00348	0.00348	0.00058	0.665
41	440	440	99.93	6.81	833	0.0667	0.0083	0.13	0.13	0.66	0.0213	0.078	0.0481	0.00945	0.0009	0.0121	0.0135	0.0135	0.0027	0.665
42	440	440	99.93	6.81	1333	0.0667	0.0083	0.13	0.13	0.66	0.00867	0.0845	0.0416	0.0116	0.00087	0.0128	0.0197	0.0197	0.00464	0.665
43*	350	440	99.93	6.81	1333	0.115	0.015	0.13	0.39	0.35	0.109	0.13	0.363	0.00115	0.00264	0.000402	0.000575	0.000575	0.00023	0.35
44*	370	440	99.93	6.81	1333	0.115	0.015	0.13	0.39	0.35	0.107	0.125	0.355	0.0025	0.00137	0.000885	0.00169	0.00169	0.000483	0.35
45*	400	440	99.93	6.81	1333	0.115	0.015	0.13	0.39	0.35	0.099	0.123	0.289	0.00354	0.000805	0.00274	0.0033	0.0033	0.00161	0.35
46*	420	440	99.93	6.81	1333	0.115	0.015	0.13	0.39	0.35	0.0885	0.114	0.211	0.00554	0.000792	0.00528	0.00607	0.00607	0.00317	0.35
47*	440	440	99.93	6.81	1333	0.115	0.015	0.13	0.39	0.35	0.06	0.107	0.0936	0.00938	0.0011	0.0116	0.00607	0.00607	0.00607	0.35

id	T	T0	Flow		Load	EtOH	H₂O	NH₃	O₂	N₂	EtOH	NH₃	O₂	MeCN	AcH	C₂H₄	CO	CO₂	HCN	N₂
48	350	440	99.93	6.81	1333	0.0667	0.0083	0.13	0.13	0.66	0.0637	0.118	0.117	0.00108	0.00045	0.00045	0.00042	0.00042	0.0003	0.665
49	370	440	99.93	6.81	1333	0.0667	0.0083	0.13	0.13	0.66	0.062	0.11	0.11	0.00141	0.000752	0.0008	0.00122	0.00122	0.00047	0.665
50	400	440	99.93	6.81	1333	0.0667	0.0083	0.13	0.13	0.66	0.0487	0.101	0.0975	0.00432	0.00198	0.00342	0.00558	0.00558	0.00216	0.666
51	420	440	99.93	6.81	1333	0.0667	0.0083	0.13	0.13	0.66	0.0253	0.0871	0.078	0.00826	0.0004	0.00826	0.014	0.014	0.00413	0.667
52	440	440	99.93	6.81	1333	0.0667	0.0083	0.13	0.13	0.66	0.006	0.0806	0.0364	0.0121	0	0.0085	0.0212	0.0212	0.00607	0.668

Table S9: reaction data relative to the VPP catalyst. (*): the data series was not used to force the parameters' optimization, and may be marked in red where shown in the figures.

id	T	T0	Flow		Load	inlet fractions					outlet fractions									
#	(°C)	(°C)	(stdml/min)	(10⁻⁵ mol/s)	(mg)	(mol/mol)					(mol/mol)									
						EtOH	H₂O	NH₃	O₂	N₂	EtOH	NH₃	O₂	MeCN	AcH	C₂H₄	CO	CO₂	HCN	N₂
1	250	320	100.2	6.8281	1336	0.045	0.005	0.13	0.13	0.69	0.040024	0.005	0.13	0.120863	0.001324	0.001659	0	0	0.001567	0.69
2	270	320	100.2	6.8281	1336	0.045	0.005	0.13	0.13	0.69	0.037871	0.005	0.124	0.124475	0.002786	0.002218	0	0	0.003696	0.69
3	300	320	100.2	6.8281	1336	0.045	0.005	0.13	0.13	0.69	0.021544	0.005	0.1070	0.116438	0.011576	0	0	0	0.016732	0.69
4	320	320	100.2	6.8281	1336	0.045	0.005	0.13	0.13	0.69	0.000952	0.005	0.0929	0.081109	0.021208	0	0	0.007341	0.029855	0.6923
5	350	320	100.2	6.8281	1336	0.045	0.005	0.13	0.13	0.69	0	0.005	0.0835	0.044561	0.012833	0	0.0015	0.016667	0.037167	0.7028
6	370	320	100.2	6.8281	1336	0.045	0.005	0.13	0.13	0.69	0	0.005	0.0690	0.024086	0.006833	0	0.002083	0.021	0.0425	0.7168
7	400	320	100.2	6.8281	1336	0.045	0.005	0.13	0.13	0.69	0	0.005	0.057	0	0.003083	0	0.003083	0.030167	0.042833	0.7255
8	420	320	100.2	6.8281	1336	0.045	0.005	0.13	0.13	0.69	0	0.005	0.057	0	0.0025	0	0.004333	0.033833	0.038667	0.7265
9	440	320	100.2	6.8281	1336	0.045	0.005	0.13	0.13	0.69	0	0.005	0.057	0	0.0025	0	0.004333	0.033833	0.038667	0.7265
10	320	320	100.2	6.8281	50.1	0.045	0.005	0.13	0.07	0.75	0.04028	0.005	0.122	0.064615	0.002047	0.002139	0	0	0.000489	0.7501
11	320	320	100.2	6.8281	83.5	0.045	0.005	0.13	0.07	0.75	0.038628	0.005	0.122	0.064003	0.002874	0.002888	0	0	0.000932	0.7501
12	320	320	100.2	6.8281	125.25	0.045	0.005	0.13	0.07	0.75	0.036267	0.005	0.119	0.05354	0.00433	0.00353	8.55E-05	0.000122	0.001612	0.7502
13	320	320	100.2	6.8281	167	0.045	0.005	0.13	0.07	0.75	0.001416	0.005	0.0952	0.013462	0.029076	0	0.000549	0.002438	0.015971	0.7501
14	320	320	100.2	6.8281	334	0.045	0.005	0.13	0.07	0.75	0.000472	0.005	0.0925	0.011871	0.028274	0	0.000623	0.00274	0.01887	0.7511
15	320	320	100.2	6.8281	50.1	0.0126	0.0014	0.036	0.017	0.933	0.01008	0.0014	0.0342	0.014405	0.000897	0.001412	<10-4	0	0.000248	0.9330
16	320	320	100.2	6.8281	83.5	0.0126	0.0014	0.036	0.017	0.933	0.009726	0.0014	0.0332	0.012139	0.001151	0.001483	<10-4	<10-4	0.000403	0.9331

id	T	T0	Flow	(10⁻⁵ mol/s)	Load	EtOH	H₂O	NH₃	O₂	N₂	EtOH	NH₃	O₂	MeCN	AcH	C₂H₄	CO	CO₂	HCN	N₂
17	320	320	100.2	6.8281	125.25	0.0126	0.0014	0.036	0.017	0.933	0.007781	0.0014	0.0324	0.011497	0.002034	0.001766	<10-4	0.000505	0.000878	0.9331
18	320	320	100.2	6.8281	167	0.0126	0.0014	0.036	0.017	0.933	0.006919	0.0014	0.0316	0.010498	0.002885	0.001666	<10-4	0.00075	0.001059	0.933
19	320	320	100.2	6.8281	334	0.0126	0.0014	0.036	0.017	0.933	0.004554	0.0014	0.0279	0.005398	0.004634	0.00164	<10-4	0.001129	0.002275	0.9334

Table S10: reaction data relative to the V(2%)/TiO catalyst.

id #	T (°C)	T0 (°C)	Flow (stdml/min)	(10⁻⁵ mol/s)	Load (mg)	inlet fractions (mol/mol)					outlet fractions (mol/mol)									
						EtOH	H₂O	NH₃	O₂	N₂	EtOH	NH₃	O₂	MeCN	AcH	C₂H₄	CO	CO₂	HCN	N₂
1	250	350	100.2	6.83	1336	0.045	0.005	0.13	0.13	0.69	0.041083	0.005	0.1246	0.126865	0.00128	0.001682	0	0	0.001418	0.69
2	270	350	100.2	6.83	1336	0.045	0.005	0.13	0.13	0.69	0.038636	0.005	0.1218	0.127879	0.002315	0.002315	0	0	0.002821	0.69
3	300	350	100.2	6.83	1336	0.045	0.005	0.13	0.13	0.69	0.01587	0.005	0.1052	0.110199	0.012599	0.001022	0	0.000646	0.019581	0.69
4	320	350	100.2	6.83	1336	0.045	0.005	0.13	0.13	0.69	0	0.005	0.0958	0.078731	0.021	0	0	0.002327	0.036731	0.6903
5	350	350	100.2	6.83	1336	0.045	0.005	0.13	0.13	0.69	0	0.005	0.0779	0.038069	0.011934	0	0.001471	0.00964	0.045374	0.7051
6	370	350	100.2	6.83	1336	0.045	0.005	0.13	0.13	0.69	0	0.005	0.0534	0.008604	0.007604	0	0.002742	0.018615	0.041219	0.7214
7	400	350	100.2	6.83	1336	0.045	0.005	0.13	0.13	0.69	0	0.005	0.0510	0	0.00482	0	0.004654	0.029917	0.038061	0.7253
8	420	350	100.2	6.83	1336	0.045	0.005	0.13	0.13	0.69	0	0.005	0.0522	0	0.003823	0	0.005934	0.033906	0.035069	0.7258
9	440	350	100.2	6.83	1336	0.045	0.005	0.13	0.13	0.69	0	0.005	0.0482	0	0.002443	0	0.007313	0.0359	0.03108	0.731
10	350	350	100.2	6.83	167	0.045	0.005	0.06	0.06	0.83	0.017018	0.005	0.037	0.0288	0.008074	0.009347	0.000716	0.00716	0.011057	0.8303
11	370	350	100.2	6.83	167	0.045	0.005	0.06	0.06	0.83	0.0045	0.005	0.0239	0.006	0.021991	0.001036	0.002303	0.011744	0.017386	0.8308
12	400	350	100.2	6.83	167	0.045	0.005	0.06	0.06	0.83	0.000409	0.005	0.0239	0.001636	0.022185	0	0.003803	0.0161	0.019142	0.8313
13	420	350	100.2	6.83	167	0.045	0.005	0.06	0.06	0.83	0.001718	0.005	0.0255	0.0024	0.019688	0	0.005845	0.02061	0.011689	0.8321
14	440	350	100.2	6.83	167	0.045	0.005	0.06	0.06	0.83	0.000982	0.005	0.0273	0.001964	0.018959	0	0.007634	0.021599	0.010637	0.8323

Table S3: reaction data relative to the V(7%)/TiO catalyst.

id	T	T0	Flow		Load	inlet fractions					outlet fractions									

#	(°C)	(°C)	(stdml/min)	(10⁻⁵ mol/s)	(mg)	(mol/mol)					(mol/mol)									
						EtOH	H₂O	NH₃	O₂	N₂	EtOH	NH₃	O₂	MeCN	AcH	C₂H₄	CO	CO₂	HCN	N₂
1	250	350	100.2	6.83	1336	0.045	0.005	0.13	0.13	0.69	0.042382	0.005	0.1295	0.127407	0.000554	0.001618	0	0	0.000439	0.69
2	250	350	100.2	6.83	1336	0.045	0.005	0.13	0.13	0.69	0.040205	0.005	0.1258	0.125757	0.001434	0.002615	0	0	0.001392	0.69
3	270	350	100.2	6.83	1336	0.045	0.005	0.13	0.13	0.69	0.027982	0.005	0.1194	0.102421	0.007001	0.002353	0	0.000588	0.009002	0.69
4	300	350	100.2	6.83	1336	0.045	0.005	0.13	0.13	0.69	0	0.005	0.0925	0.062584	0.02178	0	0.000513	0.003111	0.034226	0.6922
5	320	350	100.2	6.83	1336	0.045	0.005	0.13	0.13	0.69	0	0.005	0.0778	0.048441	0.018513	0	0.001011	0.007779	0.034693	0.7016
6	350	350	100.2	6.83	1336	0.045	0.005	0.13	0.13	0.69	0	0.005	0.0564	0.031469	0.015013	0	0.0014	0.012446	0.03236	0.7162
7	370	350	100.2	6.83	1336	0.045	0.005	0.13	0.13	0.69	0	0.005	0.0371	0.008132	0.011357	0	0.002334	0.017424	0.031893	0.7311
8	400	350	100.2	6.83	1336	0.045	0.005	0.13	0.13	0.69	0	0.005	0.0319	0	0.009412	0	0.003034	0.028704	0.036249	0.7379
9	420	350	100.2	6.83	1336	0.045	0.005	0.13	0.13	0.69	0	0.005	0.0352	0	0.008323	0	0.002956	0.031846	0.035938	0.7369

Table S4: reaction data relative to the V(7%)-Cs/TiO catalyst.

id	T	T0	Flow		Load	inlet fractions					outlet fractions									
#	(°C)	(°C)	(stdml/min)	(10⁻⁵ mol/s)	(mg)	(mol/mol)					(mol/mol)									
						EtOH	H₂O	NH₃	O₂	N₂	EtOH	NH₃	O₂	MeCN	AcH	C₂H₄	CO	CO₂	HCN	N₂
1	250	370	100.2	6.83	668	0.045	0.005	0.13	0.06	0.76	0.04324	0.1300	0.0585	0.00035	0.00118	0	0	0.00036	0.00000	0.7600
2	270	370	100.2	6.83	668	0.045	0.005	0.13	0.06	0.76	0.04281	0.1271	0.0580	0.00050	0.00134	0	0	0.00051	0.00000	0.7600
3	300	370	100.2	6.83	668	0.045	0.005	0.13	0.06	0.76	0.03834	0.1225	0.0497	0.00149	0.00212	0	0	0.00305	0.00022	0.7600
4	320	370	100.2	6.83	668	0.045	0.005	0.13	0.06	0.76	0.03022	0.1206	0.0368	0.00703	0.00197	0.00027	0.00085	0.00810	0.00080	0.7600
5	350	370	100.2	6.83	668	0.045	0.005	0.13	0.06	0.76	0.00195	0.0971	0.0015	0.02777	0.00085	0.00116	0.00490	0.01955	0.00140	0.7600
6	370	370	100.2	6.83	668	0.045	0.005	0.13	0.06	0.76	0	0.0915	0	0.03178	0.00000	0.00146	0.01103	0.01508	0.00000	0.7605
7	400	370	100.2	6.83	668	0.045	0.005	0.13	0.06	0.76	0	0.0889	0	0.03024	0.00000	0.00251	0.01443	0.01297	0.00000	0.7610
8	420	370	100.2	6.83	668	0.045	0.005	0.13	0.06	0.76	0	0.0885	0	0.02951	0.00000	0.00373	0.01524	0.01232	0.00000	0.7612
9	440	370	100.2	6.83	668	0.045	0.005	0.13	0.06	0.76	0	0.0849	0	0.02424	0.00000	0.00535	0.01768	0.01378	0.00000	0.7621
10	250	370	100.2	6.83	167	0.045	0.005	0.13	0.06	0.76	0.04400	0.1271	0.0600	0.00000	0.00092	0	0	0.00017	0.00000	0.7600

11	270	370	100.2	6.83	167	0.045	0.005	0.13	0.06	0.76	0.04410	0.1274	0.0600	0.00000	0.00084	0	0	0.00013	0.00000	0.7600
12	300	370	100.2	6.83	167	0.045	0.005	0.13	0.06	0.76	0.04152	0.1274	0.0570	0.00107	0.00216	0	0	0.00051	0.00000	0.7600
13	320	370	100.2	6.83	167	0.045	0.005	0.13	0.06	0.76	0.03989	0.1231	0.0567	0.00170	0.00283	0	0	0.00094	0.00000	0.7600
14	350	370	100.2	6.83	167	0.045	0.005	0.13	0.06	0.76	0.02520	0.1044	0.0300	0.01208	0.00236	0.00036	0.00065	0.00654	0.00073	0.7600
15	370	370	100.2	6.83	167	0.045	0.005	0.13	0.06	0.76	0.00155	0.0825	0	0.03133	0	0.00183	0.00351	0.01196	0.00446	0.7606
16	400	370	100.2	6.83	167	0.045	0.005	0.13	0.06	0.76	0.00033	0.0814	0	0.03328	0	0.00246	0.00574	0.01098	0.00525	0.7608
17	420	370	100.2	6.83	167	0.045	0.005	0.13	0.06	0.76	0	0.0817	0	0.03030	0	0.00347	0.00694	0.00974	0.00462	0.7610
18	440	370	100.2	6.83	167	0.045	0.005	0.13	0.06	0.76	0	0.0814	0	0.03022	0	0.00495	0.00776	0.00859	0.00446	0.7617
19	350	370	100.2	6.83	167	0.045	0.005	0.13	0.06	0.76	0.02468	0.1052	0.0295	0.01237	0.00246	0.00034	0.00073	0.00654	0.00069	0.7600
20	370	370	100.2	6.83	167	0.045	0.005	0.13	0.06	0.76	0.00100	0.0828	0	0.03132	0	0.00126	0.00336	0.01218	0.00446	0.7600
21	400	370	100.2	6.83	167	0.045	0.005	0.13	0.06	0.76	0	0.0813	0	0.03329	0	0.00232	0.00550	0.01098	0.00468	0.7600
22	420	370	100.2	6.83	167	0.045	0.005	0.13	0.06	0.76	0	0.0822	0	0.03020	0	0.00360	0.00681	0.00943	0.00489	0.7600
23	440	370	100.2	6.83	167	0.045	0.005	0.13	0.06	0.76	0	0.0813	0	0.02994	0	0.00489	0.00794	0.00829	0.00458	0.7600
24	350	370	100.2	6.83	167	0.045	0.005	0.06	0.06	0.83	0.00100	0.0290	0	0.02830	0.00208	0.00067	0.00477	0.01425	0.00140	0.8300
25	370	370	100.2	6.83	167	0.045	0.005	0.06	0.06	0.83	0	0.0241	0	0.03346	0.00025	0.00114	0.00638	0.01033	0.00085	0.8300
26	400	370	100.2	6.83	167	0.045	0.005	0.06	0.06	0.83	0	0.0229	0	0.03346	0	0.00215	0.00931	0.00951	0.00113	0.8300
27	420	370	100.2	6.83	167	0.045	0.005	0.06	0.06	0.83	0	0.0243	0	0.02902	0	0.00325	0.01194	0.00972	0.00170	0.8300
28	440	370	100.2	6.83	167	0.045	0.005	0.06	0.06	0.83	0	0.0255	0	0.02677	0	0.00410	0.01319	0.00935	0.00188	0.8300
29	350	370	100.2	6.83	167	0.045	0.005	0.05	0.05	0.85	0.02205	0.0431	0.0256	0.00896	0.00610	0.00035	0.00335	0.00800	0.00050	0.8500
30	370	370	100.2	6.83	167	0.045	0.005	0.05	0.05	0.85	0.00068	0.0258	0.0007	0.02726	0.00333	0.00090	0.00720	0.01138	0.00155	0.8500
31	400	370	100.2	6.83	167	0.045	0.005	0.05	0.05	0.85	0	0.0255	0	0.03003	0.00066	0.00147	0.01025	0.00931	0.00174	0.8500
32	420	370	100.2	6.83	167	0.045	0.005	0.05	0.05	0.85	0	0.0259	0	0.02936	0	0.00211	0.01075	0.00943	0.00198	0.8500
33	440	370	100.2	6.83	167	0.045	0.005	0.05	0.05	0.85	0	0.0246	0	0.02919	0	0.00321	0.01238	0.00902	0.00213	0.8500
34	350	370	100.2	6.83	167	0.018	0.002	0.03	0.02	0.93	0.00684	0.0227	0.0074	0.00452	0.00280	0.00011	0.00274	0.00401	0.00042	0.9300
35	370	370	100.2	6.83	167	0.018	0.002	0.03	0.02	0.93	0.00048	0.0178	0.0008	0.00820	0.00258	0.00015	0.00569	0.00598	0.00140	0.9300
36	400	370	100.2	6.83	167	0.018	0.002	0.03	0.02	0.93	0	0.0149	0	0.01201	0	0.00040	0.00570	0.00506	0.00029	0.9300
37	420	370	100.2	6.83	167	0.018	0.002	0.03	0.02	0.93	0	0.0153	0	0.01117	0.00011	0.00072	0.00825	0.00356	0.00045	0.9300

38	440	370	100.2	6.83	167	0.018	0.002	0.03	0.02	0.93	0	0.0141	0	0.01111	0.00043	0.00090	0.00858	0.00248	0.00023	0.9300
39	350	370	100.2	6.83	167	0.09	0.01	0.12	0.1	0.68	0.01800	0.0681	0.0205	0.04162	0.01192	0.00066	0.01000	0.01673	0.00059	0.6800
40	370	370	100.2	6.83	167	0.09	0.01	0.12	0.1	0.68	0.00495	0.0498	0.0049	0.05359	0.00941	0.00141	0.01122	0.01976	0.00089	0.6800
41	400	370	100.2	6.83	167	0.09	0.01	0.12	0.1	0.68	0.00061	0.0366	0	0.06397	0.00056	0.00444	0.02142	0.02255	0.00128	0.6800
42	420	370	100.2	6.83	167	0.09	0.01	0.12	0.1	0.68	0	0.0374	0	0.05470	0	0.00555	0.02813	0.02491	0.00029	0.6800
43	440	370	100.2	6.83	167	0.09	0.01	0.12	0.1	0.68	0	0.0431	0	0.05019	0	0.00953	0.04063	0.01854	0.00364	0.6800
44	350	370	100.2	6.83	167	0.045	0.005	0.06	0.06	0.83	0.00152	0.0289	0.0002	0.02790	0.00208	0.00069	0.00475	0.01464	0.00000	0.8300
45	370	370	100.2	6.83	167	0.045	0.005	0.06	0.06	0.83	0	0.0238	0	0.03347	0	0.00129	0.00647	0.01036	0.00083	0.8300
46	400	370	100.2	6.83	167	0.045	0.005	0.06	0.06	0.83	0	0.0227	0	0.03354	0	0.00194	0.00952	0.00971	0.00104	0.8300
47	420	370	100.2	6.83	167	0.045	0.005	0.06	0.06	0.83	0	0.0246	0	0.02888	0	0.00324	0.01191	0.00971	0.00168	0.8320
48	440	370	100.2	6.83	167	0.045	0.005	0.06	0.06	0.83	0	0.0254	0	0.02706	0	0.00401	0.01321	0.00952	0.00168	0.832

Table S5: reaction data relative to the V/ZrO catalyst.